The Role of Epigenetic Modifiers, Kdm6a and Kdm6b, in Calvarial Suture Development and Craniosynostosis

A thesis submitted in fulfilment for the degree of
DOCTOR OF PHILOSOPHY
by

Clara Mentari Putri Pribadi, B.Sc (Hons.)
Student ID: a1613995

Mesenchymal Stem Cell Group
Faculty of Health and Medical Sciences
School of Biomedicine
Discipline of Physiology
The University of Adelaide

&

Precision Medicine Theme
South Australian Health and Medical Research Institute

January 2022

Table of Contents

DECLARATION

I certify that this work contains no material which has been accepted for the award of any other degree or diploma in my name, in any university or other tertiary institution and, to the best of my knowledge and belief, contains no material previously published or written by another person, except where due reference has been made in the text. In addition, I certify that no part of this work will, in the future, be used in a submission in my name, for any other degree or diploma in any university or other tertiary institution without the prior approval of the University of Adelaide and where applicable, any partner institution responsible for the joint-award of this degree.

I give permission for the digital version of my thesis to be made available on the web, via the University's digital research repository, the Library Search and also through web search engines, unless permission has been granted by the University to restrict access for a period of time.

I acknowledge the support I have received for my research through the provision of an Australian Government Research Training Program Scholarship.

Clara Pribadi

ACKNOWLEDGMENTS

I am forever grateful for the immense support from my supervisors, my family, and my friends during this four-year journey to my greatest accomplishment thus far. During this time, I have gained not only invaluable experiences, scientific skills, and expertise, but also the understanding of the importance of perseverance and resilience.

Firstly, I would like to thank Prof Stan Gronthos for your wisdom, continuous guidance, and compassion during this incredibly unpredictable time. Thank you for your calmness and decisiveness for when I felt like the opposite of those things. Thank you to Dr Jim Cakouros for sharing your passion in epigenetics, for always being approachable and most importantly, for making this journey more fun. Thank you to Dr Esther Camp-Dotlic for patiently teaching me the most critical laboratory skills and for your guidance throughout. To my clinical supervisor, Prof Peter Anderson, thank you for sharing your knowledge, for always offering support and making time to see me every week despite your extremely busy schedule and lastly, thank you for your contagious excitement for research. I am truly blessed to have such a strong support system through this rollercoaster of a journey.

Secondly, I am incredibly thankful for Sharon Paton who went above and beyond in supporting everyone in the lab professionally and personally. Thank you for being the most compassionate listener, for being the laboratory's therapist and most importantly, for your friendship. I would also like to thank Dr Agnes Arthur for always offering a helping hand, for sharing your experiences and invaluable advice. Thank you to the current PhD students of the Mesenchymal Stem Cells laboratory: Nicholas Smith and Suzanne Motallebi for the support, the chats, and the laughter.

Thank you to all the friends that I made along the way, especially to the girls: Khatora Opperman, Laura Trainor, Natalya Plakhova, Justine Clark, Saoirse Benson, and Alanah Bradey. Thank you for showing me the intelligence, the tenacity, and the strength of women. I would not be able to do this without all of you. Thank you for keeping me sane.

Thank you to my mom who not only raised me as a single mother, but at the same time started our family business from the ground up. Thank you for showing me the importance of resilience through the most difficult times, while still showing immense compassion for other people. Thank you for always telling me how proud you are of me and thank you for shaping me into the woman I am today.

To my fiancé, Boon, thank you for never doubting me even when I doubted myself. Thank you for always being there as a shoulder to cry on, as a discussion partner, but most importantly, as a snack provider. Thank you for helping me practice every single presentation and for reading every single manuscript I have ever written. Thank you for being my biggest supporter.

Once more, thank you everyone for believing in me.

ABBREVIATIONS

3D	3-dimensional
7AAD	7-amino-actinomycin
AKT/PKB	protein kinase B
ALP	alkaline phosphatase
BCA	bicinchoninic acid
BMP	bone morphogenetic protein
BMSC	bone marrow stromal cells
bp	base pairs
BrdU	5-brome-2-deoxyuridine
BSA	bovine serum albumin
C	celsius
C-ROS-1	tyrosine kinase receptor c-ros-oncogene 1
cDNA	complimentary DNA
ChIP	chromatin immunoprecipitation
COMPASS	complex of proteins associated with Set1
DAB	3,3'-Diaminobenzidine
DAPI	4’,6-diamidino-2-phenylindole dihydrochloride
DMEM	Dulbecco’s modified eagle medium
DMSO	dimethyl sulfoxide
DNA	deoxyribonucleic acid
DNase	deoxyribonuclease
dNTP	deoxyribonucleotide triphosphate
DTT	dithiothreitol
EDTA	ethylenediaminetetra-acetic acid
ELISA	enzyme-linked immunoassay

EZH2	enhancer of zeste homolog 2
FACS	fluorescence-activated cell sorting
FCS	foetal calf serum
FGF	fibroblast growth factor
FGFR	fibroblast growth factor receptor
GLI-1	GLI family zinc finger 1
H3K27me3	tri-methylated lysine 27 on histone 3
H3K4me3	tri-methylated lysine 4 on histone 3
H4	histone 4
HEPES	4-(2-hydroxyethyl)-1-piperazineethanesulfonic acid
IgG	Immunoglobulin G
JmjC	Jumonji C
KDM6A/UTX	lysine-specific demethylase 6A
KDM6B/JMJD3	lysine-specific demethylase 6B
KDM6C/UTY	lysine-specific demethylase 6C
L	litre
M	molar
mg/ mL/ mm/ mM	milligram/ millilitre/ millimetre/ millimolar
Micro-CT	micro-computed tomography
MLL	mixed lineage leukemia
MPC	mesenchymal progenitor cells
mRNA	messenger ribonucleic acid
MSC	mesenchymal stem cells
mTOR	mammalian target of rapamycin
ng/ nm	nanogram/ nanometre
P	postnatal

P/S	penicillin/ streptomycin
PBS	phosphate buffered saline
PCR	polymerase chain reaction
PI3K	phosphatidylinositol-3-kinase
PIF	posterior interfrontal
PIN1	peptidyl-prolyl cis-trans isomerase NIMA-interacting 1
PRC2	polycomb repressive complex 2
PRX-1	paired related homeobox 1
PVDF	polyvinylidene difluoride
qPCR	reverse transcription-quantitative polymerase chain reaction
RBP2	retinoblastoma binding protein 2
rhBMP2	recombinant human bone morphogenic protein 2
RNA	ribonucleic acid
RO	reverse osmosis
ROI	regions of interest
RT	room temperature
RUNX2	runt-related transcription factor
SCS	Saethre-Chotzen syndrome
SD	standard deviation
SDS-PAGE	sodium dodecyl sulfate polyacrylamide gel electrophoresis
SEM	standard error of mean
siRNA	small interfering ribonucleic acid
SWI/SNF	switch/sucrose nonfermenting
TBS	tris-buffered saline
TET	ten-eleven-translocases
TGF-β	transforming growth factor beta

TNF-α	tumor necrosis factor alpha
TSS	transcription start site
Tween20	polyethylene glycol sorbitan monolaurate
TWIST-1	Twist family basic helix-loop-helix transcription factor 1
U	Units
v/v	volume per volume
w/v	weight per volume
WNT	wingless related protein
WT	wild type
αMEM	alpha-modified Eagle's medium
µg/ µL/ µm/ µM	microgram/ microliter/ micrometre/ micromolar

PUBLICATIONS

Scientific Manuscript

Pribadi, C., Camp-Dotlic, E., Cakouros, D., Anderson, P., Carlotta, G., Gronthos, S. (2020). Pharmacological targeting of KDM6A and KDM6B, as a novel therapeutic strategy for treating craniosynostosis in Saethre-Chotzen syndrome. *Stem Cell Research and Therapy*, 11(1), 529.

Conference Proceedings

1. 12th Annual Florey Postgraduate Research Conference, Adelaide, September 2018, Poster.
2. 3rd Annual Epigenetic Consortium of South Australia (EpiCSA) Scientific Meeting, Adelaide, October 2018, Oral presentation. Awarded the CSIRO Best Short Talk Prize.
3. SAHMRI Research Showcase, Adelaide, November 2018, Poster.
4. ASMR SA Scientific Meeting, Adelaide, June 2019, Oral presentation. Awarded the Channel 7 Children's Research Foundation Prize.
5. 6th Annual EMBL Australia PhD Course, Tasmania, July 2019, Oral presentation.
6. University of Adelaide 3-minute Thesis, August 2019, Oral presentation.
7. 13th Annual Florey Postgraduate Research Conference, September 2019, Poster.
8. Australasian Society for Stem Cell Research Joint Scientific Meeting, Brisbane, November 2019, Poster. Awarded the Adelaide Medical School Travel Award.
10. 14th Annual Florey Postgraduate Research Conference (Virtual), September 2020, Oral presentation. Awarded the Channel 7 Children's Research Foundation Prize.
11. ASMR SA Scientific Meeting, Adelaide (Virtual), October 2020, Oral presentation. Awarded the Channel 7 Children's Research Foundation Prize.

12. 14th EMBL Transcription and Chromatin Conference, Heidelberg, Germany (virtual), August 2020, Poster.

13. Cold Spring Harbour Laboratory Epigenetic and Chromatin Meeting, New York, USA (virtual), September 2020, Poster.

ABSTRACT

The five flat bones of human calvaria are held together by fibrous sutures, which remain open during development to accommodate for the growing brain. However, excessive osteogenic differentiation of mesenchymal progenitor cells (MPC) within the sutures can lead to premature suture fusion or craniosynostosis. Saethre-Chotzen Syndrome (SCS) is a common form of craniosynostosis, caused by *TWIST-1* gene mutation. Currently, the only treatment for craniosynostosis involves multiple invasive cranial surgeries, which could lead to serious complications. Thus, an attempt to identify a non-invasive therapy is paramount. The present thesis has shown that the expressions of histone demethylases, *KDM6A* and *KDM6B*, are upregulated in calvarial cells from SCS patients and from an SCS model of *Twist-1* haploinsufficient (*Twist-1*$^{del/+}$) mice. KDM6A and KDM6B have been shown previously to promote osteogenesis in MPC by removing their epigenetic target, the repressive mark of tri-methylated lysine 27 on histone 3 (H3K27me3), from the promoters of osteogenic genes. An established pre-clinical SCS mouse model was utilised to investigate the inhibition of Kdm6a and Kdm6b activity using the pharmacological inhibitor GSK-J4 on calvarial cell osteogenic potential. Furthermore, a suture mesenchyme-specific deletion of Kdm6a was established to assess the effects of Kdm6a loss, in the suture development of naturally fusing suture, the posterior interfrontal suture.

The results demonstrate for the first time that GSK-J4 treatment inhibited the osteogenic potential of calvarial stromal cells *in vitro* and the bone formation of *ex vivo* explants of *Twist-1*$^{del/+}$ calvaria, with minimal level of toxicity. ChIP analyses revealed that GSK-J4 treatment elevated the levels of the H3K27me3 mark on osteogenic genes leading to repression of their expression. *In vivo* studies showed that the local administration of GSK-J4 onto the calvaria of *Twist-1*$^{del/+}$ prevented premature suture fusion and kept the sutures open throughout calvarial development (Shpargel et al. 2017). Thus, the inhibition of Kdm6a

and Kdm6b activity by GSK-J4 could be a potential therapeutic strategy for preventing craniosynostosis in children with SCS. Furthermore, conditional knockout of *Kdm6a* prevented suture fusion of posterior interfrontal suture, suggesting that Kdm6a involvement could also contribute to non-syndromic craniosynostosis.

Chapter 1: Introduction

1.1 Mesenchymal progenitor cells within the mammalian calvaria sutures

The mammalian skull vault (calvaria) refers to the upper part of the skull, which encases the brain. Calvaria is made up of five flat bones; two frontal bones with neural crest origins and two parietal bones and occipital bone derived from the mesodermal lineage (Sahar, Longaker & Quarto 2005; Shpargel et al. 2017). These calvaria bones are held together by fibrous joints called sutures, which include the metopic suture, the sagittal suture, the coronal sutures and the lambdoid sutures (Senarath-Yapa 2012) (Figure 1.1). These sutures act like growth plates, facilitating the flexibility and expansion of the skull to assist during childbirth and accommodate for the growing brain. The complex composition of the suture includes the osteogenic fronts at the edges of the flat calvaria bones; the suture mesenchyme at the middle of the suture; the overlying pericranium and the underlying dura mater (Figure 1.1).

Within the suture mesenchyme, a reservoir of *GLI-1*$^{+}$*, PRX-1*$^{+}$*, TWIST-1*$^{+}$ mesenchymal progenitor cells (MPC) gives rise to premature osteogenic progenitors that could either remain undifferentiated or differentiate to mature bone cells, such as osteoblasts and osteocytes (terminally differentiated osteogenic cells) (Di Pietro et al. 2020; Johnson et al. 2000; Wilk et al. 2017; Zhao 2015). During development, the MPC population is involved in the calvaria outward expansion by preserving its immature proliferative state, maintained by factors such as TWIST-1 (Zhao 2015), and thus, keeping the sutures open, before mineralising to form fused sutures in mature calvaria (Beederman, MF, E. M.; Reid, R. R. 2014; Lenton et al. 2005). Initiated by osteogenic-promoting canonical WNT-signalling (Kreiborg & Cohen 2010; Krishnan, Bryant & Macdougald 2006), the differentiating MPC population is located at the suture osteogenic fronts where the bone formation is highly dependent on the expression of master osteogenic regulatory transcription factors, such as Runt-related transcription factor 2 (RUNX2) and Osterix (Nacamuli et al. 2003). *RUNX2*

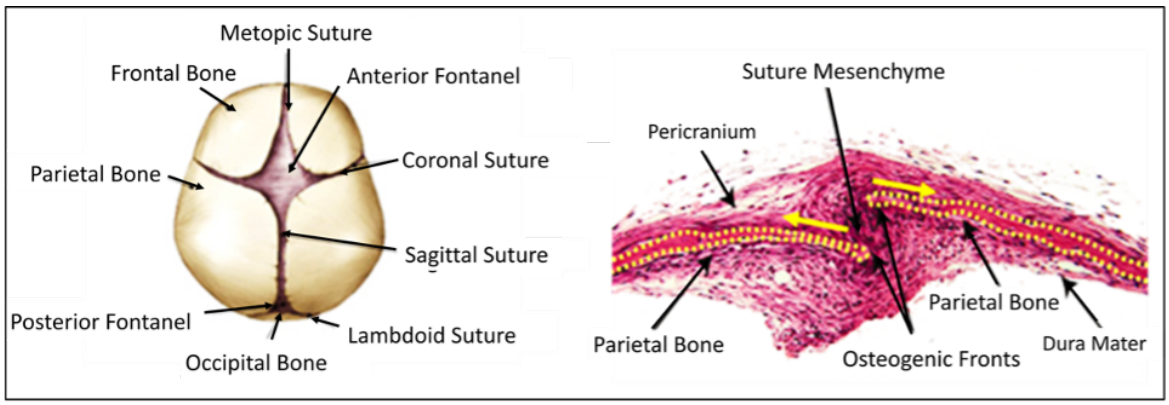
Metopic Suture
Frontal Bone
Anterior Fontanel
Parietal Bone
Coronal Suture
Sagittal Suture
Posterior Fontanel
Lambdoid Suture
Occipital Bone
Suture Mesenchyme
Pericranium
Parietal Bone
Parietal Bone
Osteogenic Fronts
Dura Mater

Figure 1.1 (Left) Schematic representation of calvarial bones and sutures of normal infant human calvaria (top view). Image adapted from Burgos-Florez et al., 2016 (Burgos-Florez, Gavilan-Alfonso & Garzon-Alvarado 2016); **(Right)** Haematoxylin and Eosin staining of murine sagittal suture. Image adapted from Lenton et al., 2005 (Lenton et al. 2005).

has been shown to be expressed in osteoprogenitor cells, responsible for initiating the osteogenic differentiation program of MPC, and is important in correct suture closure, followed by the expression of the pre-osteoblastic transcription factor, Osterix. Early osteoblasts then express the early osteogenic markers, such as Alkaline Phosphatase, before developing into mature osteoblasts. Mature functional osteoblasts express late osteogenic markers such as, Osteocalcin, Bone sialoprotein and Osteopontin (Beederman, M et al. 2013, whereas terminally differentiated osteocytes express Osteonectin and Sclerostin {Morinobu, 2003 #401; Morinobu et al. 2003) (Figure 1.2).

Most cranial sutures normally remain open and do not fuse until adulthood, with the exception of metopic suture which fuses by one year of age (Opperman 2000; Vu et al. 2001) (Idriz et al. 2015; Wilkinson et al. 2020) (Table 1.1). However, dysregulation of MPC growth or function within these sutures can cause cleft lip and palate, facial dysostosis, suture abnormalities and craniosynostosis as sutures fuse prematurely.

Table 1.1 The timing of calvarial suture fusion during human development.

Type of sutures	Time of fusion after birth
Metopic	3 months - 1 year
Sagittal	>18 years
Coronal	18 - 24 years
Lambdoid	>18 years

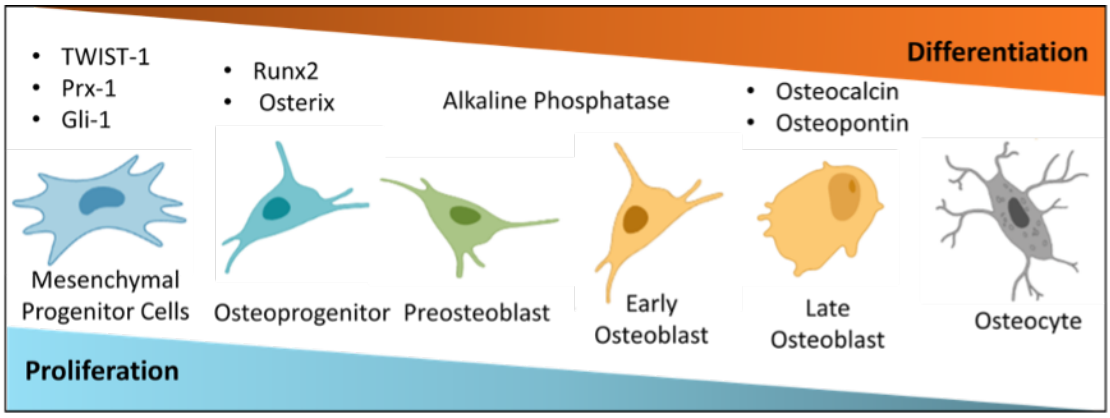
Differentiation
• TWIST-1
• Prx-1
• Gli-1
• Runx2
• Osterix
Alkaline Phosphatase
• Osteocalcin
• Osteopontin
Mesenchymal Progenitor Cells
Osteoprogenitor
Preosteoblast
Early Osteoblast
Late Osteoblast
Osteocyte
Proliferation

Figure 1.2. Diagram depicting the temporal expression of regulators involved during osteogenic differentiation of Mesenchymal Progenitor Cells. Image adapted from Beederman et al., 2013 (Beederman, M et al. 2013).

1.2 Premature fusion of calvaria sutures or Craniosynostosis

Craniosynostosis is a medical condition affecting 1 in 2,500 live births, where premature fusion of calvaria sutures occurs (Wilkie 2000). This condition could lead to unusual head shape, facial asymmetry and most importantly, increased pressure on the developing brain leading to neurological deficits (Knight et al. 2014). Currently, the only treatment option for craniosynostosis is invasive cranial surgery, involving the removal of the affected sutures and remodelling of the skull (Marchac & Renier 1990; Proctor 2012). These procedures have a major impact in the quality of life of children with craniosynostosis as it could lead to serious complications such as cerebral contusions, cerebrospinal fluid leaks, hematomas, infections and wound breakdowns and potentially death, often involving multiple operations (Han et al. 2016; Lee 2012). Thus, an attempt to identify a novel drug therapy that eliminates or limits the use of invasive surgery would be a major advancement in the management of children with craniosynostosis.

Craniosynostosis mostly exists as an isolated condition, in ~25% of all cases, craniosynostosis occurs as part of a syndrome (Wang, JC, Nagy & Demke 2016). There are a few different types of syndromic craniosynostosis, which are grouped based on their genetic mutation background and phenotypic characteristics (Table 1.2). The most common and severe type of syndromic craniosynostosis is Apert Syndrome, which is caused by missense mutations of the Fibroblast Growth Factor Receptor 2 (FGFR-2). Patients with Apert Syndrome develop craniosynostosis, midfacial hypoplasia and bony syndactyly on their fingers and toes (Wilkie et al. 1995). Point mutations in FGFR-2 and -3 could also lead to Crouzon and Pfeiffer Syndromes which exhibit similar facial abnormalities including ocular proptosis, where hand and feet anomalies characterise Pfeiffer Syndrome (Kreiborg & Cohen 2010; Lu et al. 2019; Rutland et al. 1995). The present thesis focuses on the second most prevalent forms of syndromic craniosynostosis, Saethre-Chotzen Syndrome (SCS)

which involves facial asymmetry, occasional cleft palate, droopy eyelid and mild limb deformities such as shortened, syndactyly and polydactyly fingers and toes in addition to unilateral and bilateral coronal craniosynostosis (Ahmed et al. 2017; Anderson et al. 1996; Gallagher, Ratisoontorn & Cunningham 1993)(Figure 1.3).

Table 1.2. The frequencies and the genetic mutation backgrounds of the most common types of syndromic craniosynostosis.

Syndrome	Frequency	Gene Mutation
Saethre-Chotzen	1/25000 – 50000	TWIST-1
Crouzon	1/50000 – 60000	FGFR-2 and FGFR-3
Apert	1/60000 – 100000	FGFR-2
Pfeiffer	1/100000	FGFR-2 and FGFR-3

There are more than 100 different mutations on *TWIST-1* gene that have been identified in SCS patients all resulting in loss-of-function mutation or haploinsufficiency of TWIST-1 gene (el Ghouzzi, VLM, M.; Perrin-Schmitt, F.; Lajeunie, E.; Benit, P.; Renier, D.; Bourgeois, P.; Bolcato-Bellemin, A. L.; Munnich, A.; Bonaventure, J. 1997). TWIST-1, a basic helix-loop-helix transcription factor, has been shown to mediate skeletal and head tissue development (Bildsoe et al. 2009). Its expression in MPC within the calvaria sutures is essential in maintaining proliferation activity of MPC and negatively regulating osteogenic differentiation (Cakouros, DI, S.; Cooper, L.; Zannettino, A.; Anderson, P.; Glackin, C.; Gronthos, S. 2012; Chen & Behringer 1995; Isenmann 2009). A study by Professor Gronthos and colleagues found that SCS-derived cranial cells displayed a reduced expression of *TWIST-1* and an increased capacity of forming mineral nodules under osteogenic-induced condition (Cakouros, DI, S.; Cooper, L.; Zannettino, A.; Anderson, P.; Glackin, C.; Gronthos, S. 2012). Furthermore, other groups have reported that mutation in

Figure 1.3. Frontal and Side photos and CT scans of 5-month-old Saethre-Chotzen Syndrome patient with bulging forehead (Provided by Prof Anderson, Women's and Children's Hospital, Adelaide). The arrows indicate fused coronal sutures on each side of the skull (bilateral), where the sagittal suture (SAG) remain open.

one copy or haploinsufficiency of *TWIST-1* in SCS-derived cranial cells leads to a decrease in proliferation ability and an increase in osteogenic differentiation, leading to premature fusion (Yousfi et al. 2001). Additionally, TWIST-1 has been shown to activate *GLI-1*, which is highly expressed in MPC within the suture mesenchyme (Di Pietro et al. 2020; Villavicencio et al. 2002). These studies suggest that TWIST-1 is a key regulator of cranial MPC proliferation and differentiation in SCS.

In mouse, *Twist-1*$^{del/+}$ heterozygous embryos survive post birth and show premature fusion of coronal sutures and limb abnormalities, similar to the characteristics of SCS patients. Additionally, studies have shown that *GLI-1*$^{+}$ MPC population is diminished in these mutant mice (Zhao 2015). Thus, *Twist-1*$^{del/+}$ heterozygous mouse is an excellent model to study human SCS (Carver 2002).

There are several recently proposed downstream molecular pathways targeted by TWIST-1 in MPC maintenance and differentiation to skeletal tissues. Previous studies have shown that TWIST-1 suppresses osteogenic differentiation by directly inhibiting *RUNX-2* expression (Bialek et al. 2004; Yang, DC et al. 2011); and by decreasing *Alkaline Phosphatase* and *Type I Collagen* expression (Yousfi et al. 2001). TWIST-1 has also been shown to repress chondrocyte formation by inhibiting BMP and TGF-β signalling pathways, which mediate osteogenic and chondrogenic differentiation (Dong et al. 2007; Reinhold et al. 2006). More recently, a study from Prof Gronthos laboratory identified the direct regulation by TWIST-1 of the bone promoting tyrosine kinase, C-ROS-1, during osteogenic differentiation of MPC, mediated by the PI3K/AKT/mTORC1 signalling (Camp, EA, P. J.; Zannettino, A. C.; Gronthos, S. 2017). Moreover, chemical inhibition of C-ROS-1 activity suppressed bone formation in calvarial explant cultures in the presence of BMP-2. TWIST-1 has also been shown to be involved in calvarial formation via direct regulation of TWIST-1 targets, Ddr2,

Pcolce and Tgfbi, during calvarial mesoderm development (Bildsoe et al. 2016), via TNF-α expression and caspase-2 activation in calvarial osteoblasts (Yousfi, Lasmoles & Marie 2002). Interestingly, FGFR-2, in which its mutation leads to several syndromic craniosynostosis, such as Apert and Crouzon Syndrome, has also been identified as a downstream target of TWIST-1 (Huang et al. 2014; Miraoui et al. 2010). This suggests that further investigations into the molecular mechanisms driving the development of SCS, could also reveal novel treatment targets for other types of syndromic craniosynostosis.

1.3 Epigenetics and Craniosynostosis

The fate determination of MPC either to stay as immature proliferating stem cells or to differentiate into different cell lineages is also dictated by epigenetic regulation (Ozkul & Galderisi 2016). Epigenetics is defined as changes in the chromatin structure and subsequent gene expression that results in heritable phenotypes, without altering the DNA sequence (Berger et al. 2009). The DNA strand is wrapped around a histone octamer allowing its compaction into the chromatin structure (Luger, Rechsteiner & Richmond 1999). Epigenetic modifications, placed on the DNA strands and the histone tails, are able to alter the chromatin compaction states between "open", allowing gene expression, and "closed", supressing gene expression.

The epigenetic landscapes on the promoters of master osteogenic regulatory genes are critical in determining the initiation or suppression of osteogenic differentiation pathways. One example is the enrichment of histone 3 acetylation (H3Ac) and histone 3 lysine 4 tri-methylation (H3K4me3) marks present on the RUNX2 promoter during osteogenesis via the activity of histone deacetylases, HDAC and MLL2/MLL3/COMPASS complex, respectively (Rojas et al. 2019). Additionally, reduction of the methyl group levels on the histone 3 lysine 27 position (H3K27) contributes to RUNX2 activation (Hemming, SC, D.;

Isenmann, S.; Cooper, L.; Menicanin, D.; Zannettino, A.; Gronthos, S. 2014; Rojas et al. 2015). On the other hand, removal of methyl groups on the H3K4 mark by histone demethylase, LSD1, inhibits osteogenic differentiation (Sun et al. 2018). Furthermore, Osterix activation is partly controlled by the balance between H3K4 methylation by methyltransferase, COMPASS complex, and H3K4 demethylation by demethylase, RBP2 (Ge et al. 2011). In addition to histone epigenetic modifications, DNA demethylation, catalysed by hydroxylases, TET1, and TET2, promotes ostoegenesis differentiation by binding to Runx2 and Osterix promoters (Cakouros, D & Gronthos 2020; Cakouros, D et al. 2019).

Studies of genetically identical twins, where only one of the twins had craniosynostosis, have confirmed that epigenetics plays a significant role in non-syndromic craniosynostosis (Lakin et al. 2012; Magge 2017). Furthermore, in the cases where both monozygotic twins exhibited craniosynostosis, discordant phenotypic features and variable severity levels were observed (Bin Alamer, Jimenez & Azad 2021; Farooq et al. 2020). One of the most studied epigenetic modifications is DNA methylation where methyl groups are placed onto the cytosine ring of a DNA strand (Moore, Le & Fan 2013). The levels of this epigenetic mark during maternal and paternal aging were recently associated with foetal abnormalities, including craniosynostosis (Markunas et al. 2016; Milekic et al. 2015). However, to date, there is little known regarding the epigenetic mechanism by which TWIST-1 mediates MPC differentiation in fusion progression of SCS.

1.4 Histone Demethylases, KDM6A and KDM6B roles in development and differentiation

Another epigenetic modification is the process of adding methyl groups to histone tails, called histone methylation. This process provides a unique platform to recruit methylation-reader proteins, leading to either gene activation or repression. For instance, the addition of three methyl groups to lysine 4 of histone 3 tail (H3K4me3) facilitates gene activation and in contrast, the addition of three methyl groups to lysine 27 of histone 3 tail (H3K27me3) marks gene repression (Cao et al. 2002; Sims, Nishioka & Reinberg 2003). The latter epigenetic mark is added by the methyltransferase molecule, Enhancer of Zeste Homolog 2 (EZH2), a member of the Polycomb Repressive Complex 2 (PRC2). EZH2 is essential in preserving the multipotency of hematopoietic, muscle and neural stem cells (Rao et al. 2015). Furthermore, EZH2 is involved in mediating tissue-specific differentiation, including facilitating adipogenic differentiation by adding the repressive marks on *Wnt1* gene promoters in mouse preadipocytes (Wang, Y et al. 2010), and inhibiting human MPC osteogenesis via the suppression of osteogenic genes, *RUNX2* and *Osteopontin* (Hemming, SC, D.; Isenmann, S.; Cooper, L.; Menicanin, D.; Zannettino, A.; Gronthos, S. 2014). H3K27me3 mark is reversed by histone demethylases, UTX/KDM6A and JMJD3/KDM6B, and thus, facilitate gene expression (Agger et al. 2007; De Santa et al. 2007; Hong 2007; Lan et al. 2007)(Figure 1.4). The enzymatic demethylase activity of these enzymes take place in their Jumonji C (JmjC) catalytic domain, through a dioxygenase reaction that requires Fe(II) and α-ketoglutarate as co-substrates (Kooistra & Helin 2012). Notably, KDM6A and KDM6B are associated with the MLL2 H3K4 methyltransferase complex which suggests that the removal of the repressive H3K27me3 mark works in collaboration with the addition of the activating H3K4me3 mark, allowing timely gene activation (De Santa et al. 2007; Issaeva et al. 2007).

Table 1.3 Key known epigenetic regulators of osteogenic differentiation (Cakouros, D & Gronthos 2020).

Epigenetic Enzymes	Epigenetic Marks	Target Gene
HDAC	H3Ac	RUNX2
MLL2/MLL3/COMPASS	H3K4me3	RUNX2
LSD1	H3K4me3 demethylation	RUNX2
RBP2	H3K4me3 demethylation	Osterix
TET1 & TET2	DNA demethylation	RUNX2 & Osterix
EZH2	H3K27me3	RUNX2 & Osteopontin
KDM6A & KDM6B	H3K27me3 demethylation	RUNX2, Osterix & Osteopontin

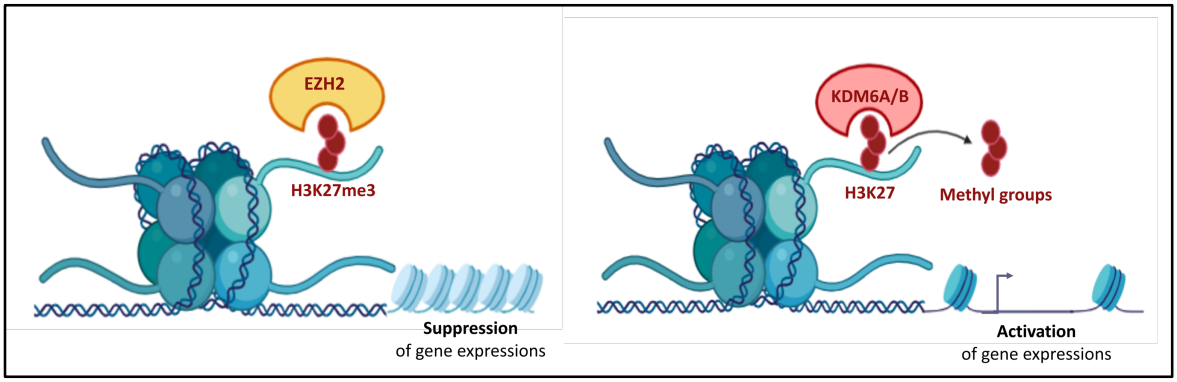
EZH2
H3K27me3
Suppression
of gene expressions
KDM6A/B
H3K27
Methyl groups
Activation
of gene expressions

Figure 1.4. Illustration of the addition and removal of three methyl groups on the lysine 27 histone 3 tail mark (H3K27me3) by histone methyltransferase, EZH2 and histone demethylases, KDM6A and KDM6B, respectively.

KDM6A is ubiquitously expressed and is located on the X-chromosome. However, it is one of the few genes that escapes chromosome X-inactivation. As a result, a higher expression of *Kdm6a* is noticed in female mouse embryonic stem cells and tissue, specifically in reproductive organs (Berletch et al. 2013), neurons and the brain (Xu et al. 2008), compared to male mice. In agreement to this, *Kdm6a*-null mouse embryos showed defects in neural crest formation and heart development, with the defects being more severe in female mice than in males. Furthermore, homozygous mutant females died before E12.5, where a subset of hemizygous males survive postnatally into adulthood, although runty (Shpargel et al. 2012; Welstead et al. 2012). This suggests that Uty/Kdm6c, a closely related paralog of Kdm6a located in the Y-chromosome, is able to compensate for the loss of Kdm6a in males. Notably, Kdm6c was considered as being enzymatically inactive (Shpargel et al. 2012), however, it was reported that it might harbor minimal demethylase activity (Walport et al. 2014). This indicates that there exists a demethylase-independent function of KDM6A. Evidently, KDM6A and KDM6B are involved in the general chromatin remodelling, independent to its demethylase activity by interacting with the SWI/SNF remodelling complexes (Miller, Mohn & Weinmann 2010). It has been previously revealed that in the absence of the demethylase activity of both Kdm6a and Kdm6b in mouse embryos, a decrease of global level of H3K27me3 was observed that leads to proper skeletal patterning and gene expression (Shpargel et al. 2014). This suggests an alternative function attributed to KDM6 subfamilies through bringing certain transcriptional complexes to the binding site, initiating gene expression, without an active demethylase function.

Since their discovery, histone demethylase involvement in embryonic development has been extensively studied. Both KDM6A and KDM6B have been shown to contribute to animal body patterning via regulation of homeobox (HOX) genes (Agger et al. 2007). These findings support studies of *Kdm6a* knockout mice and *Kdm6b* conditional knockout mice

which presented with skeletal growth retardation and were smaller in size compared to normal mice (Dai et al. 2017). Moreover, during embryonic development, KDM6A is essential in inducing appropriate ectoderm and mesoderm development upon appropriate developmental signals (Morales Torres, Laugesen & Helin 2013; Wang, C et al. 2012).

Other than their roles in development, KDM6 subfamily members are also involved in stem cell differentiation. During myogenesis, KDM6A has been reported to directly remove the repressive H3K27me3 on muscle-specific genes, allowing gene expression (Seenundun et al. 2010). During chondrogenic differentiation, inhibition of both KDM6A and KDM6B in bone marrow-derived MPC resulted in decreased expression of chondrogenic genes and reduced collagen synthesis (Yapp 2016). Additionally, a study on an inducible cartilage-specific *Kdm6b*-deficient mouse model showed defected cartilage development and accelerated osteoarthritis progression compared to control mice (Dai et al. 2017). During adipogenesis, the loss of KDM6A supresses the early formation of fat cells or adipocytes (Ota et al. 2017). Collectively, these studies showed that the KDM6 subfamilies promote myogenic, chondrogenic and adipogenic differentiation in MPC.

Previous studies have reported that the loss of *Kdm6b* resulted in a severe delay of osteogenic differentiation in mice, with *Kdm6b*-null mice displaying open calvarial sutures and less mineralised calvarial bones (Ye et al. 2012; Zhang, FX, L.; Xu, L.; Xu, Q.; Karsenty, G.; Chen, C. D. 2015); and lowered expression of *Runx2* and *Osterix*, where an increased level of the H3K27me3 mark was observed (Yang, D et al. 2013). Another study examining the role of Kdm6a in osteogenic differentiation showed that Kdm6a directly maintains the expression of *Runx2* and *Osterix* genes during early osteogenic differentiation in a murine osteogenic progenitor cell line (Ota et al. 2017). In primary bone marrow-derived MPC, enforced expression of *KDM6A* induced osteogenic differentiation, while overexpression of

EZH2 suppressed bone formation (Hemming, SC, D.; Isenmann, S.; Cooper, L.; Menicanin, D.; Zannettino, A.; Gronthos, S. 2014). Furthermore, conditional knockout of *EZH2* in the MPC of the skull and skeletal bones led to skeletal patterning defects and craniosynostosis (Hemming, S et al. 2017). Importantly, loss-of-function mutation of *KDM6A* have been previously identified to be associated with a congenital skeletal tissue disorder, called Kabuki Syndrome, with characteristics including malformed cranial bones (Miyake et al. 2013). Therefore, therapeutic targeting of *Kdm6a* expression or activity in a transient manner could potentially alleviate craniosynostosis phenotypes.

1.5 Significance

This PhD thesis examined the epigenetic modification, H3 lysine 27 trimethylation and associated demethylase, KDM6A/B in premature fusion of calvarial sutures or craniosynostosis, in order to help develop a potential non-surgical strategy for the treatment of Saethre-Chotzen Syndrome. Children with craniosynostosis are associated with asymmetrical skull and face formation and more importantly, are at risk for speech, language, behavioural and other developmental problems, if left untreated. Currently, there are two types of treatment for craniosynostosis. The main treatment is a major invasive surgery, which involves an open calvarial remodelling. This type of surgery might lead to serious complications such as cerebral contusions, cerebrospinal fluid leaks, hematomas, infections and wound breakdowns (Han et al. 2016; Lee 2012). Additionally, there is often a need for a follow up treatment with repeated surgery procedures and substantial hospitalisation, especially in severe cases of craniosynostosis (Hersh et al. 2017). The other treatment option is a less invasive alternative surgery where a small incision, assisted with an endoscope, is made to release the site of premature fusion. Following the endoscopic surgery, children are required to wear a customised helmet for 23 hours per day until 1 year of age. Although the complications of the alternative treatment are reduced compared to the

open skull surgery, they sometimes occurred. Furthermore, the alternative treatment is only available for children younger than 3 months old with non-severe cases of craniosynostosis. Thus, this treatment is only available to a small number of craniosynostosis patients, while still involving a surgical approach. Overall, these procedures can be physically and mentally traumatic for the affected children and their families. Additionally, the current use of surgical treatments has a significant financial impact on health providers. Despite the negative impacts on patients' wellbeing and health providers, a treatment which does not involve invasive surgery still does not exist. Thus, a novel drug therapy for craniosynostosis to inhibit or slow down the premature fusion of calvaria sutures could significantly minimise or possibly eliminate invasive approaches and improve the quality of life of children with SCS.

1.6 Hypothesis

TWIST-1 haploinsufficiency in SCS increases the levels of KDM6A expression or activity, which might, in part, lead to aberrant osteogenic differentiation of cranial bone cells, causing premature fusion of calvarial sutures.

1.7 Aims

Aim 1: Determine the level of H3K27me3, *Kdm6a*, *Kdm6b* and *Ezh2* gene transcript and protein expression during suture development and fusion of *Twist-1*$^{del/+}$ heterozygous mice and SCS patients.

Aim 2: Determine the effectiveness of pharmacological inhibitor of Kdm6a and Kdm6b, GSK-J4, in treating craniosynostosis in *Twist-1*$^{del/+}$ mice via local administration.

Aim 3: Determine the role of Kdm6a in suture fusion by generating *Kdm6a* conditional knockout mice in the mesenchyme lineage.

Chapter 2: Materials & Methods

2.1 Cell culture media

2.1.1 Human cell growth media

Alpha Modification of Eagle's Medium (αMEM, Cat# M4526-500mL, Sigma Aldrich, St. Louis, Missouri, United States), supplemented with 10% (v/v) Foetal Bovine/Calf Serum (FCS, Cat# AU-FBS/PG, CellSera, Rutherford, NSW, AUS), 1mM Sodium Pyruvate (Cat# S8636-100mL, Sigma Aldrich), 100μM L-ascorbate-2-phosphate (Cat#A8960-5G, Sigma Aldrich), 2mM L-Glutamine (Cat# G7513-100ml, Sigma Aldrich), and 50U/mL Penicillin, 50μg/mL Streptomycin (P/S, Cat# P4333-100mL, Sigma Aldrich) was sterilised by filtering through a sterile Nalgene® FastCap™ bottle-top filter unit with 0.2μm pore size (Sigma Aldrich) and stored in 4°C.

2.1.2 Human osteogenic inductive media

Human cell culture supplements: 5% (v/v) FCS (Cat# AU-FBS/PG, CellSera), 1mM Sodium Pyruvate (Cat# S8636-100ml, Sigma Aldrich), 100μM L-ascorbate-2-phosphate (Cat#A8960-5G, Sigma Aldrich), 2mM L-Glutamine (Cat# G7513-100ml, Sigma Aldrich), 10mM HEPES (Cat# H0887-100mL, Sigma Aldrich), 50U/mL Penicillin with 50μg/mL Streptomycin (P/S, Cat# P4333-100mL, Sigma Aldrich), and osteogenic-inducing additives: $1x10^{-7}$M dexamethasone phosphate (Cat# 163199, Royal Adelaide Hospital Pharmacy) and 1.8mM KH_2PO_4 (BDH Chemicals, Poole, UK) were added to αMEM (Cat# M4526-500mL, Sigma Aldrich). The media was filtered through a sterile 0.2μm bottle-top filter unit and stored in 4°C.

2.1.3 Mouse cell growth media

Mouse cell culture supplements: 20% (v/v) FCS (Cat# AU-FBS/PG, CellSera), 1mM Sodium Pyruvate (Cat# S8636-100mL, Sigma Aldrich), 2mM L-Glutamine (Cat# G7513-100ml, Sigma Aldrich) and 50U/mL Penicillin, 50µg/mL Streptomycin (P/S, Cat# P4333-100mL, Sigma Aldrich) were added to αMEM (Cat# M4526-500mL, Sigma Aldrich) and then filtered through a 0.2µm bottle-top filter (Sigma Aldrich).

2.1.4 Mouse osteogenic inductive media

Mouse osteogenic inductive supplements: 10% (v/v) foetal calf serum (Cat#AU-FBS/PG, CellSera), 100µg/mL L-ascorbate-2-phosphate (Cat#A8960-5G, Sigma Aldrich), 10mM β-glycerol phosphate (Cat#G9422-50g, Sigma Aldrich) , 2mM L-glutamine (Cat# G7513-100ml, Sigma Aldrich), 1mM sodium pyruvate (Cat# S8636-100ml, Sigma Aldrich), 10mM HEPES buffer (Cat#H0887-100mL, Sigma Aldrich), $1x10^{-8}$M dexamethasone (Cat# 163199, Royal Adelaide Hospital Pharmacy), 50 U/mL Penicillin and 50µg/mL Streptomycin (P/S, Cat# P4333-100mL, Sigma Aldrich) were added to αMEM (Cat#M4526-500mL, Sigma Aldrich). The media was filtered through a sterile 0.2µm bottle-top filter unit and stored in 4°C.

2.2 Isolation of human calvarial cells

Human calvarial cells were derived from the parietal bone chips from donors with informed consent in accordance with the Human Ethics Committee of the Women's and Children's Hospital, South Australia (Approval# REC1033/06/2019) (Table 2.2.1). Calvarial bone chips were washed three times in Hanks Buffered Saline Solution (Cat# H9394-500mL, Sigma Aldrich) to remove blood cells and minced into 1mm bone fragments. Approximately

10-12 bone fragments are cultured in a T25 tissue culture flasks in the presence of 5mL human cell growth media for 5 days at 37°C in a humidified environment supplemented with 5% CO_2. After this stage, adherent calvarial cells were harvested by enzymatic digestion with Collagenase I (3mg/mL; Cat# LS004196, Worthington Biochemical, NJ, USA) and Dispase (3mg/mL; Cat#17105-041-5g, Life Technologies, VIC, AUS) in 10mL of Hanks media for 1 hour and replated at $1x10^4$ cells per cm^2 until confluent before being used for experimental purposes.

Table 2.2.1. Details of SCS patients and control samples from the Women's and Children's Hospital

Code	Age	Twist-1 mutation	Tissue source
P0001	< 1 year	Compound homozygous mutation	Fused coronal suture
P0007	< 1 year	Heterozygous in-frame mutation	Fused coronal suture
P0005	< 1 year	Heterozygous missense mutation	Fused coronal suture
P0002	Adulthood	No mutation (control)	Fused coronal suture
P0014	< 1 year	No mutation (control)	Open coronal suture

2.3 Isolation of mouse calvarial cells

Mouse calvarial stromal cells were derived from the calvaria of 15-day-old *Twist-1*$^{del/+}$ heterozygous mice and wildtype mice; and from 15-day-old *Prx1*:cre;*Kdm6a*$^{fl/fl}$, *Prx1*:cre;*Kdm6a*$^{fl/y}$, and *Prx1*:cre control mice in accordance with the South Australia Health and Medical Institute (SAHMRI) Animal Ethics Committee approval #SAM262 and

#SAM347. Mouse calvaria was carefully cut out from the skull with surgical microscissors (Onyx Vanna Scissors, Able Scientific, SA, AUS), minced into 1mm fragments with surgical scalpel blades #22 (P&P Medical Surgical, Westchester, Illinois, United States) and digested in 2ml Digestion Solution: Collagenase I (3mg/mL) and DNAase I (50U/mL; Cat# 18068015, Life Technologies) in 1 x PBS (Phosphate Buffered Saline, Ca^{+}/Mg^{+}-free (Cat#D8537, Sigma-Aldrich)) for 2 x 40 min incubation periods at 37°C, with vigorous shaking by hand every 10 min. Between incubations, samples were centrifuges at 394*g* for 8 min, supernatant was removed and 2ml of new Digestion Solution was added for the second incubation. After the second incubation, samples were centrifuged as mentioned above. Bone fragments were plated in T25 tissue culture flasks and cultured in αMEM + mouse culture media additives at 37° in a humidified hypoxia incubator chamber with 5% O_2, supplemented with 5% CO_2. Cells were cultured to 80-90% confluence at which time; cells were disassociated with Collagenase I (3mg/mL) and Dispase (3mg/mL) solution, centrifuged at 394*g* for 5 min in 4°C, and cultured with a seeding density of $8x10^3$ cells/cm^2 for experiments or further expansion.

2.4 Generation of Kdm6a Conditional Knockout mice

The welfare of the animals was maintained in accordance with the South Australian Health and Medical Institute (SAHMRI) Animal Ethics Committee approval #SAM347. *Prx1*:cre-carrying mice were generated from an In-Vitro Fertilisation procedure utilising cryogenically-suspended sperm sample. *Kdm6a*-floxed mice were obtained from Jackson Laboratories, Bar Harbor, Maine, United States. Conditional *Kdm6a* knockout mice were achieved by crossing C57BL/6 heterozygous *Prx1*:cre mice with *Kdm6a*-floxed homozygous female or hemizygous male mice with a C57BL/6 background. All litters were genotyped by Polymerase Chain Reaction (PCR) using DNA extracted from ear or tail

biopsies. The biopsy samples were placed in 1.5mL Eppendorf tubes with 100µL of Chelex for 20min at 100°C on Eppendorf® Thermomixer Compact (Sigma-Aldrich) to initiate DNA extraction. The samples were then diluted in 400µL of UltraPure™ DNase/RNase-Free Distilled Water (Nuclease-free water; Cat#10977015, Invitrogen) and centrifuged at 13,793*g* for 10 min at room temperature (RT). For each PCR sample, 12µL of 2x KAPA, 0.5µL of 10µM forward and reverse primers for *Twist-1*, *Prx1* or *Kdm6a* (Table 2.4.1), 1µL of extracted DNA sample and 11µL of nuclease-free water are combined in 0.2mL Axygen™ PCR tubes and placed in Veriti™ 96-well Thermal Cycler (Thermo Fisher Scientific, Massachusetts, United States) with the following PCR conditions (Table 2.4.2). PCR samples are then loaded into 2% Agarose gel (Cat# 9010E, Scientifix, Clayton, Victoria, Australia) for *Twist-1* heterozygous mouse samples, 3% Agarose gel for *Prx1*:cre and *Kdm6a*-floxed mouse samples.

Table 2.4.1. Genotyping primers used in this study

Gene	Forward (5'-3')	Reverse (5'-3')
Twist-1	ccggatctatttgcattttaccatgggtca	cctctacctgaccgttagatggactcgg
Prx1	gcggtctggcagtaaaaactatc	gtgaaacagcattgctgtcactt
Kdm6a	ggtcacttcaacctcttattgga	acgagtgattggtctaatttgg

Table 2.4.2. PCR temperature cycling profile for each primer set.

Twist-1 Program

Temperature	Duration	
96°C	10 min	
96°C	30 sec	
64°C	30 sec	
72°C	1 min	x 35 cycles
72°C	5 min	

Prx-1:cre Program

Temperature	Duration	
94°C	5 min	
94°C	15 sec	
65°C	30 sec	
72°C	30 sec	x 35 cycles
72°C	5 min	

Kdm6a-floxed Program

Temperature	Duration	
95°C	3 min	
95°C	15 sec	
58°C	15 sec	
72°C	15 sec	x 35 cycles
72°C	1 min	

Prx1:cre control and *Prx1*:cre *Kdm6a*-floxed crossed experimental animals were sacrificed on postnatal (P) day P9, P15 and P25. The heads from culled animals were collected and the skin was carefully removed using surgical microscissors to reveal the skulls. The skulls were then fixed in 10% formalin (Thermo Fisher Scientific) for 72 hours, stored in 70% Ethanol and decalcified for 72hr with 14% EDTA (pH 7.2). Paraffin-embedded 7µm sections were cut on Epredia™ Rotary Microtome (HM 325, Fisher Scientific) and stained with Masson's trichrome and Movat's pentachrome staining (Table 2.4.3), completed by the Adelaide Medical School Histology Services.

Table 2.4.3 Brief histology solution and reagent lists

Masson's Trichrome

Reagents	Concentration
Biebrich Scarlet-Acid Fuchsin Solution	
Biebrich Scarlet	1%
Acid fuchsin	1%
Acetic Acid	1%
Phosphomolybdic-Phosphotungstic Acid Solution	
Phosphomolybdic acid	5%
Phosphotungstic acid	5%
Aniline Blue Solution	
Aniline Blue	2.5% (w/v)
Acetic Acid	1%

Movat's pentachrome (in addition to the above solutions)

Reagents	Concentration
Ferric Chloride Solution	2%
Sodium Thiosulfate Solution	5%
Acetic Acid Solution	3%

2.5 Osteogenic Differentiation Assays

Mouse calvarial cells were cultured in mouse osteogenic inductive media for 7 or 14 days, with media replaced twice weekly. GSK-J4 at 1μM and 2μM or 0.1% dimethyl sulfoxide (DMSO; Cat#DA013-2.5L-P, Chem Supply) in osteogenic-inductive media were refreshed every 24hr. Alkaline Phosphatase staining was performed on cells seeded at $8x10^3$ cells/cm^2 in 24-well plates using Leukocyte Alkaline Phosphatase kit (Cat# 86R-1KT, Sigma Aldrich), following manufacturer's protocols. Briefly, cells were fixed with Citrate-Acetone-Formaldehyde mixture, consisting of 25mL Citrate Solution (Cat#915-50mL, Sigma Aldrich), 65mL Acetone (Cat# AA008-2.5L-P, Chem Supply) and 8mL 37% Formaldehyde (Cat# FL010-10L-P, Chem Supply), at room temperature for 30 sec, rinsed in Reverse Osmosis (RO) water for 45 sec and incubated with the Alkaline-dye mixture for 15 min, protected from direct sunlight. The activity of Alkaline Phosphatase was quantitated in triplicate using StemTAG™ Alkaline Phosphatase assay kit (Cat# ab83369, Abcam Australia Pty Ltd, Victoria, Australia), following manufacturer's instructions. Briefly, cell lysates were incubated for 30 min at 37°C in the presence of StemTAG™ AP Activity Assay Substrate. The absorbance was read at 405nm on a microplate reader (iMark™ Microplate Absorbance Reader, BIO-RAD). The activity levels were then normalised to total protein level per well using Pierce BCA Protein Assay Kit (Cat# 23225, Thermo Fisher Scientific). Cell lysates were placed into 1.5ml Eppendorf test tubes and incubated for 30 min at 60°C

with BCA Working Reagent and the absorbance was read at 562nm on spectrophotometer (Genesys 10S UV-Vis, Thermo Fisher Scientific).

At 21 days, plated cells were gently washed three times in 1x PBS and fixed with 10% Neutral Buffered Formalin (Thermo Fisher Scientific). Bone mineral deposits were stained with 2% Alizarin Red S (Cat#A5533, Sigma Aldrich) in RO water. On a parallel plate, the wells were washed three times in 1x PBS and the mineralised matrix were dissolved in 0.6M HCl (Merk, Kilsyth, VIC, Australia) overnight at 4°C and transferred to 96 well plate. The extracellular calcium levels were measured, simultaneously with diluted Calcium Chloride standards, in triplicate wells using the Arsenazo III (Cat#C7529-500mL, MedTest DX, Michigan, United States) and the absorbance was read at 650nm on the microplate reader. The readings were then normalised to DNA content per well as previously described (Isenmann 2009). Following mineral dissolution, fixed cells were washed three times with 1x PBS and digested with 200µL of Proteinase K (100µg/mL) (Invitrogen, Mulgrave, Victoria, AUS) for 3 hours at 55°C. DNA concentration from 50µl of digested samples and diluted 100mg/ml DNA standards (5mg/mL, 2.5mg/mL, 1.25mg/mL, 0.625mg/mL, 0.312mg/mL and 0mg/mL) in 96-well plate were quantified using diluted Pico Green 1:300 in 1x TE Buffer from Quant-iT PicoGreen dsDNA Assay Kit (Cat# P11496, Invitrogen). The plate was then read on the VictorTM X4, PerkinElmer 2030 Multilabel Reader, under fluorescence settings with 485P excitation filter and 520P emission filter for 1 sec.

2.6 siRNA gene knock down studies

Mouse calvarial cells were seeded at $3x10^4$ cells per well in 24-well plate the day before siRNA transfections to achieve approximately 70% confluency. Sequence-specific siRNA against *Kdm6a* and *Kdm6b* or Silencer Select Negative siRNA#1 control (Life Technologies; Table 2.6.1) were transfected into the cells at concentration of 20pmol in siRNA

Transfection Medium (αMEM (Cat# M4526-500mL, Sigma Aldrich) with 10% FCS (Cat# AU-FBS/PG, CellSera)) together with 2µL Lipofectamine RNAiMAX reagent (Thermo-Fisher Scientific) and incubated for 20 min in room temperature prior to transfection. The transfection period was for 72 hours in hypoxic chamber to achieve at least a 50% knock-down of transcript levels before changing the media to osteogenic inductive media and performing osteogenic assays.

Table 2.6.1. siRNA used in this study (mouse)

siRNA	ID No.	Sense (5'-3')	Antisense (5'-3')
siKdm6a #1	s75838	cgcugcuacgaaucucuaatt	uuagagauucguagcagcgaa
siKdm6a #2	s75839	ggacuugcagcacgaauuatt	uaauucgugcugcaaguccag
siKdm6b #1	s103746	ccgugcagcuauacaugaatt	uucauguauagcugcacggtg
siKdm6b #2	s103747	cguccaauauuccuguuuatt	uaaacaggaauauuggacgca

2.7 GSK-J4 treatment

GSK-J4 (Cat# 12073, Cayman Chemical, Ann Arbor, MI, US) was reconstituted in 100% DMSO at a concentration of 50mM and stored at -80°C. Mouse calvarial cells were seeded at $4.2x10^4$ cells per well into 24-well plate. GSK-J4 at 0.1µM, 0.25µM, 0.5µM, 1µM, 2µM, 5µM, and 10µM or DMSO (0.1%) vehicle were added to the cells in the presence of either growth or osteogenic inductive media for 3, 7 or 14 days.

2.8 Gene expression studies

Total RNA from $0.5x\ 10^6$ cultured human and mouse calvarial cells was isolated using TRIzol reagent (Cat# 15596026, Thermo Fisher Scientific), according to manufacturer's

instructions. Briefly, cells cultured in 24-well plate were washed in 1x PBS and lysed in 500µL TRIzol solution for 5 min in room temperature. RNA was extracted using 100µL of Chloroform (Cat# CA038-2.5L, Chem Supply), vigorously shaken, and incubated for 2 min. Samples were then centrifuged at 12,000*g* for 15 minutes at 4°C and aqueous phase was transferred into a new 1.5mL Eppendorf tube. Total RNA was precipitated with 250µL isopropanol and 2µL RNase-free glycogen (20mg/mL; Cat#10901393001, Roche, Basel, Switzerland) overnight at -20°C and then centrifuged at the same settings as above. Pelleted RNA was washed with 75% (v/v) ethanol (Cat#EA043-2.5L-P, Chem Supply) and then resuspended and solubilised in 10µL nuclease-free water for 10 min at 55°C.

Total RNA concentration was measured with the absorbance of 260nm on a UV spectrophotometer (Nanodrop-8000, Thermo Fisher Scientific). The ratio of absorbance at 260nm and 280nm is used to detect the purity level of the samples, where a ratio of approximately 2.0 is considered as high purity. All RNA samples used in this study were in the range of 1.9-2.0.

Total RNA was then used as a template for reverse transcription into single-stranded cDNA using Superscript IV (Thermo Fisher Scientific), according to manufacturer's instructions. Briefly, 1µg total RNA, 1µL random hexanucleotide primers (100ng/mL), 1µL dNTP mix (10mM) and 1µL oligo(dT) (500ng/mL) are combined in a microcentrifuge tube, heated to 65°C for 5 min and incubated on ice for at least 1 min to allow effective primer annealing. The reverse transcription mix (4µL 5x first strand buffer, 1µL 0.1M DTT and 1µL Superscript IV (200U/mL)) is then added and incubated in room temperature for 10 min. DNA polymerization step is started by heating up the samples to 55°C for 10 min and ended with 80°C for 10 min to deactivate the enzyme, using Veriti^{TM} 96-well Thermal Cycler (Thermo Fisher Scientific). The cDNA samples were diluted in 1:5 with nuclease-free water and used for real-time Polymerase Chain Reaction (qPCR) immediately or stored in -20°C.

Real-time qPCR analyses were performed in triplicate using CFX Connect Real-Time PCR Detection System (Bio-Rad) following the cycling parameters stated in Table 2.8.1. Each reaction contained 7.5µL Sybr Green Mix (Cat# 330523, Qiagen, Hilden, Germany), 4.75µL nuclease-free water, and 0.75µL 10µM forward and reverse primer sets specific for target genes on Table 2.8.2 & 2.8.3.

Table 2.8.1. Real-time PCR temperature cycling profile.

Temperature	Duration	Objective
95°C	15 min	Enzyme activation
95°C	15 sec (cycling)	DNA denaturation
60°C	30 sec (48-52 cycles)	Primer annealing
72°C	10 sec	Primer extension
72°C	30 sec	Final extension

Table 2.8.2. Real-time PCR primers used in this thesis (Human) (GeneWorks Pty Ltd)

Gene	Forward (5'-3')	Reverse (5'-3')
β-ACTIN	gatcattgctcctcctgagc	gtcatagtccgcctagaagcat
KDM6A	gagggaagctctcattgctg	agatgaggcggatggtaatg
KDM6B	caccccagcaaaccatattatgc	cacacagccatgcagggatt
EZH2	actgctggcaccgtctgatg	cctgagaaataatctccccacag

Table 2.8.3. Real-time PCR primers used in this thesis (Mouse) (GeneWorks Pty Ltd)

Gene	Forward (5'-3')	Reverse (5'-3')
β-Actin	ttgctgacaggatgcagaag	aagggtgtaaaacggagctc
Kdm6a	ggctactggggtgttttgaa	tccaggtcgctgaataaacc

Kdm6b	cccccatttcagctgactaa	ctggaccaaggggtgtgtt
Ezh2	actgtcggcaccgtctgatg	tcctgagaaataatctccccacag
Twist-1	cagcgggtcatggctaac	tcctgagaaataatctccccacag
Runx2	cctctgacttctgcctctgg	tatggagtgctgctggtctg
Osterix	tcctcggttctctccatctg	tgcaggagagaggagtccat
Alkaline Phosphatase	gccttaccaactcttttgtgc	ggctacattggtgttgagctt

2.9 Cell proliferation assay

Mouse calvarial cells were cultured at $9x10^3$ cells/well in 96-well plates in the presence of DMSO (0.1%) or a range of GSK-J4 concentrations (0.1µM, 0.25µM, 0.5µM, 1µM, 2µM, 5µM, and 10µM) in 200µL growth inductive media for 7 days. The rate of cell proliferation was measured using cell proliferation ELISA, bromodeoxyuridine (BrdU) colorimetric kit (Cat# 11647229001, Roche Products Pty Limited, Sydney, NSW, AU), following manufacturer's directions. Briefly, the cells were incubated with 20µL/well of BrdU labelling solution for approximately 20 hours at 37°C. The labelling medium was then replaced by 200µL FixDenat solution for 30 min at RT. Fixed cells were incubated with 100µL/well Anti-BrdU-POD working solution for 90 min at RT. Colorimetric reaction was initiated by 100µL/well Substrate Solution until sufficient photometric detection is reached for approximately 20 min. The reaction was then stopped using 25µL 1M Sulphuric Acid (H_2SO_4) and the absorbance was detected at 450nm on an iMark microplate reader (Bio-Rad Laboratories, Hercules, CA, US).

2.10 Cell viability assay

Mouse calvarial cells were seeded at $2.6x10^5$ cells/well into 6-well plates in growth inductive media and in the presence of 0.1% DMSO or GSK-J4 concentration range (0.1μM-10μM) for 7 days. The rate of apoptosis was measured using Annexin V and 7AAD staining procedure. Growth media, containing dead suspended cells, was collected into cold 5mL polypropylene FACS tube and adherent cells were trypsinised, resuspended in 2mL/plate of fresh growth media and transferred into the same FACS tube. For positive controls, apoptosis and necrosis were induced by adding 100% DMSO overnight and 70% Ethanol for 5 min, respectively. FACS tubes were centrifuged at 570*g* for 2 min. Supernatant was removed and cell pellets were washed with cold PBS twice. Prior to reading, cells were resuspended in 100μL Annexin V Buffer (10mM HEPES, 140mM NaCL and 2.5mM $CaCl_2$) and 5μL of Annexin V-488 (25 mM HEPES, 140 mM NaCl, 1 mM EDTA, pH 7.4, 0.1% bovine serum albumin (BSA)) (Cat# A13202, Invitrogen/Thermo Fisher Scientific) and 20μL of 7-amino-actinomycin (7AAD; Cat# A1310, Invitrogen/Thermo Fisher Scientific) were added to ~$1x10^6$ cells. Samples were analysed immediately on LSRForessa X20 Analyzer (BD Biosciences, North Ryde, NSW, AUS).

2.11 Calvarial organ explant cultures

The calvaria of humanely culled 4-day-old *Twist-1*$^{del/+}$ mice were extracted, as previously described (Garrett 2003; Marino et al. 2016; Mohammad, Chirgwin & Guise 2008). Briefly, the scalps were removed using sterile surgical microscissors to expose the calvaria. Initial incision was created at the posterior side of the calvaria and moved towards the anterior side, avoiding the eye sockets. The whole calvaria was gently removed from the rest of the skull and washed in PBS with 10% FCS to remove the adherent connective tissue. The calvaria was then cut along the median sagittal suture to create two equal halves.

Each calvarial organ explants were placed onto stainless steel mesh, which were prepared using 0.8x1cm stainless steel sheets bent to form a bridge-like structure, in the presence of BjGb media (Fitton-Jackson Modification with L-Glutamine; Cat# B1091, US Biological, MA, US) with recombinant human bone morphogenic protein 2 (rhBMP2; 50 ng/mL, Cat# PHC7145, Thermo Fisher Scientific) and GSK-J4 at 1μM or GSK-J4 at 2μM or vehicle control (0.1% DMSO) for 10 days. Calvarial explants were then fixed in 10% formalin for 6 hours, decalcified overnight with 14% EDTA (pH 7.2), and embedded in paraffin. Sections (7μm) were stained with Masson's trichrome staining. The formation of mineralised bone shown in blue staining relative to the length of calvarial bone specimen was measured using OsteoMeasure XP Advanced Bone Histomorphometry ver.1.0.3.1 software (OsteoMetrics, Inc., Decatur, GA, US) on an Olympus BX53Microscope (Olympus, Notting Hill, VIC, Australia).

2.12 *In vivo* administration of GSK-J4 to calvaria of *Twist-1*$^{del/+}$ mice

Anaesthetic procedure using Isoflurane machine (Stinger Streamline Rodent Gas Machine; Cat#9356X, DarvallVet, NSW, AUS) with 3.5% Isoflurane and 1.0 flow rate was administered to 8-days-old *Twist-1*$^{del/+}$ mice through rodent facemasks. A 3mm incision was created at the posterior midline site of mouse heads using sterile surgical microscissors. Two 3mm^3 CollaCote sponges (Cat# 0101, Integra Life Sciences Services, Saint Priest, FRA) soaked in 0.1% DMSO as vehicle control or in GSK-J4 in the concentration of 2μM was inserted subcutaneously onto each side of the coronal sutures through the initial incision. At 20 days of age, *Twist-1*$^{del/+}$ mice were humanely culled in the accordance with SAHMRI Animal Ethics Approval (Ethics# SAM262). The harvested calvaria of treated mice fixed in 10% formalin were analysed using Masson's trichrome staining. Mineralised calvarial bone

formation relative to the length of bone analysed was quantitated on Olympus BX53 Upright Microscope (Olympus Corporation, Tokyo, Japan) using OsteoMeasure software (OsteoMetrics, Inc. Georgia, USA).

2.13 Immunohistochemical analyses

Calvaria were isolated from 10-day-old *Twist-1*$^{del/+}$ and wildtype mice, and then fixed in 10% formalin for 24 hours, decalcified with 14% EDTA (pH 7.2) overnight, and embedded in paraffin. The samples were cut transversely with thickness of 5µm and dewaxed to expose the calvarial tissue. The sections were incubated in 0.5% hydrogen peroxide (H2O2; Cat# MERC1.07209.0500, BioStrategy, Tullamarine, VIC, AUS) in methanol (Cat#MA004-2.5L-P, Chem Supply) at RT for 30 min to block endogenous peroxidase. After 2x5 min washes in PBS, sections were placed in 10mM sodium citrate (pH 6.0) and brought to boiling temperature of 98°C for 10 min using optimised domestic microwave in order to expose the antigenic sites. The sections were then blocked with 3% Normal Horse Serum (NHS) (Cat#LS-M3-20, Lifespan Bioscience, Washington, USA) prior to incubating with the primary antibody overnight at RT and washed in PBS 2x5 min. The primary antibody used was an anti-mouse H3K27me3 rabbit polyclonal antibody (Cat# 07-449, Millipore, Bayswater, VIC, AU), diluted 1:1600 in 3% NHS. Rabbit IgG (Cat# I5006, Sigma–Aldrich) replaced the primary antibody as negative control, which showed no immunoreactivity. The samples were then incubated with the secondary antibody (4µL/mL; anti-rabbit) for 30 min, washed with PBS 2x5 min, and incubated with Pierce^{TM} streptavidin horseradish peroxidase-conjugated antibodies (2µL/mL; Cat# 21130, Thermo Fisher Scientific) for 15 min at RT. Peroxidase substrate solution (13mL 0.2N HCl, 13mL 0.2M Tris (Cat# T-1378, Sigma Aldrich), 50µL 30% hydrogen peroxide and 300µL Diamino Benzidine (DAB, Cat# D-5637, Sigma Aldrich) in distilled water to a total volume of 50mL) was then applied for

approximately 7 min to achieve optimum staining reaction. Stained sections were then counterstained with Mayer's Haematoxylin (Cat#MHS32, Sigma Aldrich), and dehydrated and mounted using CV Ultra Mounting Media (Leica Biosystems, Wetzlar, Germany). The percentage of H3K27me3-positive nuclei (brown) to total number of nuclei within the white box was quantitated using Image J software (National Institutes of Health, Washington, USA).

2.14 Western blot analyses

Mouse calvarial cells were cultured at $8x10^3$ cells/cm^2 in T75 flask until confluent and then treated with GSK-J4 concentration range or 0.1% DMSO as vehicle control for 24 hours. Histone extraction protocol was adapted from Abcam (Abcam, Melbourne, VIC, AU). Briefly, $5x10^6$ cells were re-suspended in 1 ml of Triton Extraction Buffer (0.5% Triton X 100 (v/v), 2mM Phenylmethylsulfonyl Fluoride (PMSF), 0.02% NaN_3 (w/v)). The nuclei lysates were incubated on ice for 10 min with gentle stirring and centrifuged for 10 min at 6,500*g* at 4°C. Histone acid extraction was performed using 0.2M HCl at a density of $2x10^7$ nuclei/mL overnight at 4°C. Histone protein was collected in the supernatant following centrifuge spin for 10 min at 6,500*g* at 4°C, and neutralised with 2M NaOH at 1/10 of supernatant volume. Protein concentrations were measured using the Pierce Detergent Compatible Bradford Assay Kit (Cat# 1863028, Thermo Fisher Scientific) and analysed against a standard curve from serial dilutions of bovine serum albumin (2mg/ml stock). Equivalent amounts of protein were diluted with 5x Reducing Loading Buffer (50mM Tris, 1.6% SDS, 0.08% (w/v) Bromophenol Blue and 1.6% β-mercaptoethanol) and incubated for 5 min at 100°C. The samples were then loaded onto SDS-PAGE gels for Western blot analyses.

To prepare for the SDS-PAGE gel, spacer glass plate (1.5mm; Cat# 1653312, Bio-Rad) and short glass plate (Cat# 1653308, Bio-Rad) were assembled in Mini-PROTEAN® casting frame (Cat# 1653304, Bio-Rad). 10mL of 13.5% acrylamide separating gel and 5mL of stacking gel were prepared as described in Table 2.14.1. Separating gel was poured in between the glass plates up to 2cm below the top of the short plate and was allowed to set before the stacking gel was poured and a 15-well comb (Cat# 4560016, Bio-Rad) were inserted. Two sets of plates were then placed into the Mini-PROTEAN® Tetra Electrode Assembly (Cat# 1658037, Bio-Rad) to create a sealed chamber. The assembly was placed into a Mini-PROTEAN® Tetra Vertical Electrophoresis Cell (Cat# 1658005, Bio-Rad) and the inside chamber was half-filled with 1x SDS Running Buffer (0.3% (w/v) Tris-HCl, 1.44% (w/v) glycine and 0.1% (w/v) SDS). The comb was removed prior to loading the prepared protein samples and 5µL of Dual Precision Plus Ladder (Cat #1610374, Bio-Rad). The samples were run through the stacking gel at 15mA/gel and were then resolved through the separating gel at 30mA/gel, until the loading buffer dye reaches the end of the gel.

The resolved protein was then transferred to Polyvinylidene Difluoride (PVDF) membrane (Hybond-P membrane, Amersham Biosciences, GE Healthcare, Little Chalfont, UK), which was pre-equilibrated in 100% methanol for 5 min. The membrane, Foam Pads (Cat# 1703933, Bio-Rad), and filter papers were soaked in Transfer Buffer (12.104g of Tris and 57.66g of Glycine in 3L RO water with 0.6L methanol). The electrophoresis transfer system (Mini Trans-Blot® Cell, Bio-Rad) was assembled in a gel holder cassette, following manufacturer's instructions. The assembled cassette and a cooling unit were placed into the Mini Trans-Blot Electrophoretic Transfer Cell (Cat# 1703930, Bio-Rad) filled with Transfer Buffer. The protein transfer was then performed for 1 hour at 100 volts in 4°C.

Tris-buffered Saline (TBS) was prepared by dissolving 24.3g Tris and 80g sodium chloride in 1L RO water (pH 7.6). TBS buffer (100mL) was diluted in 899mL RO water with 1mL Tween 20 (Cat#P1379-500mL, Sigma Aldrich) to produce TBS-T buffer.

The PVDF membrane was then carefully removed from the gel holder cassette, equilibrated with TBS-T buffer, and blocked with 5% fat-free skim milk (Cat# 7910660P, Coles, AUS) as blocking solution and probed overnight at 4°C with an anti-mouse H3K27me3 rabbit polyclonal antibody (Cat# 07-449, Millipore Corporation, North Ryde, NSW, AU) and a rabbit anti-H4 antibody (Cat#ab10158, Abcam), both at 1:1,000 dilution in 5mL blocking solution. Following two washes with TBS/0.1% Tween 20, the blots were incubated for 1 hour in room temperature with fluorescence secondary antibody (anti-rabbit 800nm or 680nm, Li-Cor Biosciences, VIC, AUS), in 1:20,000 dilution with TBS-T Buffer. Blots were washed two more times and then scanned on Odyssey CLX Near-Infrared Fluorescence Imaging System (Li-Cor Biosciences). Analyses and measurements were performed on Image Studio Lite software (Li-cor Biosciences).

Table 2.14.1. Separating and Stacking Gel

Separator Gel	Volume	Supplier
40% acrylamide	3.4mL	Bio-Rad
2% bis-acrylamide	1.813mL	Bio-Rad
1.5M Tris-HCl pH 8.8	2.5mL	ChemSupply
Milli-Q water	2.127mL	Merck Millipore
10% SDS	100µL	Sigma Aldrich
10% APS	50µL (Immediately before use)	Sigma Aldrich
TEMED	10µL (Immediately before use)	Sigma Aldrich

Stacking Gel	Volume	Supplier
40% acrylamide	0.62mL	Bio-Rad
2% bis-acrylamide	0.33mL	Bio-Rad
0.5M Tris-HCl pH 6.8	1.26mL	ChemSupply
Milli-Q water	2.71mL	Merck Millipore
10% SDS	50µL	Sigma Aldrich
10% APS	25µL (Immediately before use)	Sigma Aldrich
TEMED	5µL (Immediately before use)	Sigma Aldrich

2.15 Chromatin Immunoprecipitation (ChIP) Analyses

Mouse calvarial cells were seeded at density of $8x10^3$ cells/cm^2 in T75 flasks. Once the cells were confluent, the cells were cultured in growth or osteogenic-inductive media in the presence of GSK-J4 at 1µM or vehicle control (0.1% DMSO) for 24hr. ChIP protocol was adapted from Abcam (www.abcam.com/protocols). Chromatin was cross-linked with a final of 0.75% formaldehyde for 10 min at room temperature with gentle rocking on a platform mixer (Ratek Laboratory Equipment, Victoria, Australia). Glycine (Cat# GA007-500G, Chem Supply, Gillman, SA, Australia) at a final concentration of 125mM was added and incubated whilst rocking for 5 min. The media is then removed, and the adherent cells were washed with ice cold PBS. Cross-linked cells were detached using 1x trypsin, and the remaining cells were scraped. Cells were lysed with the lysis buffer (50mM HEPES KOH pH7.5, 140mM NaCl, 1mM EDTA pH8, 1% Triton X-100, 0.1% Sodium deoxycholate, 0.1% SDS, and 1x protease inhibitors (Sigma Aldrich; one complete EDTA-free Protease Inhibitor cocktail tablet diluted in 5.6mL RO water)) at 400µl per 1 million cells. DNA was

sheared into 200-500bp in length with a probe sonicator (Diagenode Bioruptor Inc, Denville, NJ, US) at 3 watts for 30 seconds on ice.

Prior to processing the samples for immunoprecipitation, 10µL of sample was transferred to a new Eppendorf tube to be used as a genomic input control and stored in -20°C. The sample volume was then halved into a new tube to be used as the IgG isotope control. Both the IgG control and experimental samples are diluted in RIPA buffer (50mM Tris-HCl pH 8, 150mM NaCl, 2mM EDTA pH 8, 1% NP40, 0.5% Sodium Deoxycholate, 0.1% SDS, 1x Protease Inhibitor) to make up 1mL in total volume. Pre-clean step was performed on the samples using 20µL ChIP-Grade Protein G-conjugated magnetic beads (Cat# 9006S, Cell Signalling, Massachusetts, USA) for 2 hours at 4°C, gently mixed on a tube rotator. The magnetic beads with non-specific protein complex were separated using a magnetic rack and the supernatant was transferred into new tubes. Anti-mouse H3K27me3 rabbit polyclonal (1µg; Cat# 07-449, Millipore) and IgG rabbit polyclonal control (1µg; Cat#12-370, Millipore) were added to respective samples and incubated overnight at 4°C on a tube rotator. Magnetic beads (20µL) were then gently mixed with the samples for 2 hours at 4°C to bind with the antibody and chromatin complex. The magnetic bead, antibody and chromatin complex were separated, and the supernatant was removed. The beads were washed three times in 1mL Low Salt Immune Complex Wash Buffer (0.1% SDS, 1% Triton X-100, 2mM EDTA pH8, 150mM NaCL, 20mM Tris-HCl pH 8) and two times in 1mL High Salt Immune Complex Wash Buffer (0.1% SDS, 1% Triton X-100, 2mM EDTA pH8, 500mM NaCL, 20mM Tris-HCl pH8). The DNA were then eluted from the complex by adding 120µL Elution Buffer (1% SDS and 100mM $NaHCO_3$) and 1µL of Proteinase K at 65°C for 4 hours on Eppendorf® Thermomixer Compact (Sigma-Aldrich) with 800rpm setting. The supernatant containing DNA was separated from the magnetic beads and transferred into new tubes. DNA samples were purified using QIAquick® PCR Purification Kit (Cat# 28104, Qiagen) according to

manufacturer's instructions. Purified DNA samples were then used in qPCR. Transcription start site (TSS) primer sets (GeneWorks Pty Ltd) used in this study: mouse *Runx2* TSS (Fwd: 5'-aggccttaccacaagccttt-3'; Rev: 5'-gtgggactgcctaccactgt-3'), mouse *Alkaline Phosphatase* TSS (Fwd: 5'-agggaaagagagaggcaagg-3', Rev: 5'-ttccttacctgcaggcactc-3').

2.16 Micro-Computed Tomography Analyses

High-resolution three-dimensional (3D) images of 25-days-old control and experimental mouse skulls were analysed using micro-computed tomography (Micro-CT; Skyscan 1076 X-ray Micro-CT, Bruker MicroCT, Kontich, Belgium). Skulls were scanned at 8.5µm resolution, 800ms exposure, 4K pixelation, 80kV voltage, 200µA current, 0.2 rotation step, and 2-frame averaging with AI 0.5mm filter for P9 and P15 and AI 1mm filter for P25. Reconstruction of the Micro-CT scans was conducted on NRecon Reconstruction (64-bit, ver.1.6.10, Bruker MicroCT) with a smoothing of 2, ring artefact reduction of 8 and beam hardening correction of 30%. Reconstructed images were realigned in Data Viewer (64-bit, ver. 1.5.2., Bruker MicroCT). Region of Interest (ROI) of the Coronal and Posterior Interfrontal (PIF) suture were selected from the realigned data and evaluated in a Comprehensive Tex Archive Network CT-analyzer (CTan, ver.1.15, Bruker MicroCT) using optimised 3D morphometric parameters. A surface rendered 3D model was constructed from the ROI in CTVol and viewed in CTVox (ver.2.3, Bruker MicroCT).

2.17 Statistics

The sample size of 3 for in vitro experiments and 5 for ex vivo and in vivo experiments for each sex were determined based on previous SD values to achieve 30% or greater difference with 80% power (Arthur et al. 2013; Hemming, SC, D.; Codrington, J.; Vandyke, K.; Arthur, A.; Zannettino, A.; Gronthos, S. 2017; Nguyen et al. 2016). Calculation of statistical significance was carried out using GraphPad PRISM 8 (GraphPad Software, La Jolla, CA,

RRID: CR_002798, http://www.graphpad.com/). The software was also used for the generation of graphs which showed statistical differences (*) of $p \leq 0.05$ between samples, based on Student's t-test and One-way ANOVA statistical tests as indicated.

Chapter 3: Identification of Histone Demethylases, Kdm6a and Kdm6b, as Novel Targets for Treating Aberrant Osteogenic Differentiation in Saethre-Chotzen Syndrome Mouse Model

3.1 Introduction

Calvarial sutures are comprised of active mesenchyme forming the osteogenic fronts at the edges of the flat calvarial bones (Doro, Grigoriadis & Liu 2017; Lenton et al. 2005). The active mesenchyme contains a *TWIST-1*$^{+}$/*GLI-1*$^{+}$/*PRX-1*$^{+}$ MPC population which has the potential for osteogenic differentiation (Connerney et al. 2006; Johnson et al. 2000; Rice et al. 2000; Yoshida et al. 2005; Zhao 2015). *TWIST-1* expression in suture mesenchyme maintains MPC proliferative characteristics, and suppresses osteogenic differentiation by directly inhibiting major osteogenic genes (Bildsoe et al. 2016; Isenmann 2009; Katsianou et al. 2016; Yang, DC et al. 2011; Yousfi et al. 2001). Furthermore, previous studies found that *Twist-1* expression is required for correct establishment of the coronal sutures in mice, where trisomy of the *Twist-1* locus preserved open calvarial sutures (Bildsoe et al. 2009; Yoshida et al. 2005). On the other hand, haploinsufficiency of the *TWIST-1* gene in humans, results in a rare clinical condition called Saethre-Chotzen Syndrome (SCS). Calvarial cells derived from SCS patients exhibit a decreased proliferation rate and an increased osteogenic differentiation, leading to premature suture fusion or craniosynostosis (Cakouros, DI, S.; Cooper, L.; Zannettino, A.; Anderson, P.; Glackin, C.; Gronthos, S. 2012; Camp, E et al. 2018; Yousfi et al. 2001). Craniosynostosis patients are divided into two main types: non-syndromic craniosynostosis, which are non-inherited isolated incidents and syndromic craniosynostosis, which are driven by underlying genetic mutations, such as *TWIST-1* mutation in SCS.

Recently, it has been revealed that epigenetic mechanisms play a significant role in non-syndromic craniosynostosis where studies of genetically identical twins reported that one twin displayed craniosynostosis, whereas the other displayed normal skull development (Lakin et al. 2012; Magge 2017). However, until now, no study has examined the role of epigenetics in syndromic craniosynostosis.

TWIST-1 expression and function has been correlated with the epigenetic regulator EZH2 in mediating SCS cranial bone cell growth and differentiation (Cakouros, DI, S.; Cooper, L.; Zannettino, A.; Anderson, P.; Glackin, C.; Gronthos, S. 2012), where *Ezh2* knockdown in the mesenchymal lineage leads to craniosynostosis and other skeletal deformities (Hemming, S et al. 2017). EZH2 is a member of the Polycomb Repressive Complex 2 (PRC2) and acts as a methyltransferase which tri-methylates lysine 27 of the histone 3 tail (H3K27me3), to repress gene activation (Sims, Nishioka & Reinberg 2003). The counter demethylases, KDM6A and KDM6B, remove the tri-methylation mark on H3K27me3 to promote gene activation (Agger et al. 2007; De Santa et al. 2007; Hong 2007; Lan et al. 2007). The enzymatic demethylase activity of these epigenetic modifiers is carried out by their Jumonji C catalytic domain (Kooistra & Helin 2012). Previous studies have reported that KDM6A and KDM6B promote osteogenic differentiation of MPC (Hemming, SC, D.; Isenmann, S.; Cooper, L.; Menicanin, D.; Zannettino, A.; Gronthos, S. 2014; Ota et al. 2017), whereas EZH2 represses bone gene activation and MPC osteogenic differentiation (Hemming, SC, D.; Isenmann, S.; Cooper, L.; Menicanin, D.; Zannettino, A.; Gronthos, S. 2014). Additionally, loss-of-function mutation of KDM6A has been previously identified to be associated with a congenital skeletal tissue disorder, called Kabuki Syndrome (Miyake et al. 2013; Shpargel et al. 2017; Van der Meulen 2014). Infants with this syndrome are manifested with unconventional facial appearance, growth retardation, and skeletal defects, including abnormal fingers, joints, spine and malformed cranial (Faundes et al. 2021). These observations provide further affirmation of the importance of KDM6A in skeletal development. Similarly, loss of *Kdm6b* results in a severe delay of osteogenic differentiation in mice (Ye et al. 2012; Zhang, FX, L.; Xu, L.; Xu, Q.; Karsenty, G.; Chen, C. D. 2015) and lowered expression of *Runx2* and *Osterix*, as a result of increased levels of H3K27me3 (Yang, D et al. 2013). These observations provide affirmation that both KDM6A and B play important roles in promoting osteogenic differentiation of MPC.

To examine epigenetic changes in SCS, *Twist-1* heterozygous mutant mice (*Twist-1*$^{del/+}$) were utilised, which display craniofacial defects including unilateral or bilateral coronal synostosis and limb abnormalities similar to the characteristic abnormalities described for SCS human patients (Carver 2002). The present study investigated the expression levels and role of histone demethylases, *Kdm6a* and *Kdm6b*, in the osteogenic potential of calvarial cells and calvarial explants derived from *Twist-1*$^{del/+}$ mice.

3.2 Results

3.2.1 Calvarial cells of SCS patients exhibit upregulated level of *KDM6A* and *KDM6B* gene expression.

The expression of *TWIST-1* and histone demethylases, *KDM6A* and *KDM6B* in SCS patients were observed by extracting stromal cells from calvarial bone chips derived from SCS patients. Following induction in osteogenic conditions, lowered expression of TWIST-1 was confirmed and upregulated levels of both *KDM6A* and *KDM6B* were observed in SCS calvarial cells using real-time qPCR analyses, compared with calvarial cells from healthy calvaria (Figure 3.2.1A-C). Furthermore, human SCS calvarial cells displayed a significant increase in the levels of mineralised deposits. On the other hand, forced overexpression of *TWIST-1* in human calvarial cells significantly supressed the expression levels of *KDM6A* and *KDM6B* and mineral formation capacity (Figure 3.2.2A-D).

3.2.2 *Twist-1*$^{del/+}$ calvarial cells exhibit increased expression and upregulated enzymatic activity of Kdm6a and Kdm6b.

Calvarial cells derived from 15-day-old *Twist-1*$^{del/+}$ heterozygous mice (SCS mouse model), cultured under osteogenic inductive conditions were found to express reduced transcript levels of *Twist-1* and *Ezh2*, whereas gene expression levels of *Kdm6a*, *Kdm6b*, and the early (*Runx2*) and late (*Alkaline Phosphatase*) bone associated markers and mineral formation level were upregulated, compared to wild type calvarial cells (Figure 3.2.3-4). Western blot analyses to detect protein levels of Kdm6a and Kdm6b were attempted; however, no bands were detected, which could potentially be caused by low antibody sensitivity levels (Figure 3.2.4G). However, immunohistochemical analyses demonstrated a decrease in H3K27me3-positive cells within the coronal suture mesenchyme of day 8 (pre-fusion) *Twist-1*$^{del/+}$ mice (Figure 3.2.5).

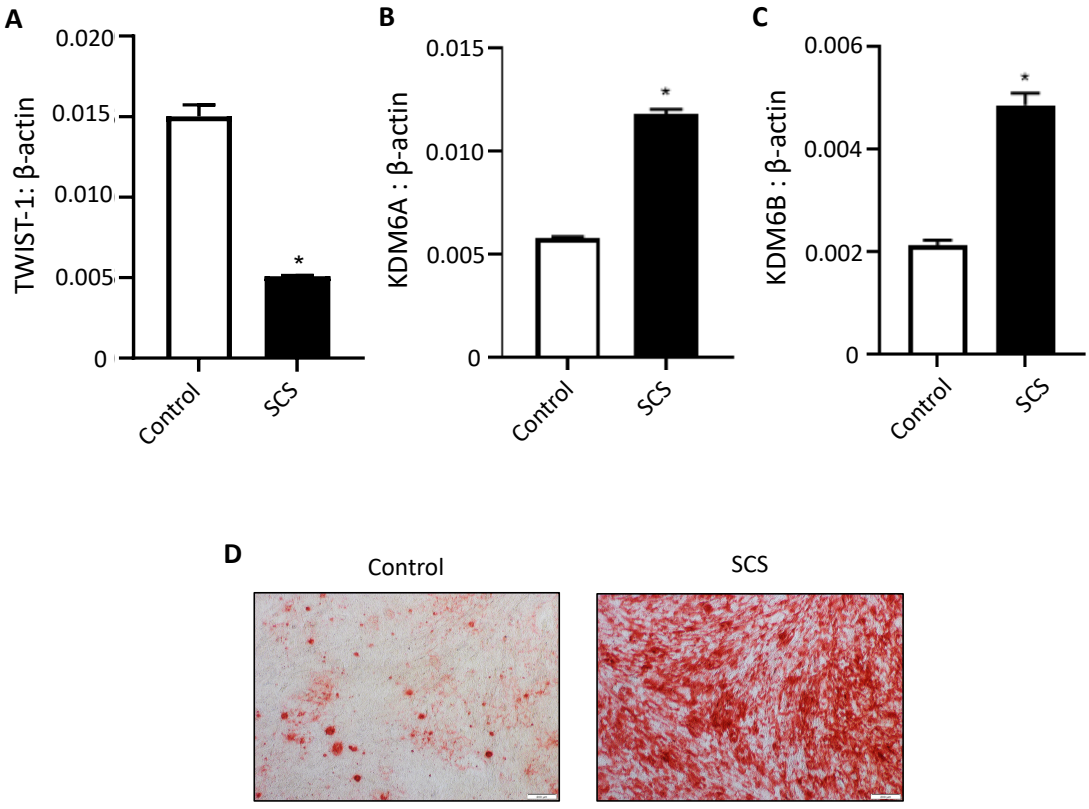
A
0.020
0.015
0.010
0.005
0
TWIST-1: β-actin
*
Control
SCS
B
0.015
0.010
0.005
0
KDM6A : β-actin
*
Control
SCS
C
0.006
0.004
0.002
0
KDM6B : β-actin
*
Control
SCS
D
Control
SCS

Figure 3.2.1. Calvarial cells from SCS patients exhibit upregulated expression of histone demethylases, KDM6A and KDM6B and increased level of mineral deposits. Calvarial cells collected from normal calvaria as control and SCS patients were cultured under osteogenic conditions for 7 days. Gene expression levels of (A) *TWIST-1*, (B) *KDM6A* and (C) *KDM6B* from prepared cDNA were analysed with real-time qPCR and normalised to *β-Actin.* (D) Representative images of mineral deposits present in control and SCS calvarial cell cultures stained with Alizarin Red, following 4 weeks of osteogenic induction. Data represent mean ± S.E., * $p \leq 0.05$, two-tailed, unpaired, student's t-test, n = 3 Control and n = 3 SCS.

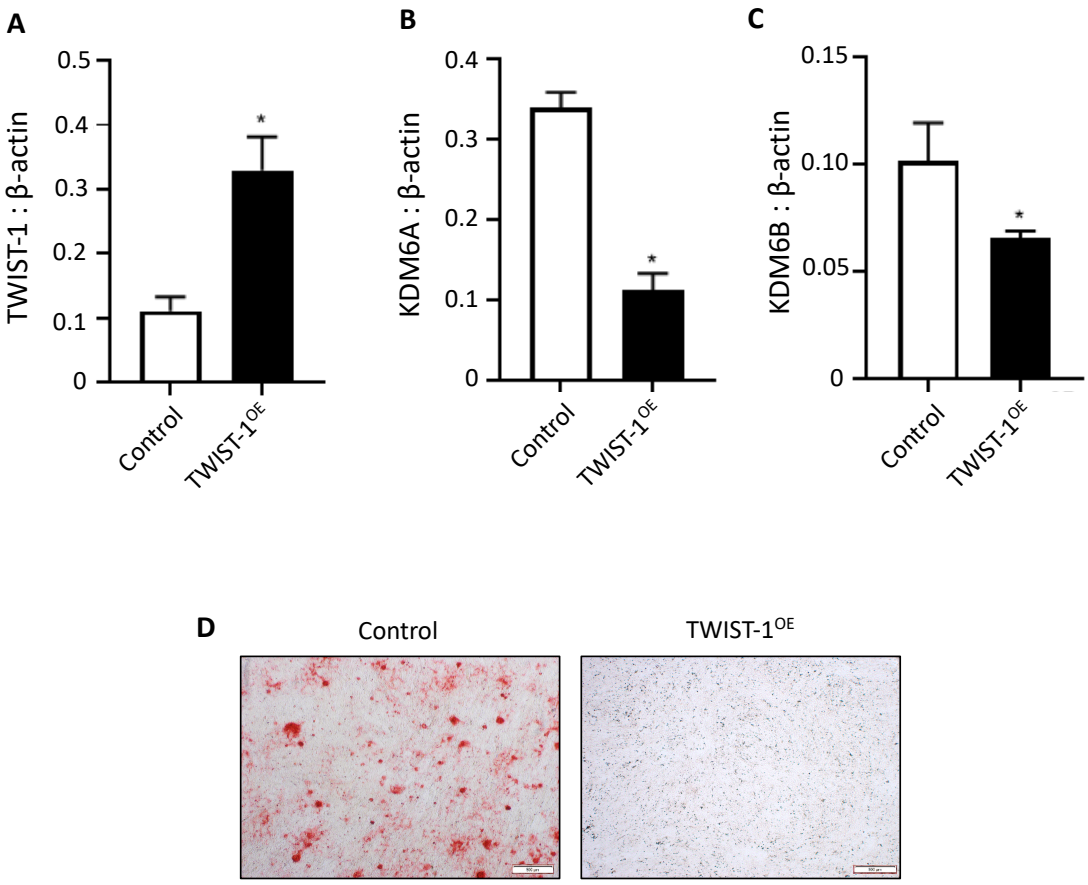
A
TWIST-1 : β-actin
0.5
0.4
0.3
0.2
0.1
0
*
Control
TWIST-1OE
B
KDM6A : β-actin
0.4
0.3
0.2
0.1
0
*
Control
TWIST-1OE
C
KDM6B : β-actin
0.15
0.10
0.05
0
*
Control
TWIST-1OE
D
Control
TWIST-1OE

Figure 3.2.2. Overexpression of *TWIST-1* in calvarial cells supressed expression of histone demethylases, KDM6A and KDM6B and mineral formation capacity. Gene expression levels of (A) *TWIST-1*, (B) *KDM6A* and (C) *KDM6B* in vector only (Control) and *TWIST-1* overexpressing ($TWIST^{OE}$) calvarial cells, cultured under osteogenic conditions for 7 days, were analysed with real-time qPCR and normalized to *β-actin*. (D) Representative images of Alizarin Red mineral staining of control and $TWIST^{OE}$ calvarial cells following 4 weeks of osteogenic induction. Data represent mean ± S.E., * $p \leq 0.05$, two-tailed, unpaired, student's t-test, n = 3 Control and n = 3 $TWIST^{OE}$.

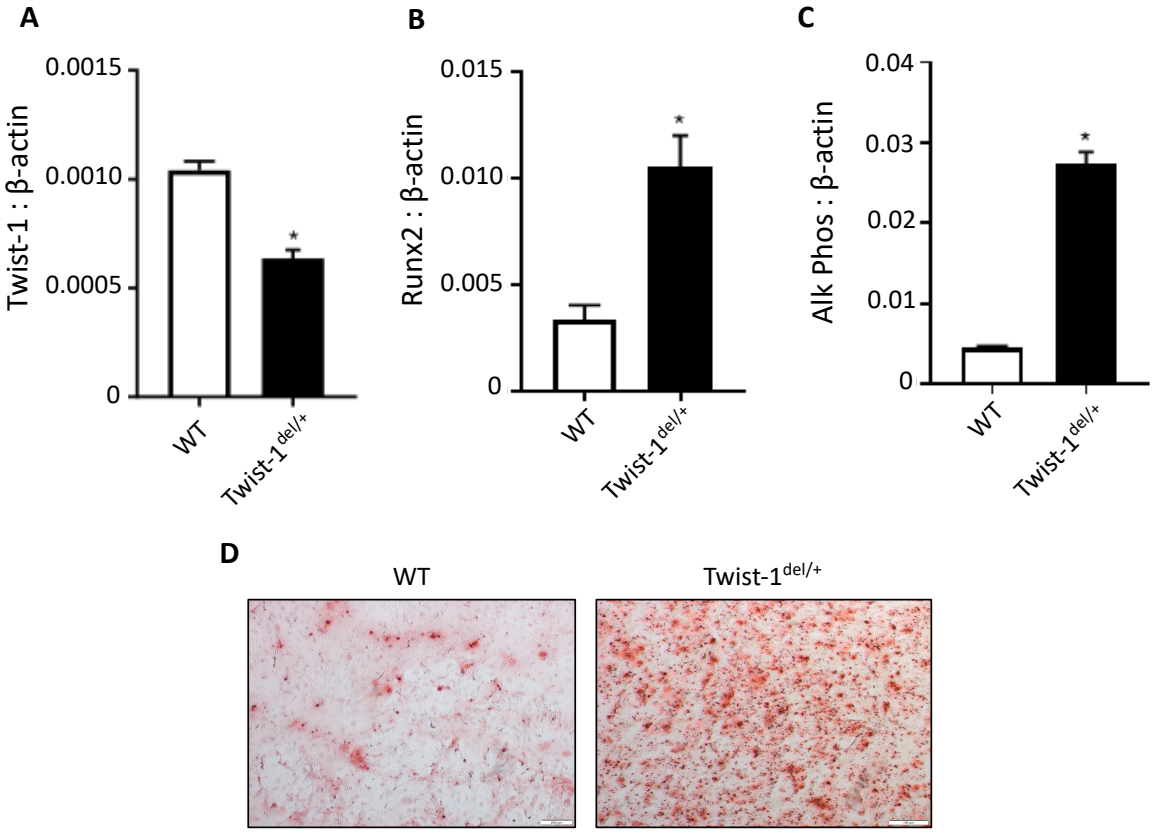
A
Twist-1 : β-actin
0.0015
0.0010
0.0005
0
*
WT
Twist-1del/+
B
Runx2 : β-actin
0.015
0.010
0.005
0
*
WT
Twist-1del/+
C
Alk Phos : β-actin
0.04
0.03
0.02
0.01
0
*
WT
Twist-1del/+
D
WT
Twist-1del/+

Figure 3.2.3. *Twist-1*$^{del/+}$ calvarial cells exhibit increased expression of osteogenic promoting genes and mineral formation capacity. Gene expression levels of (A) *Twist-1*, (B) *Runx2,* (C) *Alkaline Phosphatase (Alk Phos)* in calvarial cells from wild-type (WT) and *Twist-1* haploinsufficient (*Twist-1*$^{del/+}$) mice, cultured under osteogenic conditions for 7 days, were analysed with real-time qPCR and normalised to *β-Actin*. (D) Representative images of Alizarin Red mineral staining of WT and *Twist-1*$^{del/+}$ calvarial cells, cultured in osteogenic conditions for two weeks. Data represent mean ± S.E., *$p \leq 0.05$, two-tailed, unpaired, student's t-test, n = 3 WT and n = 3 *Twist-1*$^{del/+}$ mice.

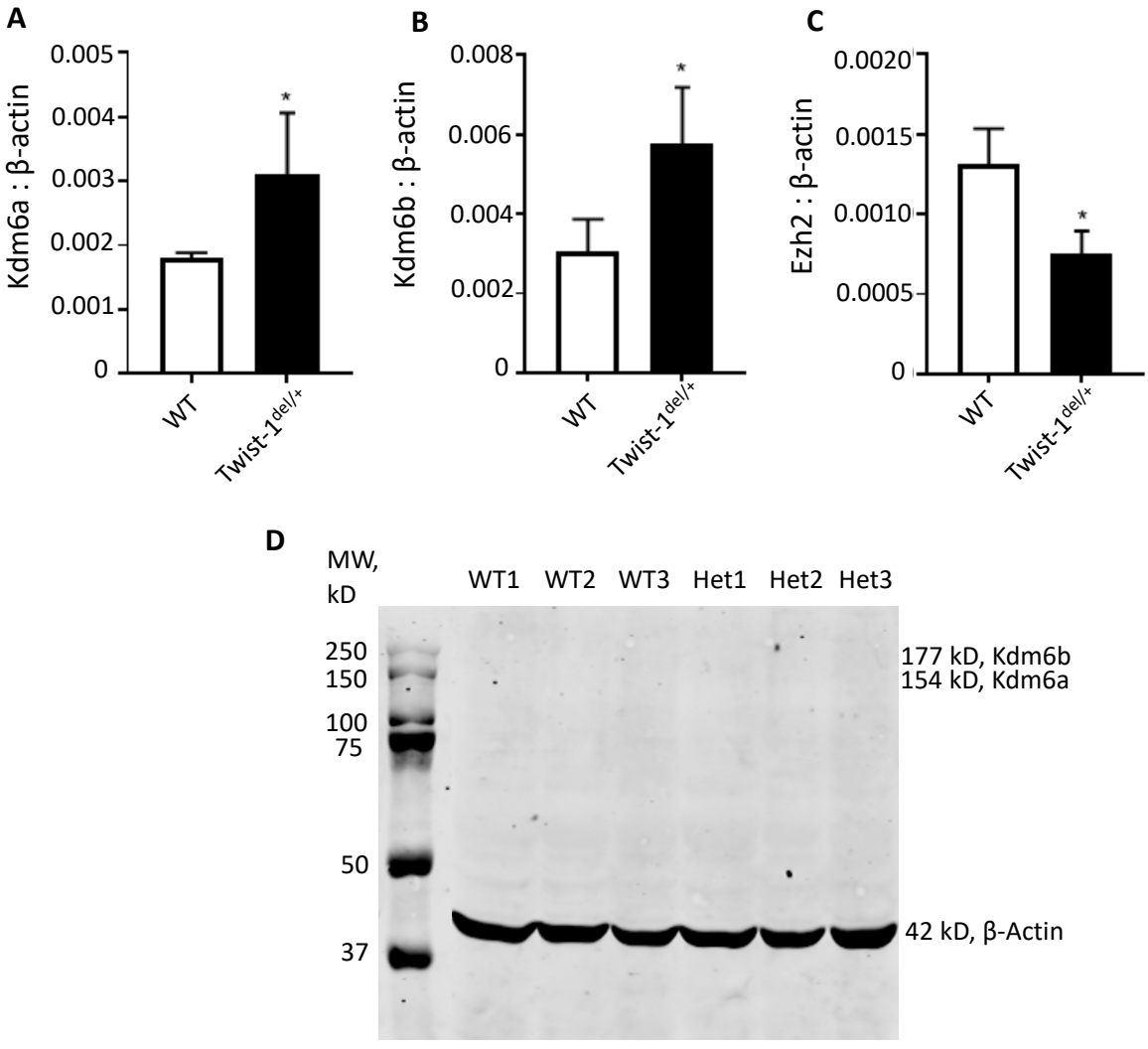
A
Kdm6a : β-actin
0.005
0.004
0.003
0.002
0.001
0
*
WT
Twist-1del/+
B
Kdm6b : β-actin
0.008
0.006
0.004
0.002
0
*
WT
Twist-1del/+
C
Ezh2 : β-actin
0.0020
0.0015
0.0010
0.0005
0
*
WT
Twist-1del/+
D
MW, kD
WT1 WT2 WT3 Het1 Het2 Het3
250
150
100
75
50
37
177 kD, Kdm6b
154 kD, Kdm6a
42 kD, β-Actin

Figure 3.2.4. *Twist-1*$^{del/+}$ calvarial cells display differential expression levels of histone epigenetic enzymes. Gene expression levels of (A) *Kdm6a,* (B) *Kdm6b* and (C) *Ezh2* in calvarial cells from wild-type (WT) and *Twist-1* haploinsufficient (*Twist-1*$^{del/+}$) mice were analysed with real-time qPCR and normalised to *β-Actin,* following 7 days of osteogenic induction. (D) Western blot analysis of protein extracts isolated from wild-type (WT1-3) and *Twist-1*$^{del/+}$ calvaria cells (Het1-3) for Kdm6a/b and β-Actin. Data represent mean ± S.E., *p ≤ 0.05, two-tailed, unpaired, student's t-test, n = 3 WT and *Twist-1*$^{del/+}$ mice.

A

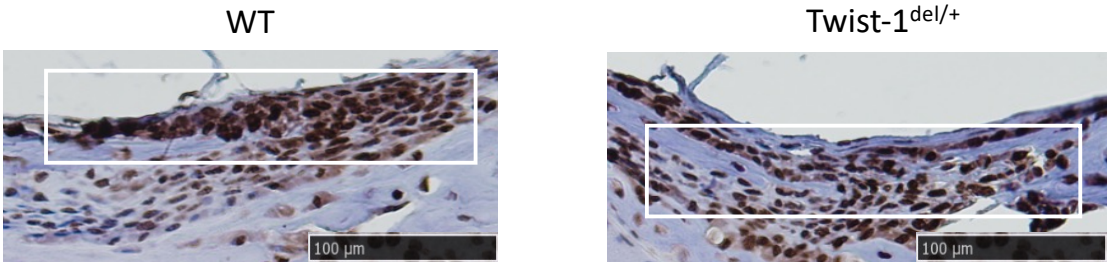
WT
Twist-1del/+
100 µm
100 µm

B

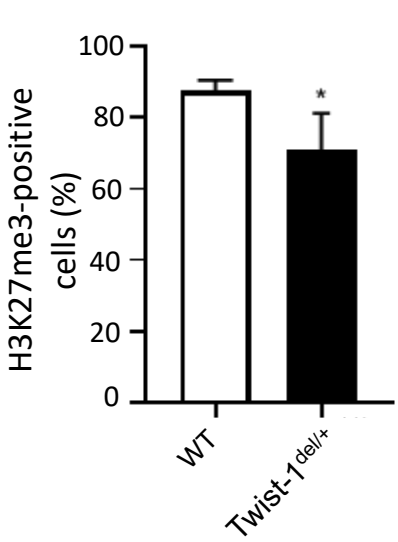
H3K27me3-positive cells (%)
100
80
60
40
20
0
*
WT
Twist-1del/+

Figure 3.2.5. Coronal sutures of SCS mouse model displayed reduced level of histone repressive mark, H3K27me3. (A) Representative images of calvarial sections focusing on open coronal sutures (white box) of 8 day old WT and *Twist-1*$^{del/+}$ mice using an antibody specific to H3K27me3 (brown stain) counterstained with Hematoxylin, scale bar = 100μm. (B) Quantitative measurement of the percentage of H3K27me3-positive nuclei to total number of nuclei within the white box using Image J software. Data represent mean ± S.E, *$p \leq 0.05$, two-tailed, unpaired, student's t-test, n = 3 WT and n = 3 Twist mice.

3.2.3 Kdm6a and Kdm6b promote the osteogenic differentiation capacity of *Twist-1*$^{del/+}$ calvarial cells

The role of Kdm6a and Kdm6b during osteogenic differentiation in calvarial cells from *Twist-1*$^{del/+}$ mice, was assessed using two specific siRNA molecules targeting either *Kdm6a* or *Kdm6b*. Reduced gene expression levels were observed for both *Kdm6a* and *Kdm6b* using each siRNA molecule suggesting an overlap in specificity (Figure 3.2.6). A reduction in the early osteogenic markers, *Runx2* and *Osterix* and mature osteoblast marker, *Alkaline Phosphatase* were also observed using real-time qPCR analyses following siRNA treatment (Figure 3.2.7). Furthermore, the data showed a decrease in Alkaline Phosphatase enzymatic activity in siRNA *Kdm6a* or *Kdm6b* transfected *Twist-1*$^{del/+}$ calvarial cells under osteogenic conditions, compared with scrambled siRNA controls (Figure 3.2.8). Parallel studies found that the level of Alizarin red-positive mineralised deposits was significantly reduced in cultures of siRNA *Kdm6a* or *Kdm6b* knockdown *Twist-1*$^{del/+}$ calvarial cells under osteogenic conditions, compared with scrambled siRNA-treated cells (Figure 3.2.9A). This was confirmed by reduced amounts of extracellular calcium levels in replicate cultures of siRNA *Kdm6a* or *Kdm6b*-treated *Twist-1*$^{del/+}$ calvarial cells, compared to the scrambled siRNA controls (Figure 3.2.9B & C). Collectively, these findings demonstrate that knockdown of *Kdm6a* and *Kdm6b* resulted in the suppression of osteogenic differentiation capacity of calvarial cells from both *Twist-1*$^{del/+}$ female and male mice.

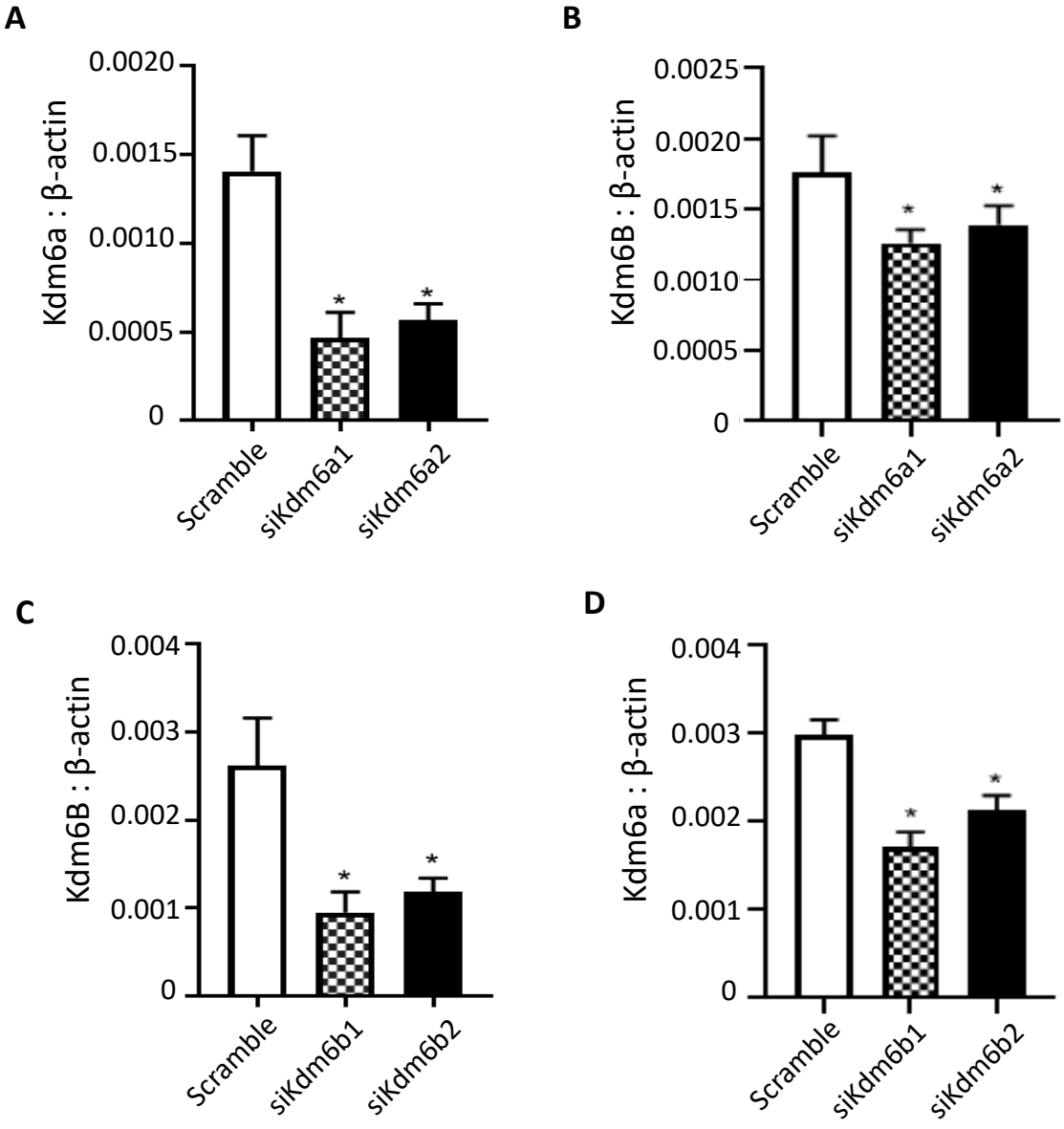
A
Kdm6a : β-actin
0.0020
0.0015
0.0010
0.0005
0
Scramble
siKdm6a1
siKdm6a2
B
Kdm6B : β-actin
0.0025
0.0020
0.0015
0.0010
0.0005
0
Scramble
siKdm6a1
siKdm6a2
C
Kdm6B : β-actin
0.004
0.003
0.002
0.001
0
Scramble
siKdm6b1
siKdm6b2
D
Kdm6a : β-actin
0.004
0.003
0.002
0.001
0
Scramble
siKdm6b1
siKdm6b2

Figure 3.2.6. Knockdown of *Kdm6a* and *Kdm6b* in *Twist-1*$^{del/+}$ calvarial cells. (A) Real-time qPCR analysis of *Kdm6a* and *Kdm6b* in *Twist-1*$^{del/+}$ calvarial cells treated with siRNAs targeting either (A & B) *Kdm6a* (siKdm6a1 or siKdm6a2) or (C & D) *Kdm6b* (siKdm6b1 or siKdm6b2), compared to the siRNA scrambled control (Scramble), under osteogenic inductive conditions. Data represent mean gene expression levels normalised to *β-Actin* ± S.E. expression, *$p \leq 0.05$, two-tailed, unpaired, student's t-test, n = 3 *Twist-1*$^{del/+}$ mice.

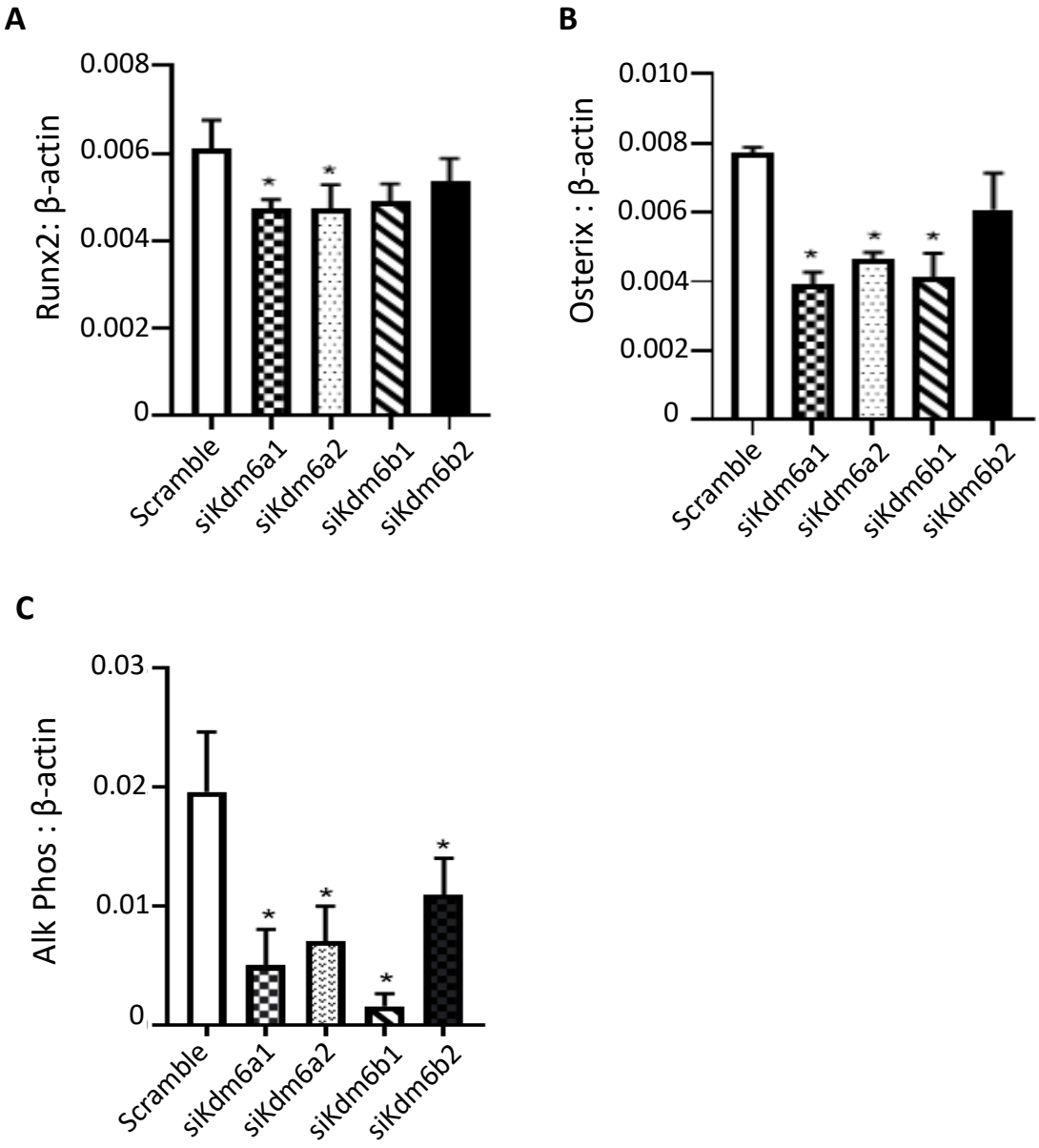
A
Runx2: β-actin
0.008
0.006
0.004
0.002
0
Scramble
siKdm6a1
siKdm6a2
siKdm6b1
siKdm6b2
B
Osterix : β-actin
0.010
0.008
0.006
0.004
0.002
0
Scramble
siKdm6a1
siKdm6a2
siKdm6b1
siKdm6b2
C
Alk Phos : β-actin
0.03
0.02
0.01
0
Scramble
siKdm6a1
siKdm6a2
siKdm6b1
siKdm6b2

Figure 3.2.7. Suppression of Kdm6a and Kdm6b inhibit the expression of osteogenic master genes in *Twist-1*$^{del/+}$ calvarial cells. Gene expression levels of osteogenic promoting genes, (A) *Runx2*, (B) *Osterix* and (C) *Alkaline Phosphatase* (Alk Phos) levels analysed with real-time qPCR in *Twist-1*$^{del/+}$ calvarial cells treated with siRNAs targeting either *Kdm6a* (siKdm6a1 or siKdm6a2) or *Kdm6b* (siKdm6b1 or siKdm6b2), compared to the siRNA scrambled control (Scramble), under osteogenic inductive conditions. Data represent mean gene expression levels normalised to *β-Actin* ± S.E. expression, *$p \leq 0.05$, two-tailed, unpaired, student's t-test, n = 3 *Twist-1*$^{del/+}$ mice.

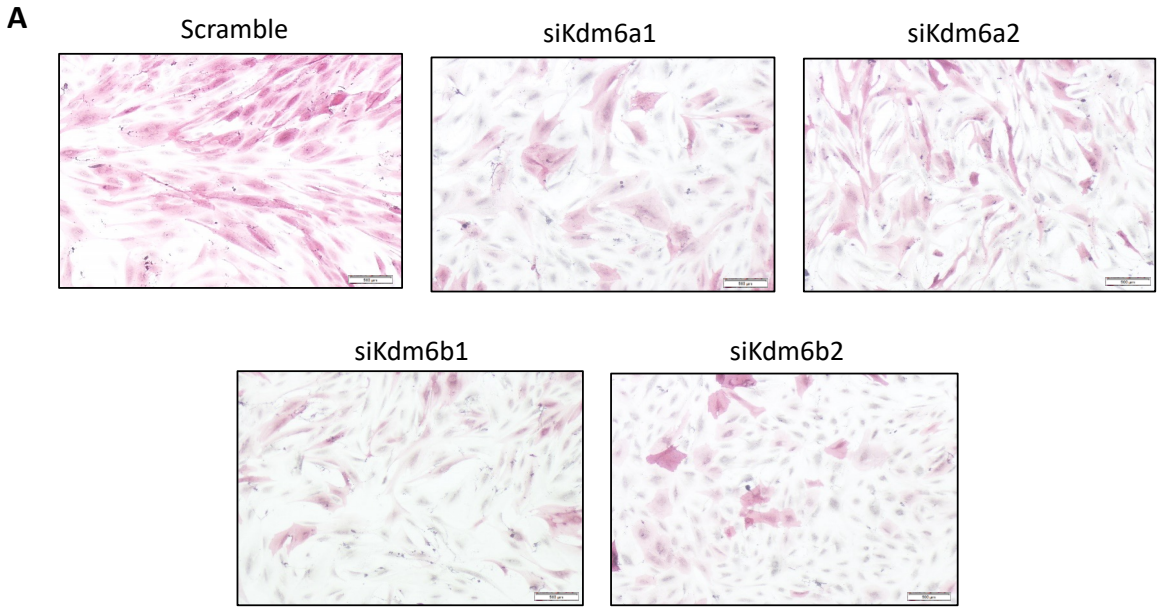
A
Scramble
siKdm6a1
siKdm6a2
siKdm6b1
siKdm6b2

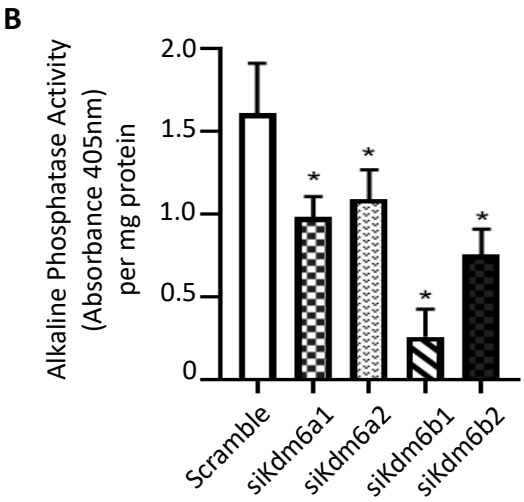
B
Alkaline Phosphatase Activity
(Absorbance 405nm)
per mg protein
2.0
1.5
1.0
0.5
0
*
Scramble
siKdm6a1
siKdm6a2
siKdm6b1
siKdm6b2

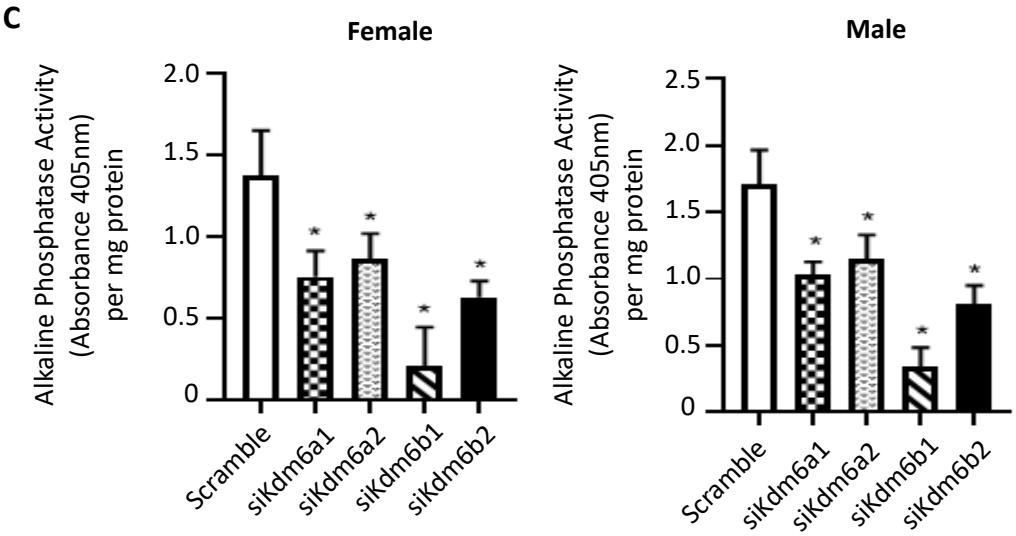
C
Female
Male
Alkaline Phosphatase Activity
(Absorbance 405nm)
per mg protein
2.0
1.5
1.0
0.5
0
2.5
*
Scramble
siKdm6a1
siKdm6a2
siKdm6b1
siKdm6b2

Figure 3.2.8. Kdm6a and Kdm6b promote early osteogenic differentiation in *Twist-1*$^{del/+}$ calvarial cells. (A) Representative images of Alkaline Phosphatase staining of *Twist-1*$^{del/+}$ calvarial cells treated with siRNA Scramble control or *Kdm6a* and *Kdm6b*-specific siRNA, following one week of osteogenic induction, scale bar = 100μm at 50X magnification. (B) Quantitative analysis of Alkaline Phosphatase activity relative to total protein for *Twist-1*$^{del/+}$ calvarial cells treated with Scramble control and *Kdm6a* and *Kdm6b*-specific siRNA, following osteogenic induction for 7 days. (C) Comparison analysis of Alkaline Phosphatase activity following siRNA knockdown between calvarial cells extracted from female and male *Twist-1*$^{del/+}$ male mice. Data represent mean ± S.E., *$p \leq 0.05$, two-tailed, unpaired, student's t-test, n = 4 *Twist-1*$^{del/+}$ mice.

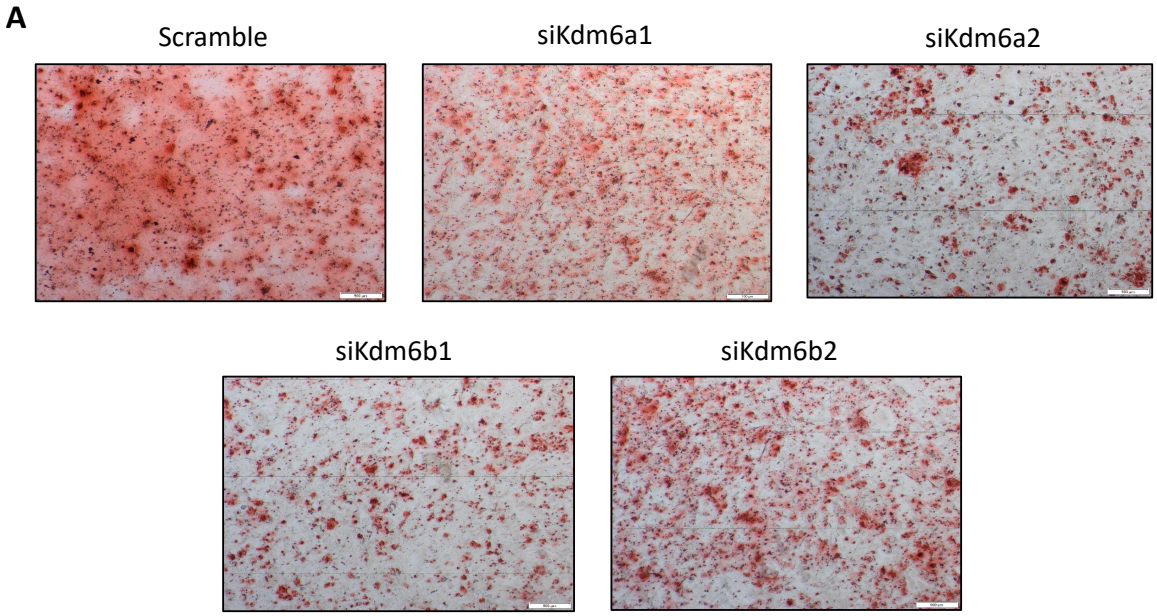
A
Scramble
siKdm6a1
siKdm6a2
siKdm6b1
siKdm6b2

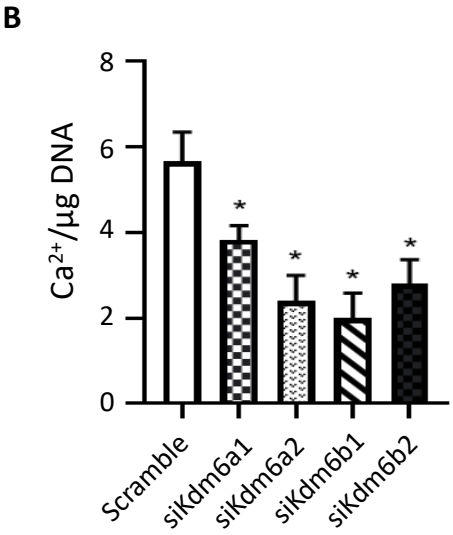
B
Ca2+/µg DNA
0
2
4
6
8
*
Scramble
siKdm6a1
siKdm6a2
siKdm6b1
siKdm6b2

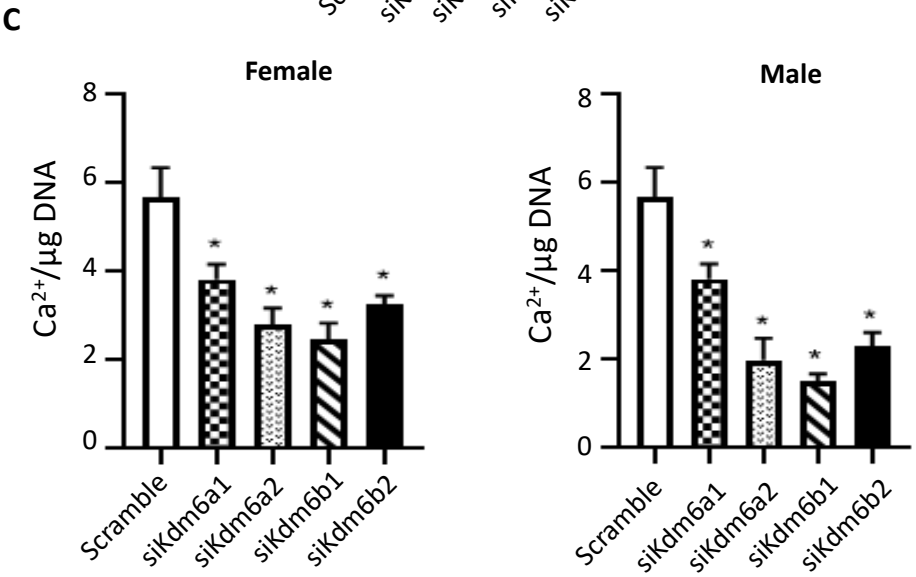
C
Female
Male
Ca2+/µg DNA
0
2
4
6
8
*
Scramble
siKdm6a1
siKdm6a2
siKdm6b1
siKdm6b2

Figure 3.2.9. Kdm6a and Kdm6b promote late osteogenic differentiation in *Twist-1*$^{del/+}$ calvarial cells. (A) Representative images of Alizarin Red mineral staining of *Twist-1*$^{del/+}$ calvarial cells treated with siRNA Scramble control or *Kdm6a* and *Kdm6b*-specific siRNA, following two weeks of osteogenic induction (scale bar = 100μm at 50X magnification). (B) Analysis of extracellular calcium levels relative to total DNA for *Twist-1*$^{del/+}$ calvarial cells treated with siRNA Scramble control or *Kdm6a* and *Kdm6b*-specific siRNA, following two weeks of osteogenic induction. (C) Extracellular calcium levels were compared between calvarial cells extracted from either female or male *Twist-1*$^{del/+}$ male mice, following siRNA knockdown. Data represent mean ± S.E., *$p \leq 0.05$, two-tailed, unpaired, student's t-test, n = 4 *Twist-1*$^{del/+}$ mice.

3.3 Discussion

In this chapter, the results demonstrate, for the first time, that calvarial cells extracted from SCS patients with *TWIST-1* loss-of-function mutations express elevated levels of histone demethylases, *KDM6A* and *KDM6B*. On the other hand, forced overexpression of *TWIST-1* in normal human calvarial cells caused a reduction in *KDM6A* and *KDM6B* gene expression levels. These observations suggested that TWIST-1 might indirectly regulate the expression of KDM6 members in SCS patients. This may occur by TWIST-1 increasing the expression of repressor transcription factors or other epigenetic enzymes which are then recruited to *KDM6A* and *KDM6B* promoters. To identify the indirect pathways, future studies would include ChIP-seq on potential key regulators to identify protein-DNA interactions. Furthermore, the results demonstrated that calvarial cells extracted from SCS mouse model, *Twist-1*$^{del/+}$ mice revealed elevated levels of *Kdm6a* and *Kdm6b*, whereas the gene expression levels of the counter histone methyltransferase, *Ezh2*, was reduced, compared to cells derived from littermate wildtype mice. This correlated to a reduction in the amount of H3K27me3 within the coronal sutures of *Twist-1*$^{del/+}$ mice. These findings suggest that the altered balance in epigenetic enzymes that deposit or remove H3K27me3 are pivotal in driving the craniosynostosis phenotype.

Both histone demethylases have been previously reported to promote osteogenic differentiation in human BMSC by removing the repressive mark, H3K27me3, on the promoter of osteogenic-promoting genes (Hemming, SC, D.; Isenmann, S.; Cooper, L.; Menicanin, D.; Zannettino, A.; Gronthos, S. 2014). Similarly, the present study found that knockdown of *Kdm6a* and *Kdm6b* expression in *Twist-1*$^{del/+}$ calvarial cells reduced gene transcript levels of osteogenic associated genes, *Runx2, Osterix* and *Alkaline Phosphatase*. Previous studies have shown that TWIST-1 induces *EZH2* in cultured human BMSC increasing levels of *EZH2* and H3K27me3 along the Ink4A locus and bone gene promoters

to promote proliferation but suppress osteogenesis, which was diminished in cranial bone cells derived from SCS patients (Cakouros, DI, S.; Cooper, L.; Zannettino, A.; Anderson, P.; Glackin, C.; Gronthos, S. 2012; Camp, E et al. 2018; Hemming, SC, D.; Isenmann, S.; Cooper, L.; Menicanin, D.; Zannettino, A.; Gronthos, S. 2014). These observations support the findings that *TWIST-1* mutations lead to altered *EZH2* and *KDM6A/B* expression levels, suggesting that a balance of histone demethylases and methyltransferase is essential in maintaining the correct fate determination of cranial MPC. The epigenetic dysregulation seen in the *Twist-1* haploinsufficient cells may therefore mediate the premature maturation of bone cells as a result of *Twist-1* mutation within the suture mesenchyme of the SCS mouse model. The aberrant osteogenesis in *Twist-1* mutant cells has been reported previously in other studies and further confirmed in this present study with an observed increased expression of *Runx2* and *Alkaline Phosphatase* when compared to wildtype cells (Camp, E et al. 2018; Yousfi et al. 2001; Yousfi, Lasmoles & Marie 2002). Both of these osteogenic genes have been previously shown to be expressed within mouse calvarial cells at the osteogenic fronts and within the suture mesenchyme and thus, have essential roles in the development of mouse calvaria (Nam et al. 2019; Rice, Rice & Thesleff 2003).

Functional studies using *Twist-1*$^{del/+}$ calvarial cells determined that suppressing the expression of *Kdm6a* and *Kdm6b* led to the inhibition of early osteogenic differentiation shown in the reduced activity and expression of *Alkaline Phosphatase*, and late osteogenic differentiation as seen in the reduced amount of mineral deposition and reduced calcium production. This is in agreement with previous studies reporting that less mineralised calvarial bones with open calvarial sutures were observed in *Kdm6b*-null mice (Zhang, FX, L.; Xu, L.; Xu, Q.; Karsenty, G.; Chen, C. D. 2015), whereas *Kdm6a*-null mice exhibit defects in neural crest formation (Shpargel et al. 2017). Notably, the defects in *Kdm6a* knockout mice are more severe in female mice than in males (Welstead et al. 2012; Xu et al.

2008). This suggested that Uty/Kdm6c, an enzymatically-inactive paralog of Kdm6a located on the Y-chromosome, is able to compensate for the loss of Kdm6a in males (Shpargel et al. 2012; Walport et al. 2014). However, comparison between the sexes showed similar response to the osteogenic potential following *Kdm6a* and *Kdm6b* knockdown. This indicated that the enzymatic activity is essential in the regulation of H3K27me3 levels during calvarial osteogenic differentiation and thus, Kdm6c activity was not able to compensate during Kdm6a and Kdm6b inhibition in this instance. Collectively, the findings of this chapter provide evidence that *Kdm6a* and *Kdm6b* are important factors in aberrant cranial bone formation in *Twist-1*$^{del/+}$ mutant mice, and confirmed previous studies that deregulated epigenetic patterns play significant roles in the development of craniosynostosis (Lakin et al. 2012; Magge 2017). The data also indicate that *Kdm6a* and *Kdm6b* are putative molecular targets that could be exploited for the treatment of craniosynostosis.

Chapter 4: Pharmacological targeting of Kdm6a and Kdm6b, as a novel therapeutic strategy for treating craniosynostosis in Saethre-Chotzen Syndrome

4.1 Introduction

During embryonic and postnatal development, the sutures remain open up to adulthood, providing flexibility to the calvaria and allowing the cranium to expand during brain development (Beederman, MF, E. M.; Reid, R. R. 2014; Bildsoe et al. 2016; Goodnough, Dinuoscio & Atit 2016; Vu et al. 2001). However, dysregulation of MPC differentiation within these sutures results in excessive ossification and premature fusion of the suture space otherwise called craniosynostosis.

Craniosynostosis occurs in 1 in 2,500 live births and can result in an unusual head shape, facial asymmetry and most importantly, pre-fusion of the cranial sutures, causing increased pressure on the developing brain leading to neurological deficits (Knight et al. 2014; Wilkie & Morriss-Kay 2001). Currently, there are two different types of treatment for craniosynostosis, both involving surgical interventions. Traditional treatments, first introduced in the 1890s, involve invasive open cranial surgery to remove the affected sutures allowing for remodelling of the skull using metal plates, which were later improved by using osteosynthesis absorbable meshes (Jimenez, McGinity & Barone 2018; Marchac & Renier 1990; Proctor 2012). These complicated procedures require long operating times and extensive exposure to anaesthetic agents, which could negatively impact the quality of life of children with craniosynostosis. Moreover, these surgeries often lead to serious complications, such as blood loss requiring transfusions, facial scars and swelling, highlighting the need for less invasive surgical procedures (Bergquist et al. 2016; Han et al. 2016; Lee 2012). In 1998, a minimally invasive surgery, involving an endoscopy-assisted craniectomy, was first performed, with decreased surgical and recovery time and significantly less blood loss. However, this procedure is exclusively accessible to early onset craniosynostosis cases with early diagnosis and surgical intervention, and is only effective with the assistance of post-operative orthotic therapy (Jimenez, McGinity & Barone 2018).

Furthermore, the correction from these procedures frequently regresses overtime and requires further surgical interventions throughout childhood (Wes et al. 2014). Additionally, skull vault corrective surgery could disrupt normal suture anatomy creating a secondary craniosynostosis, where other previously-open sutures develop premature synostosis (Adamo & Pollack 2010; Kim, SY, Shin & Lim 2017; Seruya et al. 2011). This effect was proposed to be caused by interrupting the signalling mechanism of normal suture growth by detaching the dura mater from the healthy sutures, and by the sudden decrease in intracranial pressure (Kim, SY, Shin & Lim 2017). Therefore, a non-surgical therapeutic treatment that prevents or reverses premature suture fusion, allowing for gradual expansion of the skull vault, is paramount in improving the quality of life of children with craniosynostosis.

Suture patency regression and secondary suture fusion are more frequently observed in syndromic craniosynostosis because of the underlying untreated genetic mutation. The most prevalent mutation is the ligand-independent activation of the Fibroblast Growth Factor Receptor 2 (FGFR2), which causes syndromic craniosynostosis, including Apert, Crouzon, and Pfeiffer Syndromes. In the last decade, the FGF/FGFR signalling pathway has served as a pharmacological target for a number of studies with varying levels of success. One example is the injection of Juglone, an inhibitor of PIN1 enzyme which stabilises Runx2 and FGF/FGFR signalling complex, into the embryos of an Apert Syndrome mouse model. The data showed that this approach prevented premature coronal suture fusion in newborn Apert Syndrome mice (Shin et al. 2018). Another study delivered a soluble form of a mutated FGFR2 as a decoy receptor to prevent excessive FGFR2 activation. The treatment inhibited osteogenic differentiation and maintained suture patency in calvarial explant cultures derived from Apert Syndrome mice (Yokota et al. 2014). On the other hand, subcutaneous injection of BMN11, an inhibitor of the FGF/FGFR signalling via the Natriuretic Peptide Receptor 2 expressed within the coronal sutures of a Crouzon mouse model, resulted in no

significant changes to suture patency (Holmes et al. 2018). These approaches possess the clinical potential to alleviate or minimise the frequency of the surgical procedures required for treating craniosynostosis.

More recently, our laboratory identified, for the first time, a potential therapeutic strategy for the second most common mutation underlying syndromic craniosynostosis, *TWIST-1* deletion or non-sense mutations, which leads to the loss of function or haploinsufficiency of the *TWIST-1* gene resulting in Saethre-Chotzen Syndrome (SCS) (El Ghouzzi, V et al. 2000). This condition involves unilateral and bilateral coronal synostosis, facial asymmetry, occasional cleft palate, droopy eyelid and mild limb deformities such as shortened and united fingers and toes (Anderson et al. 1996; Gallagher, Ratisoontorn & Cunningham 1993). Our laboratory's study showed that inhibition of TWIST-1 target, tyrosine kinase receptor c-ros-oncogene 1 (C-ROS-1), using tyrosine kinase chemical inhibitor called Crizotinib, prevented bone formation potential in calvarial organotypic cultures from SCS mouse model and aberrant osteogenic differentiation of calvarial cells extracted from SCS patients(Camp, E et al. 2018). However, no study to date has investigated epigenetic enzymes as therapeutic targets to prevent craniosynostosis in SCS.

In the previous thesis chapter, a novel association was identified between the *Twist-1* mutation in SCS mouse calvarial cells and the upregulation of the expression and activity of the epigenetic enzymes, Kdm6a and Kdm6b. Furthermore, suppression of *Kdm6a* and *Kdm6b* gene expression was shown to inhibit osteogenic differentiation potential of *Twist-1*$^{del/+}$ calvarial cells. Therefore, the present chapter aimed to assess a pharmacological based therapy approach to prevent craniosynostosis in *Twist-1*$^{del/+}$ mice by targeting Kdm6a and Kdm6b activity in a pre-clinical study, using a small-molecule cell-permeable selective inhibitor, GSK-J4 (Kruidenier 2012). *Twist-1*$^{del/+}$ mutant mice exhibit premature unilateral or bilateral fusion of the coronal sutures, which normally remain open throughout adulthood

in wildtype mice (Table 4.1.1). Additionally, this mouse model displays syndactyly and polydactyly which mimics the characteristics of SCS patients.

Table 4.1.1. The timing of suture fusion in wildtype and *Twist-1*$^{del/+}$ mice

Mouse Suture	Time of Fusion (after birth)
Wildtype Interfrontal	9 – 15 days
Wildtype Coronal, Sagittal, Lambdoid	Remain open
Twist-1$^{del/+}$ Interfrontal	9 – 15 days
Twist-1$^{del/+}$ Coronal	9 – 15 days
Twist-1$^{del/+}$ Sagittal, Lambdoid	Remain open most of the time

The chemical compound, GSK-J4 was designed to target KDM6A and KDM6B enzymatic activities by competitively binding with their active sites, responsible for the interaction between the co-substrate, α-ketoglutarate, and a histone-3 peptide (Kruidenier 2012). Since then, GSK-J4 has been highly utilised in studies of novel therapeutic strategies against various types of diseases, including acute lymphoblastic and myeloid leukemia (Benyoucef et al. 2016; Li et al. 2018), and breast (Yan et al. 2017), prostate (Morozov et al. 2017), ovarian cancers (Sakaki et al. 2015), osteoarthritis (Yapp 2016), and brainstem glioma (Hashizume et al. 2014; Sui et al. 2017). The studies on human brainstem glioma cell lines demonstrate that GSK-J4 reduced cell proliferation and migration and promoted cellular apoptosis. However, these effects were not observed on normal brain cells. Furthermore, GSK-J4 treatment reduced brain glioma tumour size in mouse organotypic explants and extend mouse survival *in vivo*. Moreover, GSK-J4 has also been used to understand the role of KDM6 subfamily members in regulating differentiation of embryonic stem cells and bone marrow-derived mesenchymal stem cells. The data showed that the presence of GSK-J4 inhibited chondrogenic differentiation *in vitro* (Lhuissier et al. 2019; Yapp 2016).

The present study investigated the role of Kdm6a and Kdm6b in regulating the osteogenic capacity of *Twist-1*$^{del/+}$ calvarial cells *in vitro* and calvarial explants *ex vivo*. Furthermore, a potential drug therapy approach to suppress osteogenic differentiation of the calvarial bones and to prevent premature suture fusion using the selective Kdm6a and Kdm6b inhibitor, GSK-J4, was assessed *in vivo* using the *Twist-1*$^{del/+}$ mutant mouse model.

4.2 Results

4.2.1 Kdm6a and Kdm6b inhibitor, GSK-J4, shows minimal toxicity in *Twist-1*$^{del/+}$ calvarial cells

Twist-1$^{del/+}$ calvarial cells were cultured with increasing concentrations of GSK-J4 to assess potential cytotoxic effects. Observable differences in cell density occurred in the presence of GSK-J4 between 2-10μM (Figure 4.2.1A). Quantitative analyses found that the proliferation rate was unaffected in the presence of 0.1-0.5μM GSK-J4, but cell proliferation was significantly reduced between 1-10μM GSK-J4, as assessed by BrdU incorporation (Figure 4.2.1B). Flow cytometric analyses of *Twist-1*$^{del/+}$ calvarial cells found that the percentage of early apoptotic (Annexin V positive), necrotic (7AAD positive) and late-stage apoptotic (Annexin V + 7AAD positive) cells significantly increased with GSK-J4 treatment at the higher doses of 5μM and 10μM (Figure 4.2.2A-D). Furthermore, analyses using cell impermeant stain, Trypan Blue, showed an increased percentage of non-viable *Twist-1*$^{del/+}$ calvarial cells treated with 2-10μM GSK-J4 (Figure 4.2.2E). Therefore, concentrations higher than 2μM were eliminated from further studies.

4.2.2 Inhibition of Kdm6a and Kdm6b activity by GSK-J4 suppresses the osteogenic differentiation of *Twist-1*$^{del/+}$ calvarial cells *in vitro*

In order to assess whether inhibition of Kdm6a and Kdm6b activity could suppress the osteogenic differentiation capacity of *Twist-1*$^{del/+}$ calvarial cells, the osteogenic regulatory gene expression levels and osteogenic capacity of *Twist-1*$^{del/+}$ calvarial cells were analysed following the addition of GSK-J4 optimised concentrations. The data showed that *Twist-1*$^{del/+}$ calvarial cells, exhibited a reduction in *Runx2*, *Osterix*, *Alkaline Phosphatase* and *Osteonectin* gene expression levels in the presence of 1 or 2μM GSK-J4 compared to vehicle

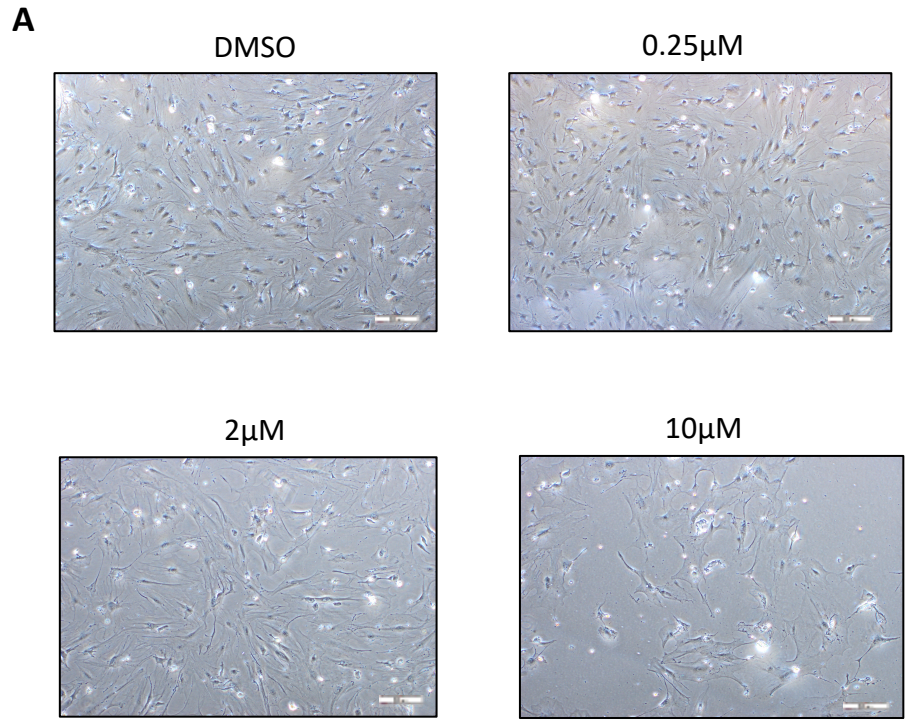
A
DMSO
0.25μM
2μM
10μM

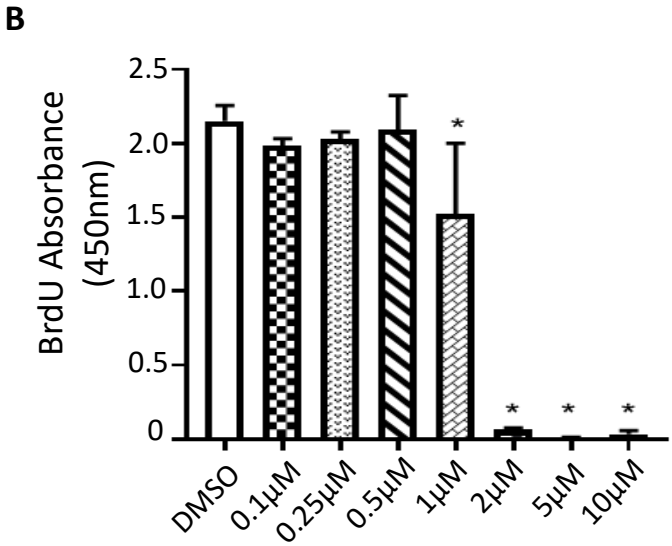
B
BrdU Absorbance (450nm)
2.5
2.0
1.5
1.0
0.5
0
*
*
*
*
DMSO
0.1μM
0.25μM
0.5μM
1μM
2μM
5μM
10μM

Figure 4.2.1. Increasing concentration of Kdm6a and Kdm6b inhibitor, GSK-J4, supresses *Twist-1*$^{del/+}$ proliferation. (A) Representative cell densities of *Twist-1*$^{del/+}$ calvarial cells are shown following treatment with low, medium and high doses of GSK-J4 for 1 week, scale bar = 100μm at 50X magnification. (B) Proliferation rates were measured by BrdU incorporation for *Twist-1*$^{del/+}$ calvarial cells following GSK-J4 treatment with a range of concentrations (0.1μM-10μM or 0.1% DMSO vehicle control) for 1 week. Data represent mean ± S.E., *$p \leq 0.05$, One-way ANOVA with Tukey's multiple comparisons, n = 3 *Twist-1*$^{del/+}$ mice.

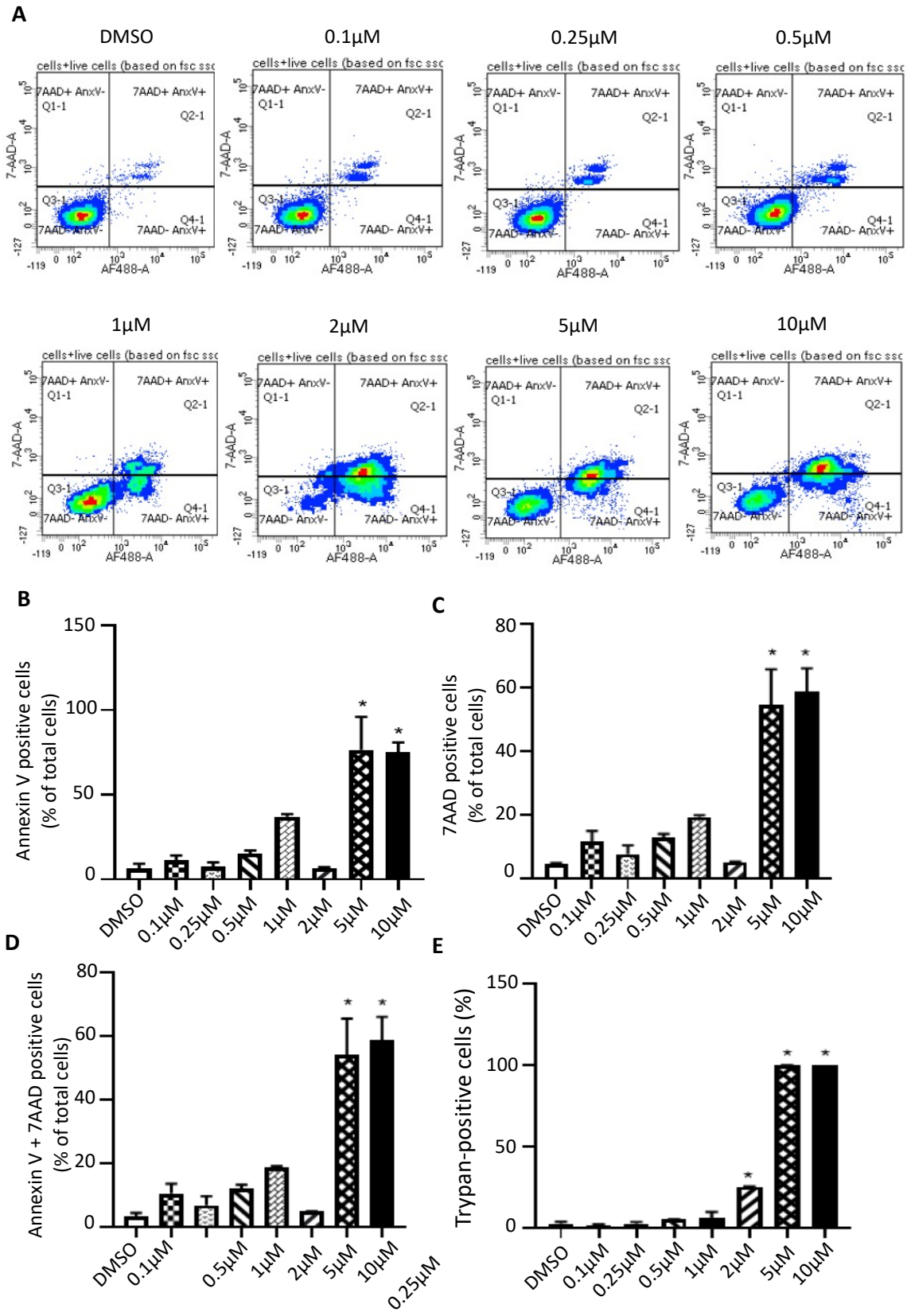
A
DMSO
0.1μM
0.25μM
0.5μM
1μM
2μM
5μM
10μM
cells+live cells (based on fsc ssc
7AAD+ AnxV-
Q1-1
7AAD+ AnxV+
Q2-1
Q3-1
7AAD- AnxV-
Q4-1
7AAD- AnxV+
7-AAD-A
AF488-A
B
Annexin V positive cells
(% of total cells)
C
7AAD positive cells
(% of total cells)
D
Annexin V + 7AAD positive cells
(% of total cells)
E
Trypan-positive cells (%)

Figure 4.2.2. GSK-J4 affected the rate of apoptosis and necrosis of *Twist-1*$^{del/+}$ calvarial cells. (A) Flow cytometric analysis of Annexin V/ 7AAD staining in *Twist-1*$^{del/+}$ calvarial cells in the presence of GSK-J4 (0.1μM-10μM or 0.1% DMSO vehicle control) for 1 week. Representative histograms depicting early apoptotic cells (Annexin V^+), necrotic cells ($7AAD^+$), and late apoptotic cells (Annexin V^+/ $7AAD^+$). (B-D) Quantitation of percentage of Annexin V/ 7AAD stained *Twist-1*$^{del/+}$ calvarial cells by flow cytometric analysis in the presence of GSK-J4 (0.1μM-10μM or 0.1% DMSO vehicle control) for 1 week. (E) Percentage of Trypan-positive cells were quantitated utilising a hemocytometer following treatment of GSK-J4 (0.1μM-10μM or 0.1% DMSO vehicle control) for 1 week. Data represent mean ± S.E., *$p \leq 0.05$, One-way ANOVA with Tukey's multiple comparisons, n = 3 *Twist-1*$^{del/+}$ mice.

alone controls, when cultured under osteogenic inductive conditions (Figure 4.2.3). Supportive studies showed that Alkaline Phosphatase activity was significantly suppressed in *Twist-1*$^{del/+}$ calvarial cells treated with 2μM GSK-J4, compared to vehicle controls (Figure 4.2.4). Furthermore, Western Blot analyses showed an increase in H3K27me3 levels in histone lysates extracted from *Twist-1*$^{del/+}$ calvarial cells treated with 1μM or 2μM GSK-J4, compared to 0.1% DMSO vehicle control (Figure 4.2.5A), confirming the specificity of GSK-J4 as previously described (Kruidenier 2012).

Chromatin collected from replicate experiments was used to assess levels of the inhibitory mark, H3K27me3, present on the *Runx2* and *Alkaline Phosphatase* promoter transcription start sites (TSS), using ChIP analyses. The results demonstrated that H3K27me3 levels decreased dramatically on the *Runx2* and *Alkaline Phosphatase* TSS, under osteogenic inductive conditions compared to normal growth conditions (Figure 4.2.5B&C). However, treatment with GSK-J4 resulted in increased levels of H3K27me3 on the *Runx2* and *Alkaline Phosphatase* TSS, correlating with the suppression of these genes following GSK-J4 treatment (Figure 4.2.5B&C). These findings suggested that the addition of GSK-J4 to *Twist-1*$^{del/+}$ calvarial cell cultures increased the amount of H3K27me3 found on the promotors of osteogenic genes by inhibiting the activity of Kdm6a and Kdm6b histone demethylases during osteogenesis.

The effect of GSK-J4 on osteogenic differentiation was further examined using a murine calvarial organotypic explant model. Calvaria derived from *Twist-1*$^{del/+}$ mice were cultured in media containing hrBMP2, which provides sequence homology with mouse BMP-2, to stimulate bone formation and in the presence or absence of GSK-J4. The calvarial explants were then stained with Masson's trichrome stain to identify newly mineralised bone (Figure 4.2.6A). Histomorphometric analyses revealed a reduction in total bone formation and

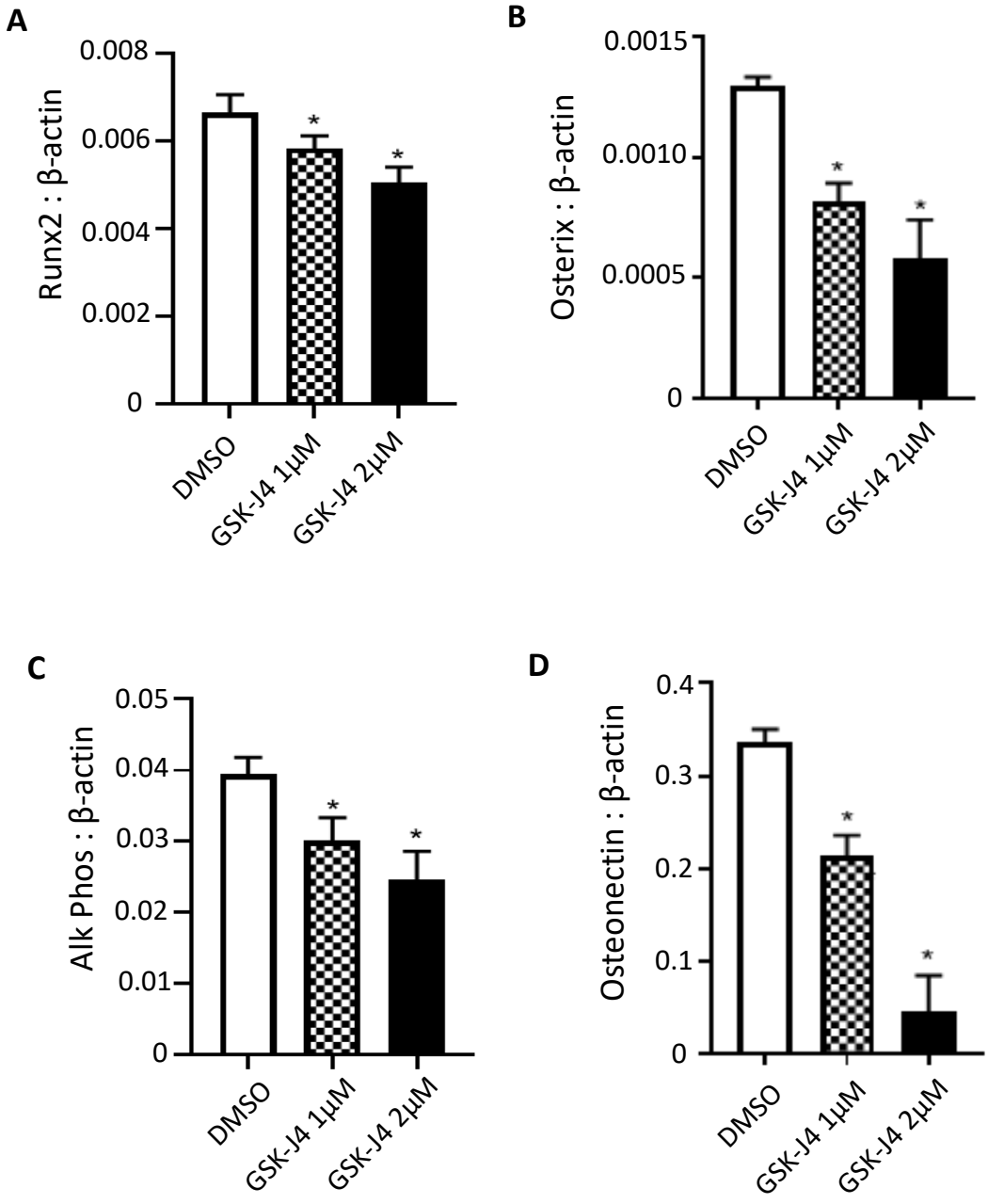
A
Runx2 : β-actin
0.008
0.006
0.004
0.002
0
DMSO
GSK-J4 1μM
GSK-J4 2μM
B
Osterix : β-actin
0.0015
0.0010
0.0005
0
C
Alk Phos : β-actin
0.05
0.04
0.03
0.02
0.01
D
Osteonectin : β-actin
0.4
0.3
0.2
0.1

Figure 4.2.3. Inhibition of Kdm6a & Kdm6b activity supresses osteogenic gene expressions of *Twist-1*$^{del/+}$ calvarial cells. GSK-J4 optimised concentrations were administered on *Twist-1*$^{del/+}$ calvarial cells for 24 hours under osteogenic inductive conditions. Transcript levels of (A) *Runx2*, (B) *Osterix*, (C) *Alkaline Phosphatase* (Alk Phos) and (D) *Osteonectin* in *Twist-1*$^{del/+}$ calvarial cells were analysed with real-time qPCR. Data represent mean gene expression levels normalised to *β-Actin* ± S.E. expression, *$p \leq 0.05$, two-tailed, unpaired, student's t-test, n = 3 *Twist-1*$^{del/+}$ mice.

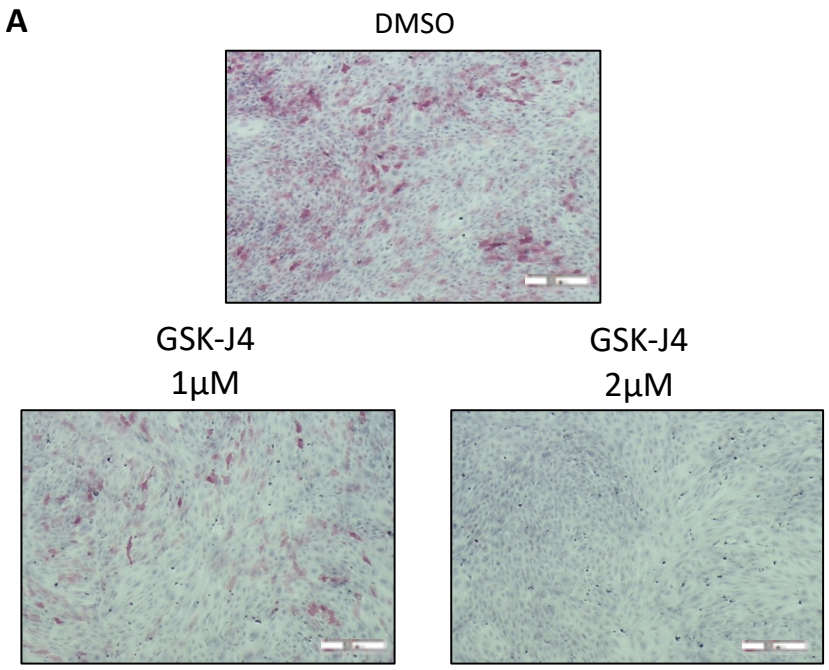
A
DMSO
GSK-J4
1μM
GSK-J4
2μM

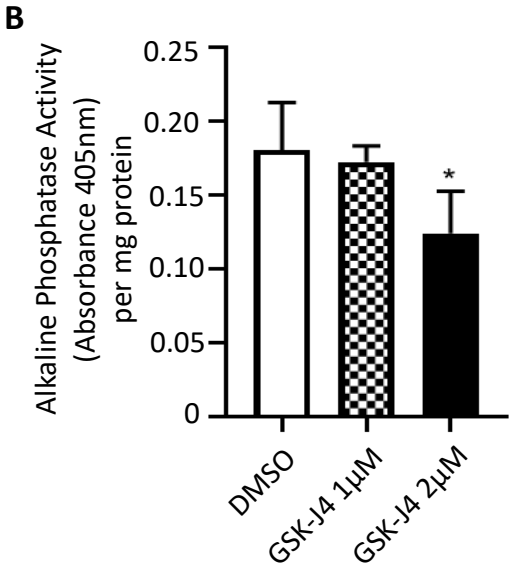
B
Alkaline Phosphatase Activity
(Absorbance 405nm)
per mg protein
0.25
0.20
0.15
0.10
0.05
0
*
DMSO
GSK-J4 1μM
GSK-J4 2μM

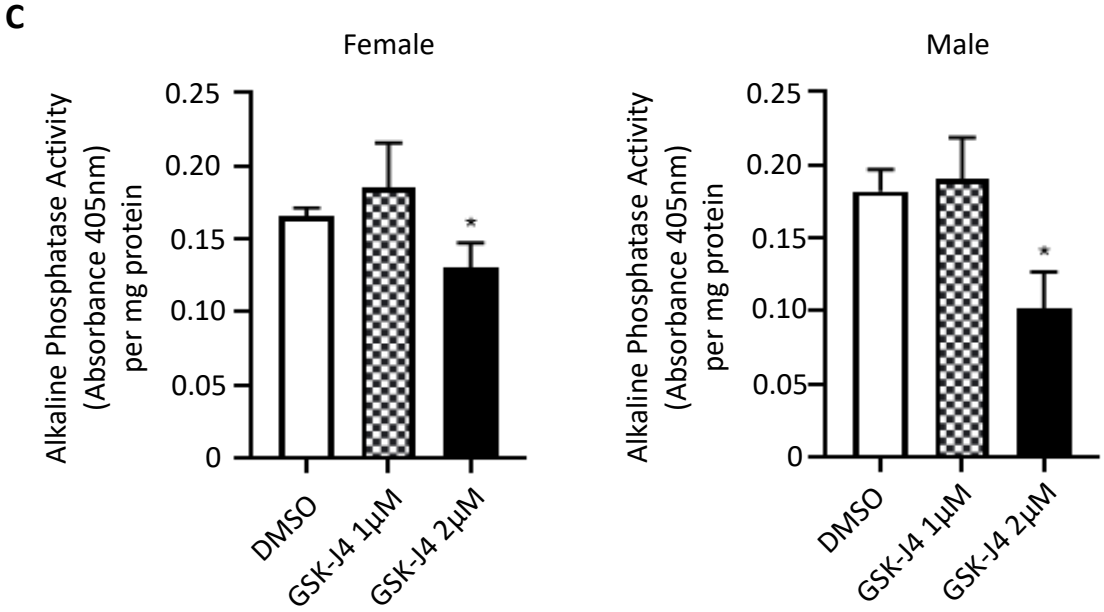
C
Female
Male
Alkaline Phosphatase Activity
(Absorbance 405nm)
per mg protein
0.25
0.20
0.15
0.10
0.05
0
*
DMSO
GSK-J4 1μM
GSK-J4 2μM

Figure 4.2.4. Inhibition of Kdm6a and Kdm6b activity by GSK-J4 suppresses osteogenic differentiation in *Twist-1*$^{del/+}$ calvarial cells. (A) Representative images of Alkaline Phosphatase staining and (B) quantitation of Alkaline Phosphatase activity relative to total protein for *Twist-1*$^{del/+}$ calvarial cells treated with either 1μM or 2μM GSK-J4 or 0.1% DMSO, following 1 week of osteogenic induction. (C) Analysis on the effects of GSK-J4 on Alkaline Phosphatase activity between calvarial cells extracted from female and male *Twist-1*$^{del/+}$ mice. Data represent mean ± S.E., *$p \leq 0.05$, One-way ANOVA with Tukey's multiple comparisons, n = 4 *Twist-1*$^{del/+}$ mice.

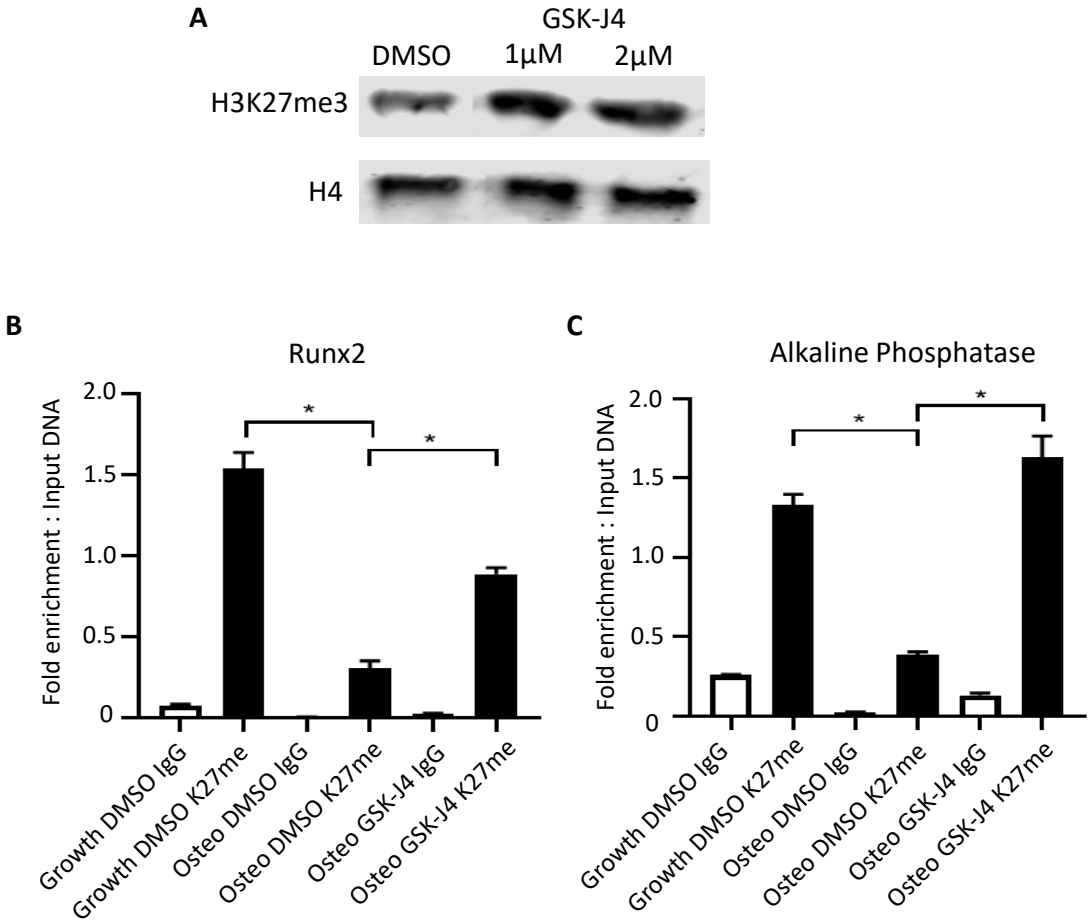
A
GSK-J4
DMSO
1μM
2μM
H3K27me3
H4
B
Runx2
Fold enrichment : Input DNA
2.0
1.5
1.0
0.5
0
*
*
Growth DMSO IgG
Growth DMSO K27me
Osteo DMSO IgG
Osteo DMSO K27me
Osteo GSK-J4 IgG
Osteo GSK-J4 K27me
C
Alkaline Phosphatase
Fold enrichment : Input DNA
2.0
1.5
1.0
0.5
0
*
*
Growth DMSO IgG
Growth DMSO K27me
Osteo DMSO IgG
Osteo DMSO K27me
Osteo GSK-J4 IgG
Osteo GSK-J4 K27me

Figure 4.2.5. GSK-J4 exposure alleviate the level of histone repressive mark on osteogenic gene promoters in *Twist-1*$^{del/+}$ calvarial cells. (A) Western blot analysis of nuclear extracts isolated from *Twist-1*$^{del/+}$ calvarial cells treated with GSK-J4 (1μM, 2 μM) or 0.1% DMSO vehicle control for 24 hours to assess H3K27me3 levels relative to histone 4 (H4). Chromatin immunoprecipitation (ChIP) analysis of H3K27me3 levels on the transcriptional start sites of (B) *Runx2* and (C) *Alk Phos* for *Twist-1*$^{del/+}$ calvarial cells cultured under normal growth media (Growth) or osteogenic inductive conditions (Osteo) for 1 week in the presence of either GSK-J4 (1μM) or 0.1% DMSO. ChIP was performed using either IgG control antibody (IgG) or H3K27me3-specific antibody (K27me). Enriched genomic DNA was used to amplify the transcription start site of target genes. Data represent mean fold enrichment relative to input DNA ± S.E., *$p \leq 0.05$, One-way ANOVA with Tukey's multiple comparisons, n = 4 *Twist-1*$^{del/+}$ mice.

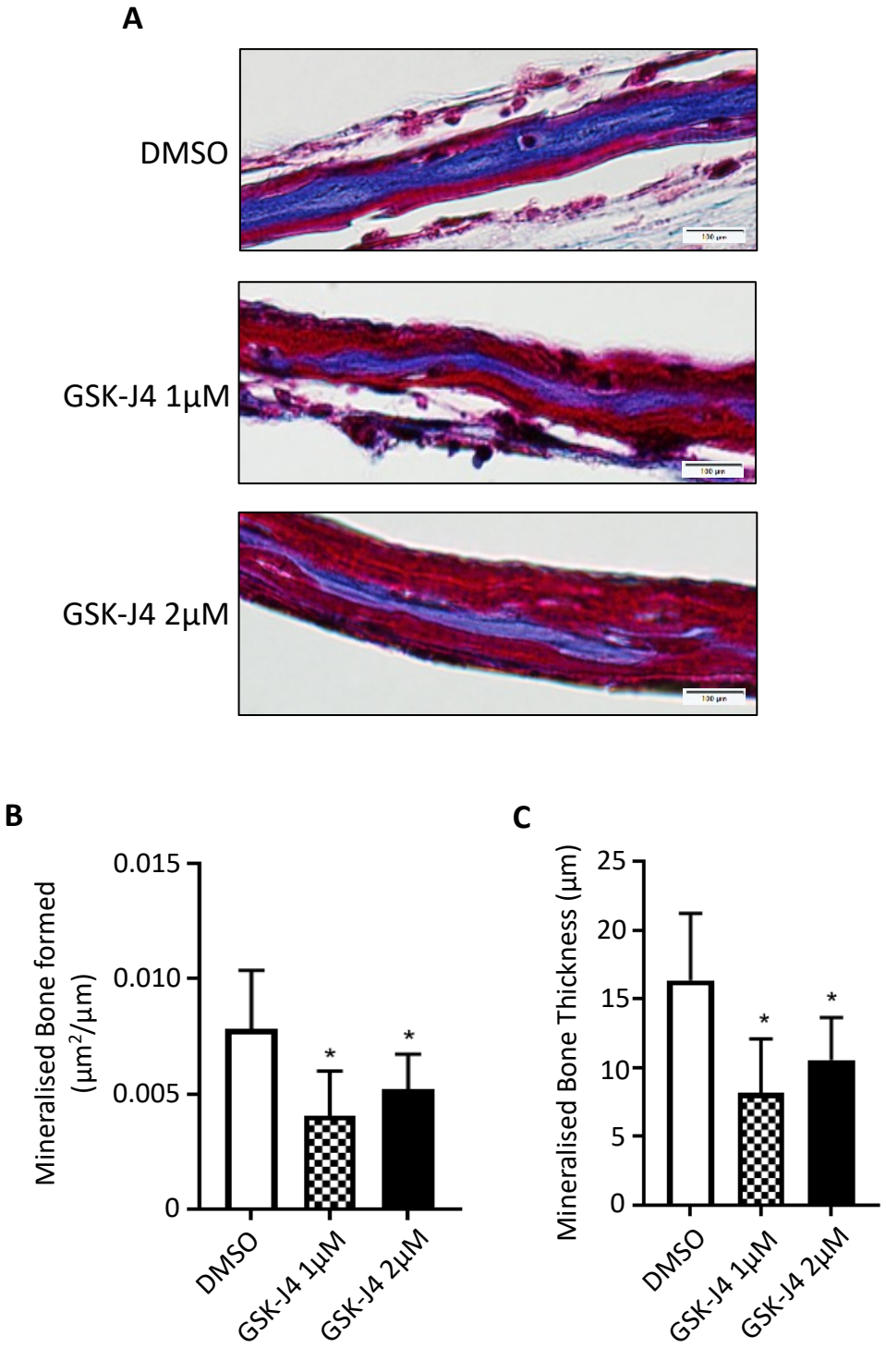
A
DMSO
GSK-J4 1µM
GSK-J4 2µM
B
Mineralised Bone formed (µm²/µm)
0.015
0.010
0.005
0
*
*
DMSO
GSK-J4 1µM
GSK-J4 2µM
C
Mineralised Bone Thickness (µm)
25
20
15
10
5
0
*
*
DMSO
GSK-J4 1µM
GSK-J4 2µM

Figure 4.2.6. GSK-J4 treatment inhibits calvarial bone mineralisation in *Twist-1*$^{del/+}$ mice. (A) Representative images of the stained *Twist-1*$^{del/+}$ calvarial explants treated with BMP2 for 10 days in the presence of either 1μM, 2μM GSK-J4 or 0.1% DMSO vehicle control, then stained with Masson's trichrome. The blue stain depicts mineralized bone and the red stain depicts unmineralized osteoid, scale bar = 100μm. Histomorphometric analysis of (B) mineralized bone formed and (C) bone thickness of treated calvarial explants. Data represent mean ± S.E., *$p \leq 0.05$, One-way ANOVA with Tukey's multiple comparisons, n = 5-7 *Twist-1*$^{del/+}$ mice / treatment group.

thickness in calvarial explants treated with 1 or 2μM GSK-J4, compared to 0.1% DMSO vehicle alone treated explants (Figure 4.2.6B&C).

4.2.3 GSK-J4 treatment prevents craniosynostosis in *Twist-1*$^{del/+}$ mice

The ability of GSK-J4 treatment to prevent fusion of the coronal sutures *in vivo* was assessed using 3mm^2 Collacote^{TM} sponges (used in routine oral surgery) containing either DMSO vehicle alone or GSK-J4 placed subcutaneously on top of the coronal sutures in pre-fusion 8-day-old *Twist-1*$^{del/+}$ mice. Paraffin sections of coronal sutures derived from post-fusion 20-day-old *Twist-1*$^{del/+}$ mice were stained with Masson's trichrome stain and examined by histomorphometric analyses. The data showed that 80% of *Twist-1*$^{del/+}$ mice treated with 2μM GSK-J4 exhibited open coronal sutures at postnatal day 20, whereas unilateral or bilateral coronal craniosynostosis was observed in 83% of the *Twist-1*$^{del/+}$ mice treated with DMSO alone (Table 4.2.1 & Figure 4.2.7). Furthermore, there was a significant reduction in the total mineralised bone formed and bone thickness in the coronal sutures of GSK-J4-treated *Twist-1*$^{del/+}$ mice compared to DMSO treated control mice (Figure 4.2.8A&C). Of note, the brain tissue underneath the parietal bones around the DMSO- and GSK-J4-treated coronal sutures exhibit normal morphology as previously described (Brat 2018; Garman 2011), with intact dura mater and pericranium layers (Figure 4.2.8B). These findings demonstrate that local administration of GSK-J4 underneath the skull cap can prevent premature coronal suture fusion that occurs in *Twist-1*$^{del/+}$ mice between postnatal days 9-20, without negatively affecting the brain tissue. However, histomorphometric analyses of MicroCT scans of the coronal sutures region revealed that 2μM GSK-J4 subcutaneous treatment did not affect bone volume and surface area of *Twist-1*$^{del/+}$ mice (Figure 4.2.9).

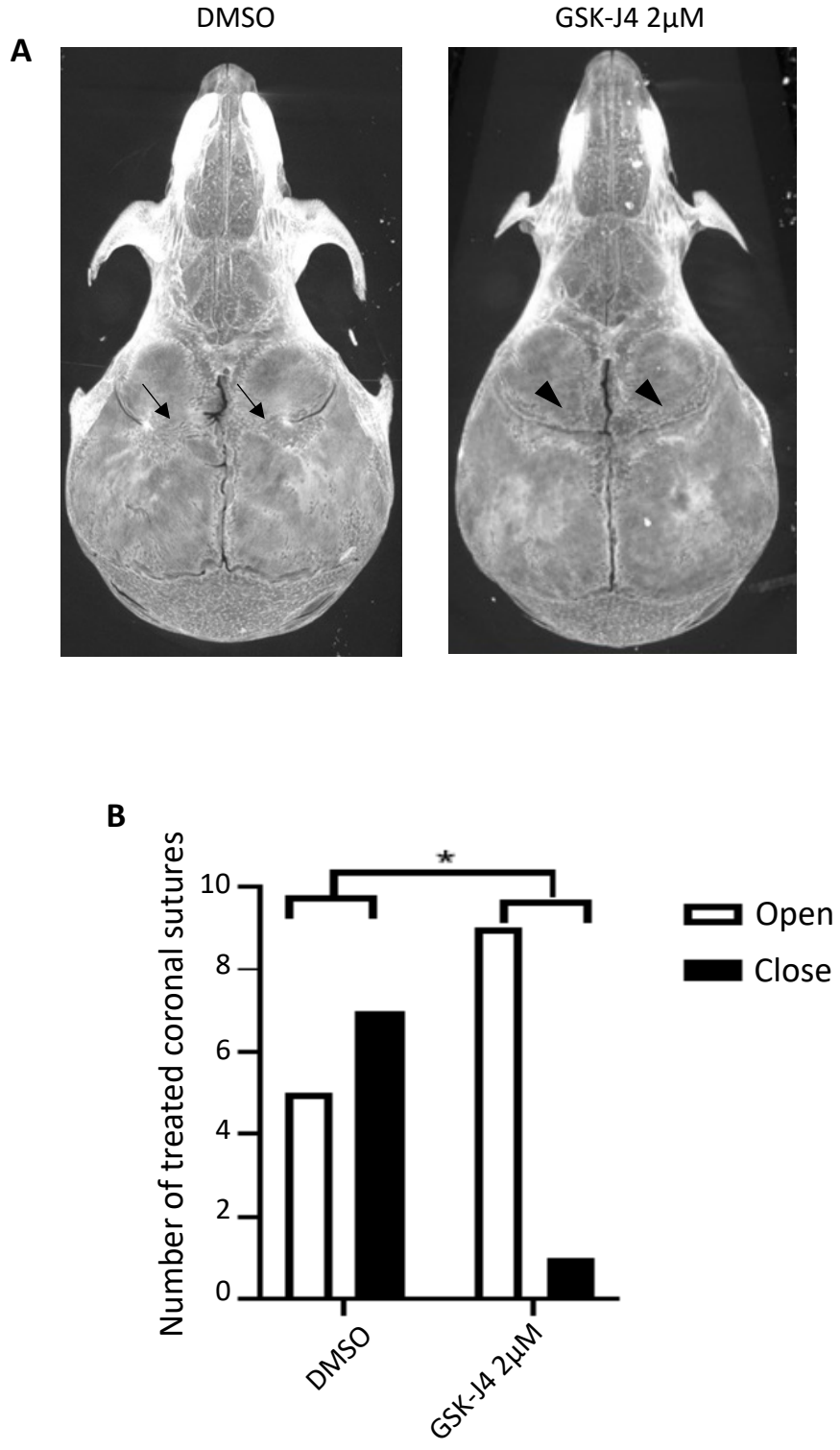
A
DMSO
GSK-J4 2μM
B
Number of treated coronal sutures
10
8
6
4
2
0
*
Open
Close
DMSO
GSK-J4 2μM

Figure 4.2.7. Local GSK-J4 treatment prevented coronal synostosis in Twist-1$^{del/+}$ mice. (A) Representative 3D images of Micro CT scans of 20-days-old calvaria of *Twist-1*$^{del/+}$ mice following local implantation of CollaCote sponge carriers containing either 0.1% DMSO or 2μM GSK-J4 at postnatal 8 day old (P8) mice, with arrows indicating fused coronal sutures and arrowheads marking open coronal sutures. (B) Total number of open and close *Twist-1*$^{del/+}$ coronal sutures following treatment with DMSO or 2μM GSK-J4. Data represent mean ± S.E., *$p \leq 0.05$, contingency table with two-sided Fisher's exact test, n = 5-6 *Twist-1*$^{del/+}$ mice/treatment group.

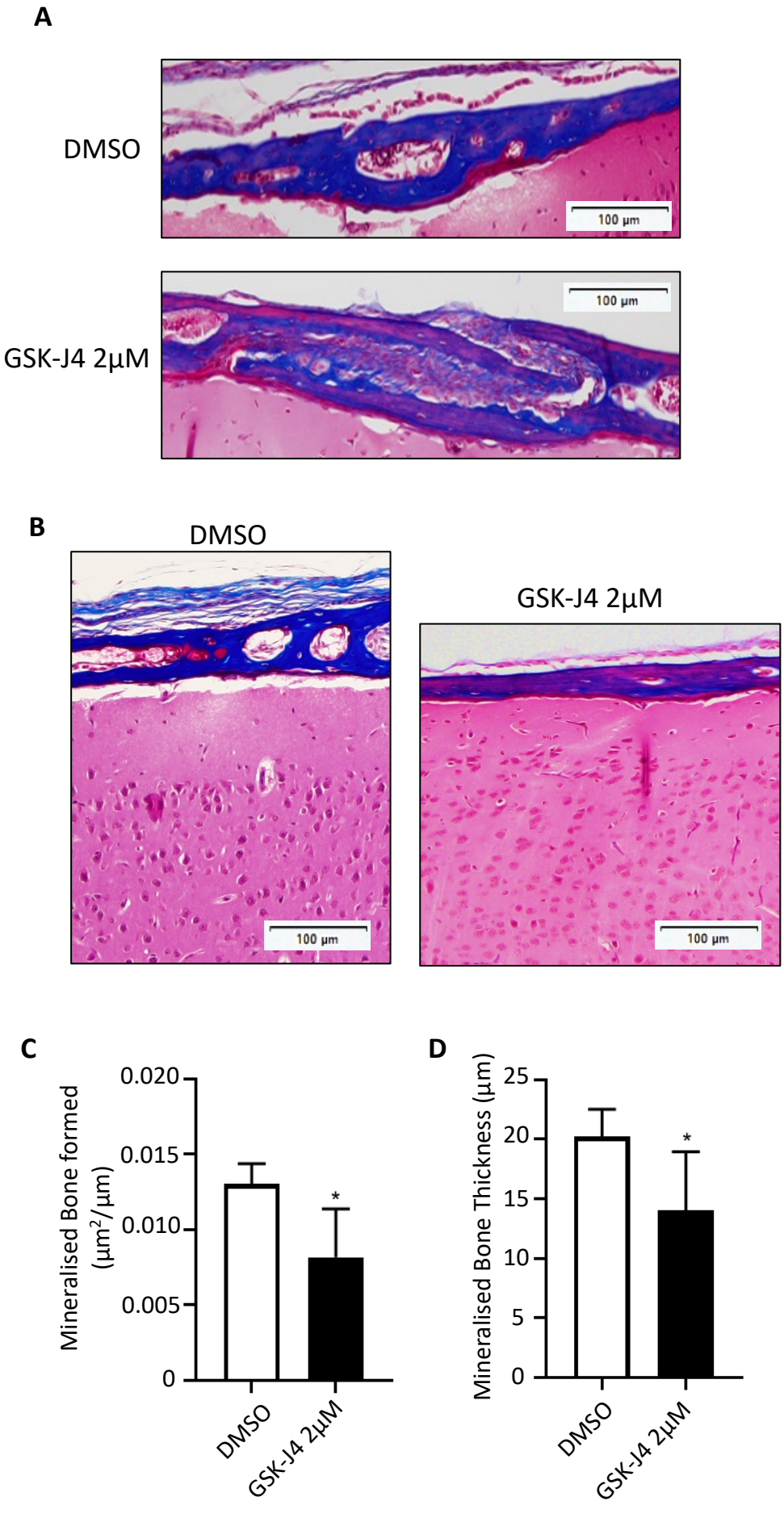
A
DMSO
100 µm
GSK-J4 2µM
100 µm
B
DMSO
100 µm
GSK-J4 2µM
100 µm
C
Mineralised Bone formed (µm²/µm)
0.020
0.015
0.010
0.005
0
*
DMSO
GSK-J4 2µM
D
Mineralised Bone Thickness (µm)
25
20
15
10
5
0
*
DMSO
GSK-J4 2µM

Figure 4.2.8. GSK-J4 treatment prevents coronal suture fusion and bone formation of *Twist-1*$^{del/+}$ mice *in vivo*. Representative images of Masson's trichome-stained (A) coronal sutures and (B) brain tissue of 20 day old *Twist-1*$^{del/+}$ mice following local treatment of 2μM GSK-J4 or 0.1% DMSO at P8, scale bar = 100μm. Histomorphometric analysis of (C) mineralised bone formed and (D) bone thickness of locally treated coronal sutures. Data represent mean ± S.E., *$p \leq 0.05$, One-way ANOVA with Tukey's multiple comparisons, n = 5-6 *Twist-1*$^{del/+}$ mice/treatment group.

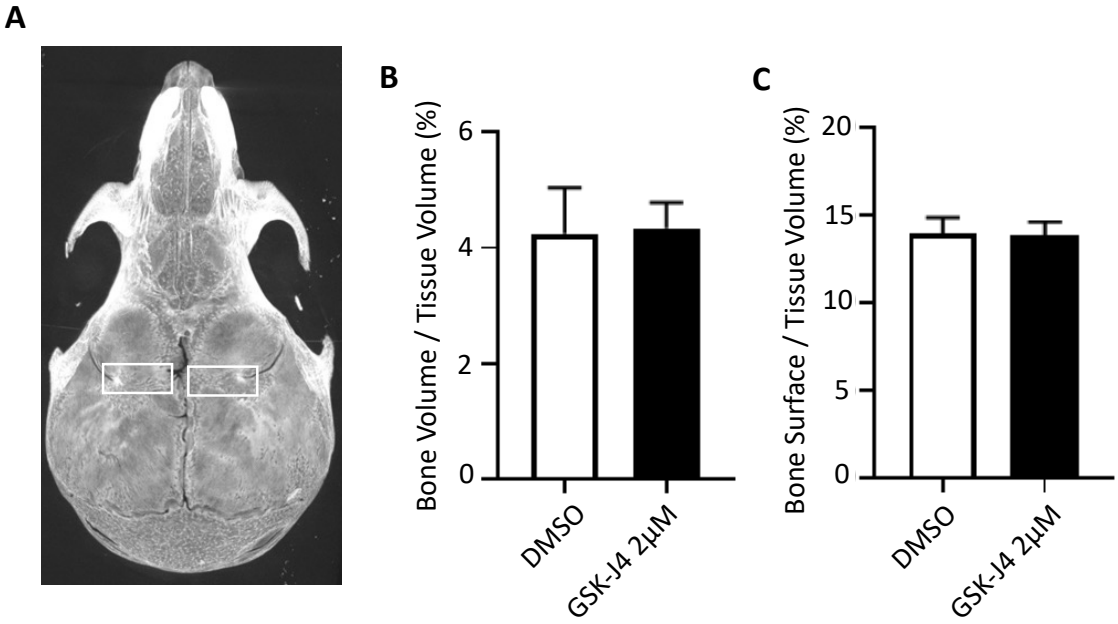
A
B
C
Bone Volume / Tissue Volume (%)
6
4
2
0
DMSO
GSK-J4 2μM
Bone Surface / Tissue Volume (%)
20
15
10
5
0
DMSO
GSK-J4 2μM

Figure 4.2.9. Inhibition of Kdm6a and Kdm6b activity by GSK-J4 does not significantly supress calvarial suture bone formation. (A) The Region of Interest (ROI), indicated in white boxes, of the coronal sutures of *Twist-1*$^{del/+}$ mice treated with either DMSO or 2μM GSK-J4 was selected. (B) The bone volume and (C) bone surface of the ROI were analysed and quantitated on Bruker MicroCT software suite. Data represent mean ± S.E., *$p \leq 0.05$, two-tailed, unpaired, student's t-test, n = 5-6 *Twist-1*$^{del/+}$ mice/treatment group.

Table 4.2.1. GSK-J4 treatment prevents unilateral and bilateral craniosynostosis in *Twist-1*$^{del/+}$ mice. The present table shows the number of *Twist-1*$^{del/+}$ mice with open coronal sutures, unilateral or bilateral coronal craniosynostosis following treatment of either DMSO (0.1%) or 2μM GSK-J4 (n = 5-6 *Twist-1*$^{del/+}$ mice/treatment group).

	DMSO Control	2μM GSK-J4
Open coronal sutures	1	4
Unilateral coronal craniosynostosis	2	1
Bilateral coronal craniosynostosis	3	-

4.3 Discussion

Chapter 4 explored the utility of a chemical inhibitor, GSK-J4, in supressing the osteogenic potential of *Twist-1*$^{del/+}$ calvarial cells. This inhibitor was designed to target KDM6A and KDM6B enzymatic activities by competitively binding with their active sites, responsible for the interaction between the co-substrate, α-ketoglutarate, and a histone-3 peptide (Kruidenier 2012). Our study showed that the treatment of GSK-J4 using concentrations of 1μM and 2μM on *Twist-1*$^{del/+}$ calvarial cells resulted in a reduction in *Runx2*, *Osterix*, *Alkaline Phosphatase* and *Osteonectin* gene expression and activity, correlating to lower levels of H3K27me3 on *Runx2* and *Alkaline Phosphatase* promoters. Notably, the dosage used had little or no effect in the cell viability rate of the *Twist-1*$^{del/+}$ calvarial cells, however higher doses significantly reduced the proliferation rate. This anti-proliferative effect of GSK-J4 has been previously described for embryonic bodies and tumour cells such as bone sarcoma (Lhuissier et al. 2019), paediatric brain glioma (Hashizume et al. 2014) and acute lymphoblastic leukaemia (Benyoucef et al. 2016). Whilst the reduction of proliferation rate was found to be caused by accumulation of cells at S-phase inhibiting cell cycle progression, our study also showed that *Twist-1*$^{del/+}$ calvarial cells undergo apoptosis in the presence of 5μM GSK-J4.

In the present study, functional studies demonstrated that GSK-J4 treatment reduced the development of total bone on whole calvarial organotypic explant cultures derived from *Twist-1*$^{del/+}$ mice. In a pre-clinical model of SCS, local administration of GSK-J4 to the calvaria of *Twist-1*$^{del/+}$ mice prevented premature coronal suture fusion and reduced the amount of mineralised calvarial bone formation. GSK-J4 was administered locally based on the ubiquitous expressions of both Kdm6a and Kdm6b, which are essential in the correct skeletal patterning, brain and heart development (Miyake et al. 2013; Tang et al. 2020; Welstead et al. 2012; Yapp 2016; Zhang, FX, L.; Xu, L.; Xu, Q.; Karsenty, G.; Chen, C. D.

2015). Furthermore, total bone volume and surface area of the parietal bones surrounding the coronal sutures of whole calvarial explants were quantitated using Micro-CT as previously conducted in our laboratory (Camp, E et al. 2018). However, the present data suggested that, while GSK-J4 maintained open coronal sutures, its local treatment did not affect the overall bone volume and surface area of the parietal bones. Alternatively, the potential changes of the bone volume and surface area might be masked by the sensitivity level of the Micro-CT scanner. Collectively, the present study demonstrated that GSK-J4 treatment effectively supressed osteogenic differentiation of *Twist-1*$^{del/+}$ calvarial cells in both sexes and whole calvarial explants *in vitro,* and prevented coronal suture craniosynostosis of *Twist-1*$^{del/+}$ mice *in vivo* by inhibiting the enzymatic activity of aberrant Kdm6a and Kdm6b levels and thus, recovering the level of H3K27me3 marks on osteogenic genes. Additionally, a time course analyses on the long-lasting phenotypes of GSK-J4 treatment on coronal sutures of *Twist-1*$^{del/+}$ mice would be conducted in future experiments.

The delivery system used in the present study demonstrated effective drug-releasing capacity and biocompability, which are in support of previous studies utilising absorbable collagen sponge to deliver craniofacial defect treatments (Moioli et al. 2007; Springer et al. 2007). However, a rate-controlled delivery system may allow for the use of lower concentrations of GSK-J4 to generate a similar efficacy response. One potential delivery system is the use of Titania-nanotube based protein, which has been previously tested on Crouzon Syndrome mouse model and demonstrated prolonged and sustained drug release with non-toxic and chemically-stable characteristics (Bariana et al. 2017). Another previously reported biomaterial is mesoporous silica nanoparticles and nanogels which exhibited high-loading capacity and targeted and controlled drug release qualities as shown for studies utilising an Apert Syndrome mouse model (Finlay 2015; Yokota et al. 2014).

Previous studies have employed GSK-J4 to understand the roles of the KDM6 subfamily members in regulating differentiation of embryonic stem cells and bone marrow-derived MPC (Yapp 2016). Moreover, GSK-J4 has been highly utilised in the studies of novel therapeutic strategies against various types of diseases, including osteoarthritis (Yapp 2016), and brainstem glioma (Hashizume et al. 2014; Sui et al. 2017). The study on osteoarthritis demonstrated that GSK-J4 supresses collagen output, osteoarthritis-related genes and improves collagen organisation *ex vivo*. Of note, the study on brainstem glioma showed that normal brain cells from healthy children are unaffected by GSK-J4 treatment. This observation was confirmed by histological assessment of the brain tissue of Twist-1$^{del/+}$ mice following the localised treatment of GSK-J4 in the present study. This implies that the use of localised GSK-J4 treatment to reverse craniosynostosis may have little or no adverse impact on brain development in children with SCS. However, further studies are required to perform pathological assessments of any potential GSK-J4 toxicity issues for various tissues and organs, as well as cognitive evaluations, using *Twist-1*$^{del/+}$ mice in the absence of pre-clinical large animal models of SCS. Toxicity studies would include weight and histology of the thymus, spleen and lymph nodes, and blood parameters, and liver, and kidney function analyses using serum samples, including identification of antibodies against infection, and microscopic histopathological examination. These studies will be conducted on a time course covering pre-treatment (8-day-old) to adulthood (3-month-old) time points to analyse short- and long-term effects of GSK-J4. Behavioural studies could include assessments of spatial learning and memory, such as passive avoidance, radial arm maze, and Morris water maze tests on adult mice (Salimi & Pourahmad 2018), and evaluation of mouse development milestones from the start of treatment until adulthood (Van Meer & Raber 2005).

Currently, the main treatment for craniosynostosis involves an open calvarial remodelling surgery. This type of surgery might lead to serious complications such as cerebral

contusions, cerebrospinal fluid leaks, hematomas, infections and wound breakdowns (Han et al. 2016; Lee 2012). Additionally, in severe cases of craniosynostosis, there is often a need for a follow up treatment with repeated surgery procedures and substantial hospitalisation, as there is the possibility that sutures might fuse before the cranium has had the opportunity to expand appropriately to accommodate for the growing brain (Hersh et al. 2017). Despite the negative impacts on a patient's wellbeing, quality of life and family, and the financial burden for health providers, therapies which do not involve invasive surgery have yet to be developed.

Chapter 5: Conditional Knockout of Kdm6a Prevents Naturally Occurring Suture Fusion in Female Mice

5.1 Introduction

Mammalian calvarial bone plates are formed through intramembranous ossification during which mesenchymal stromal cells within the ossification centres differentiate, commit into osteogenic precursors, and ossify to form the skull vault. The stromal cells forming the parietal bones and the sagittal sutures between them are of the mesodermal origin, while the frontal bones and the posterior interfrontal sutures (PIF) originate from the neural crest, where the coronal sutures are located between the mesodermal and neural crest interface (Behr 2011; Jiang et al. 2002). Within these sutures, *PRX-1*-expressing stem cells are located in a small niche and overlap with other *GLI-1*$^{+}$ cells which make up the majority of the suture mesenchyme cells. The *PRX-1*$^{+}$ cells are capable of differentiating into osteoblasts upon WNT-signalling during craniofacial bone formation (Mani et al. 2010) (Ouyang et al. 2014). Previous studies from our laboratory have shown that *Ezh2* knockout in *Prx-1* positive mesenchymal cells causes craniosynostosis (Hemming, SC, D.; Codrington, J.; Vandyke, K.; Arthur, A.; Zannettino, A.; Gronthos, S. 2017). Therefore, the present chapter utilised the *Prx-1* gene as a driver for suture mesenchyme-specific knockdown of *Kdm6a* during mouse development, since *Kdm6b* null mice have previously been reported to display open calvarial sutures and less mineralised calvarial bones (Zhang, FX, L.; Xu, L.; Xu, Q.; Karsenty, G.; Chen, C. D. 2015). In the present study, the assessment of *Kdm6a* loss were focused on the PIF suture, the only naturally-fusing suture in mice and equal to the metopic suture in human. Unlike the other sutures which remain patent throughout mouse life span, the PIF closes during the first month through the endochondral ossification pathway. Examination of the stages of PIF suture development showed initiation by chondrogenesis with upregulations of *Sox9* and *Type II Collagen* expressions, which are required for cartilage formation, followed by expressions of bone marker genes, such us *Type I Collagen* and *Osteocalcin* (Sahar, Longaker & Quarto 2005). These cellular changes in the suture mesenchyme are first observed at postnatal day 7 (P7) and slowed down at P10. At P9-10,

ossification of the suture appearing as bony bridges between the frontal plates are observed starting anteriorly in the endocranial layer of the suture and proceeding posteriorly. However, other studies observed that the bridges are presented as intermittent fusion points starting sporadically throughout the PIF sutures and alternating with patent areas (Sahar, Longaker & Quarto 2005). At P13, late osteogenic maturation starts and peaks at P15 which leads to complete fusion of the endocranial layer of the PIF suture, but leaving the ectocranial open until P25 (Cohen 1993). These observations highlight the PIF complex and unique architecture of a double layer interface of the endocranial and ectocranial layers separated by a vein (Moss 1958).

Previous chapters showed that the inhibition of *Kdm6a* and *Kdm6b* expression and enzymatic activity supresses aberrant osteogenic inhibition of calvarial stromal cells and maintain suture patency in *Twist-1*$^{del/+}$ mice. Both *Kdm6a* and *Kdm6b* expression are ubiquitous, and are located on the X-chromosome and chromosome 17, respectively. Of note, *Kdm6a* partially escapes X-inactivation resulting in an increased *Kdm6a* gene expression level in females (Lederer et al. 2012). These Kdm6 members have been shown to have an activating role on osteogenic gene promoters via their histone demethylase capacities (Hemming, SC, D.; Isenmann, S.; Cooper, L.; Menicanin, D.; Zannettino, A.; Gronthos, S. 2014; Hong 2007; Yang, D et al. 2013). However, recent studies have revealed Kdm6 demethylase-independent potential for general chromatin-remodelling, where deletion of demethylase function on both Kdm6a and Kdm6b displayed normal embryonic development phenotypes in mice (Miller, Mohn & Weinmann 2010; Shpargel et al. 2014). Furthermore, the demethylase-independent activity of Kdm6a was observed to attenuate an osteoporotic phenotype in mice, which was achieved through the loss of H3K27me3 on *Runx2* and *Osterix* gene promoters (Wang, FS et al. 2017). The capability of Kdm6a and Kdm6b in alleviating H3K27me3 independent of their catalytic functions was previously

identified, where enzymatic mutation of both Kdm6a and Kdm6b led to a typical decrease in global H3K27me levels during early embryonic differentiation. This was thought to occur via mediating interactions between the T-Box family of transcription factors and SWI/SNF chromatin remodelling complex, which modulates H3K27 acetylation regulating the enhancer landscape during essential developmental processes (Alver et al. 2017).

These activities were previously present in the catalytically inactive member of the KDM6 family, KDM6C or UTY, encoded by the Y-chromosome. Although when first discovered KDM6C was identified as the demethylase-dead homolog of KDM6A and KDM6B, recent studies revealed that the catalytic capability of KDM6C exists in a significantly reduced level (Walport et al. 2014). Kdm6c was shown to be capable of partially compensating the phenotypic severity of neural crest-specific knockout of *Kdm6a* in hemizygous male. On the other hand, homozygous female, lacking *Kdm6c* gene, exhibited enhanced phenotypic traits, such as cranial deformities and heart defects (Lang et al. 2005). This was further observed during mouse embryonic development, where knockout of *Kdm6a* was lethal in female mice before embryonic day 11, whereas male embryos survived until birth with less severe defects in mesoderm-derived development, suggesting redundancy of Kdm6a and Kdm6c in embryonic stem cell differentiation (Wang, C et al. 2012). These observations were eliminated in $Kdm6a^{-/y}$ and $Kdm6c^{-/y}$ hemizygous male mice, which were mid-gestationally lethal with developmental defects (Shpargel et al. 2012). The ability of the catalytically supressed Kdm6c in compensating for Kdm6a loss in male further confirmed the demethylase-independent roles of the Kdm6 family members during embryonic mouse development.

Previous studies on the skeletal structure on a *Kdm6a* knockout model, specifically on the neural crest lineage using *Wnt-1*:cre driver, showed that male $Kdm6a^{fl/y}$ mice exhibited

frontonasal hypoplasia, increased facial angle with prominent forehead, reduced palpebral fissures, and significant shortening and reduced thickness of nasal and frontal bones which presented more severely in female *Kdm6a*$^{fl/fl}$ mice with an addition of severe cases of cleft palate and significant shortening of nasal and frontal bones. Additionally, both male and female knockout mice showed reductions in weight. These phenotypic features mimicked the characteristics of the Kabuki Syndrome in human, including the craniofacial defects and postnatal growth retardation (Shpargel et al. 2017). Furthermore, previous studies on the intramembranous and endochondral ossification processes on *Kdm6b* knockout model revealed that *Kdm6b*$^{-/-}$ homozygous mouse embryos died shortly after birth and exhibited open fontanelles, reduced mineralisation in calvarial bones and long bones, deformed collarbones, dwarfism and decreased cartilage proliferation and differentiation (Zhang, F et al. 2015; Zhang, FX, L.; Xu, L.; Xu, Q.; Karsenty, G.; Chen, C. D. 2015). On the other hand, studies of hemizygous *Kdm6c* mutant mice showed that the loss of *Kdm6c* did not affect the viability and fertility in male mice with no reported phenotypical defects (Shpargel et al. 2012). Collectively, these studies demonstrated that the Kdm6 subfamily members are essential in the correct calvarial and skeletal development in mice.

The present chapter focuses on assessing the role of Kdm6a during calvarial development *in vivo*. To achieve this aim, a conditional knockout mouse model was generated utilising a *Prx1:Cre* driver to knockout *Kdm6a* gene expression in the suture mesenchyme and skeletal limb bones to asses cranial development.

5.2 Results

5.2.1 Conditional knockout of *Kdm6a* in *Prx-1*-expressing cells of adolescence female mice exhibit decreased body weight.

To analyse the role of Kdm6a during calvarial suture development *in vivo*, mesenchyme-specific deletion of a conditional *Kdm6a* was generated by crossing *Kdm6a* floxed mice (*Kdm6a*$^{fl/fl}$) with cre recombinase mice driven by the *Prx-1* promoter (*Prx1*:cre) to generate *Prx1*:cre;*Kdm6a*$^{-/-}$ female (FKO) and *Prx1*:cre;*Kdm6a*$^{-/y}$ male (MKO) mice (Figure 5.2.1A). The Prx-1 transcription factor has previously been identified in precursor mesenchymal cells populating the calvarial suture niche and the skeletal bones of the limbs (Logan et al. 2002; Ouyang et al. 2014; Wilk et al. 2017). The detection of *Kdm6a* knockout was assessed by genotyping analyses with *Kdm6a* and *Prx1* primer sets of extracted DNA from FKO and MKO tails or ear notches (Figure 5.2.1B&C). The levels of *Kdm6a* expression in FKO and MKO mice were then confirmed with qPCR analyses. The results showed approximately 50% reduction in *Kdm6a* gene expression levels in both FKO and MKO calvarial cells (Figure 5.2.1D). This partial knockout of *Kdm6a* is likely due to the heterogeneity of the bulk calvarial cell population characterised as *Gli-1* positive, whereas *Prx-1* expression identified a more discrete subset (Doro, Grigoriadis & Liu 2017).

Initial studies first compared the body weight of postnatal day 9 (P9), 15 (P15) and 25 (P25) FKO and MKO mice with *Prx1*:cre control mice. The weight of P9 and P15 FKO and MKO mice were found to be comparable to *Prx1*:cre control mice (Figure 5.2.2A&B). However, P25 FKO mice showed a significant decrease in body weight, whereas P25 MKO mice showed an increasing body weight trend, although non-significant (Figure 5.2.2C). These results suggested that conditional loss of *Kdm6a* in the mesenchymal department affected the body weight of female mice more severely than male mice.

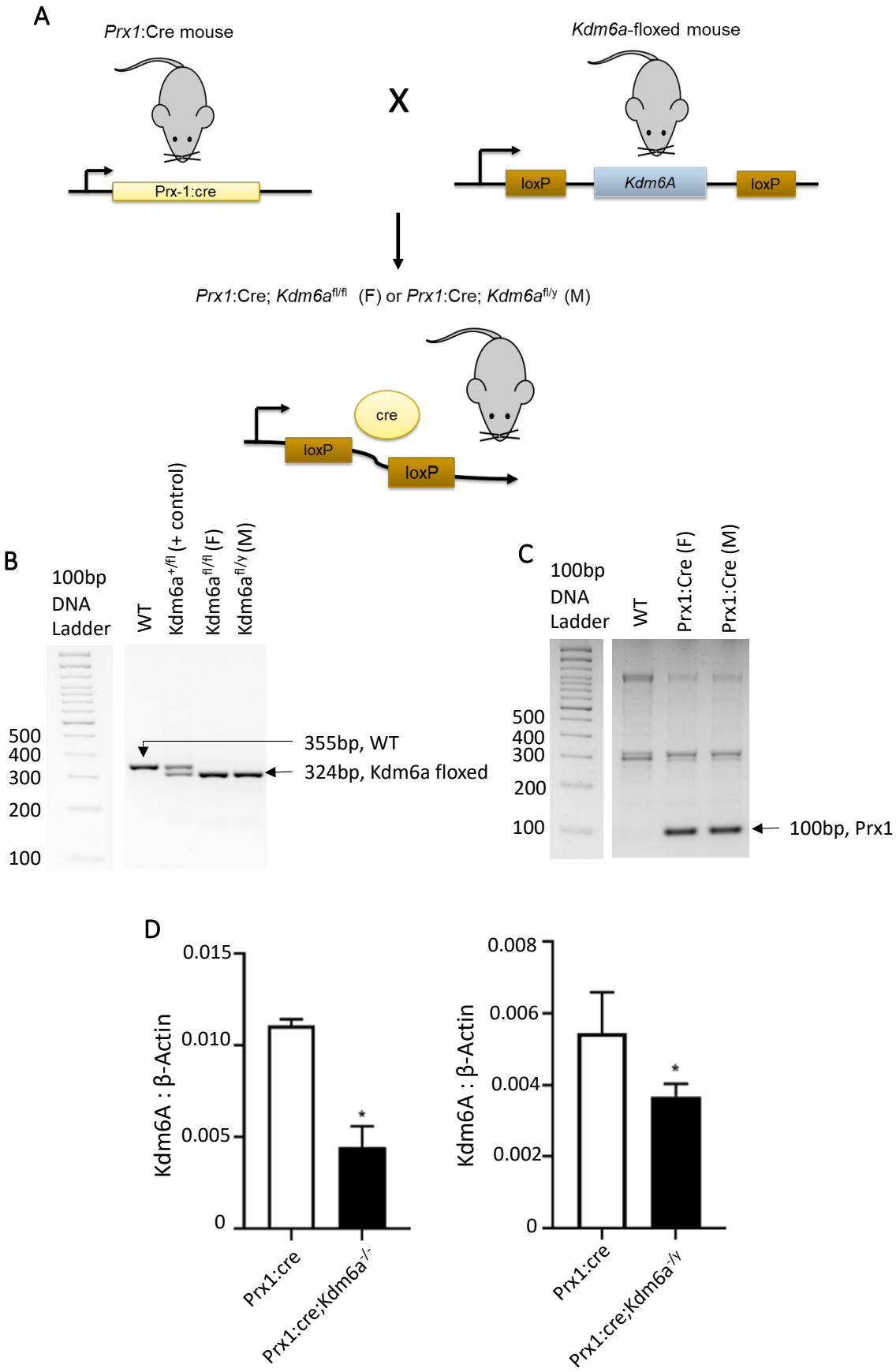
A
Prx1:Cre mouse
Kdm6a-floxed mouse
X
Prx-1:cre
loxP
Kdm6A
loxP
Prx1:Cre; Kdm6a fl/fl (F) or Prx1:Cre; Kdm6a fl/y (M)
cre
loxP
loxP
B
100bp DNA Ladder
WT
Kdm6a +/fl (+ control)
Kdm6a fl/fl (F)
Kdm6a fl/y (M)
500
400
300
200
100
355bp, WT
324bp, Kdm6a floxed
C
100bp DNA Ladder
WT
Prx1:Cre (F)
Prx1:Cre (M)
500
400
300
200
100
100bp, Prx1
D
Kdm6A : β-Actin
0.015
0.010
0.005
0
Prx1:cre
Prx1:cre;Kdm6a -/-
Kdm6A : β-Actin
0.008
0.006
0.004
0.002
0
Prx1:cre
Prx1:cre;Kdm6a -/y

Figure 5.2.1. *Kdm6a* conditional knockout model using *Prx-1* driver. (A) Cross breeding flow chart of *Kdm6a*-floxed mouse colony with *Prx1*:cre mice, resulting in *Prx1*:cre;*Kdm6a*$^{-/-}$ female and *Prx1*:cre;*Kdm6a*$^{-/y}$ male mice. Genotyping results of *Kdm6a* conditional knockout mouse samples using (B) *Kdm6a* and (C) *Prx1* primer sets. (D) Gene expression levels of *Kdm6a* in calvarial cells extracted from *Prx1*:cre;*Kdm6a*$^{-/-}$ and *Prx1*:cre;*Kdm6a*$^{-/y}$ mice and sex-matched *Prx1*:cre control mice, cultured in growth media and analysed with real-time qPCR, normalised to *β-Actin.* Data represent mean ± S.E. expression, *$p \leq 0.05$, two-tailed, unpaired, student's t-test, n=3 per group.

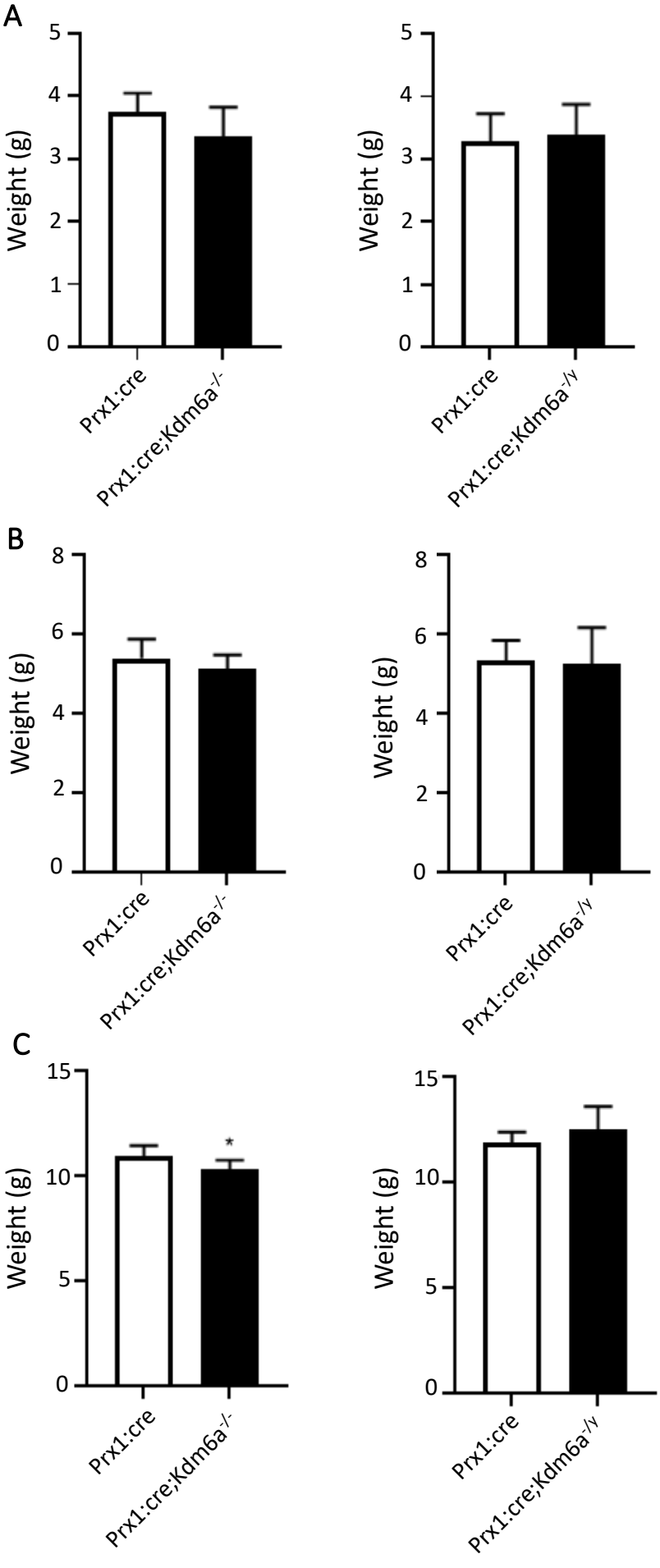
A
Weight (g)
0
1
2
3
4
5
Prx1:cre
Prx1:cre;Kdm6a-/-
Prx1:cre;Kdm6a-/y
B
Weight (g)
0
2
4
6
8
Prx1:cre
Prx1:cre;Kdm6a-/-
Prx1:cre;Kdm6a-/y
C
Weight (g)
0
5
10
15
*
Prx1:cre
Prx1:cre;Kdm6a-/-
Prx1:cre;Kdm6a-/y

Figure 5.2.2. Conditional knock out of *Kdm6a* does not significantly affect the body weight of postnatal 9 day old (P9) and P15 mice, but reduces the weight of P25 female mice. Weight analysis of (A) P9, (B) P15 and (C) P25 female *Prx1*:cre*;Kdm6a*$^{-/-}$ and (B) male *Prx1*:cre*;Kdm6a*$^{-/y}$ knockout mice compared to the gender-respective *Prx1*:cre controls. Data represent mean ± S. E, *p ≤ 0.05, two-tailed, unpaired, student's t-test, n=6 per group.

5.2.2 The loss of Kdm6a in suture mesenchyme changes the dimensions of the calvaria during mouse development.

As the majority of the craniofacial bones are derived from the suture mesenchyme via intramembranous ossification (Jiang et al. 2002; Rice, Rice & Thesleff 2003), the effects of the loss of *Kdm6a* within the suture mesenchyme population on craniofacial formation were investigated. The quantitative analyses of the calvaria form was performed using MIMICS software (Materialise NV, Belgium) to extract the morphometrics data based on specified calvarial landmarks. The calvaria of the MKO mice showed increased anterior and posterior width size at P9 (Table 5.2.1, Figure 5.2.3 & 5.2.5), increased anterior and posterior length at P15 (Table 5.2.2, Figure 5.2.6 & 5.2.8) and increased anterior width at P25 (Table 5.2.3, Figure 5.2.9 & 5.2.11). However, P9 and P15 FKO mice showed no significant differences in the calvarial width or length compared to age-matched female *Prx1*:cre controls (Table 5.2.1 & 5.2.2, Figure 5.2.3, 5.2.4 & Figure 5.2.6, 5.2.7). In P25 FKO mice, the anterior calvarial width and length were increased, whereas the posterior length was decreased (Table 5.2.3, Figure 5.2.9 & 5.2.10). The differential changes of calvarial formation for both FKO and MKO mice during development suggested the importance of *Kdm6a* expression within the suture mesenchyme population required for correct calvarial patterning.

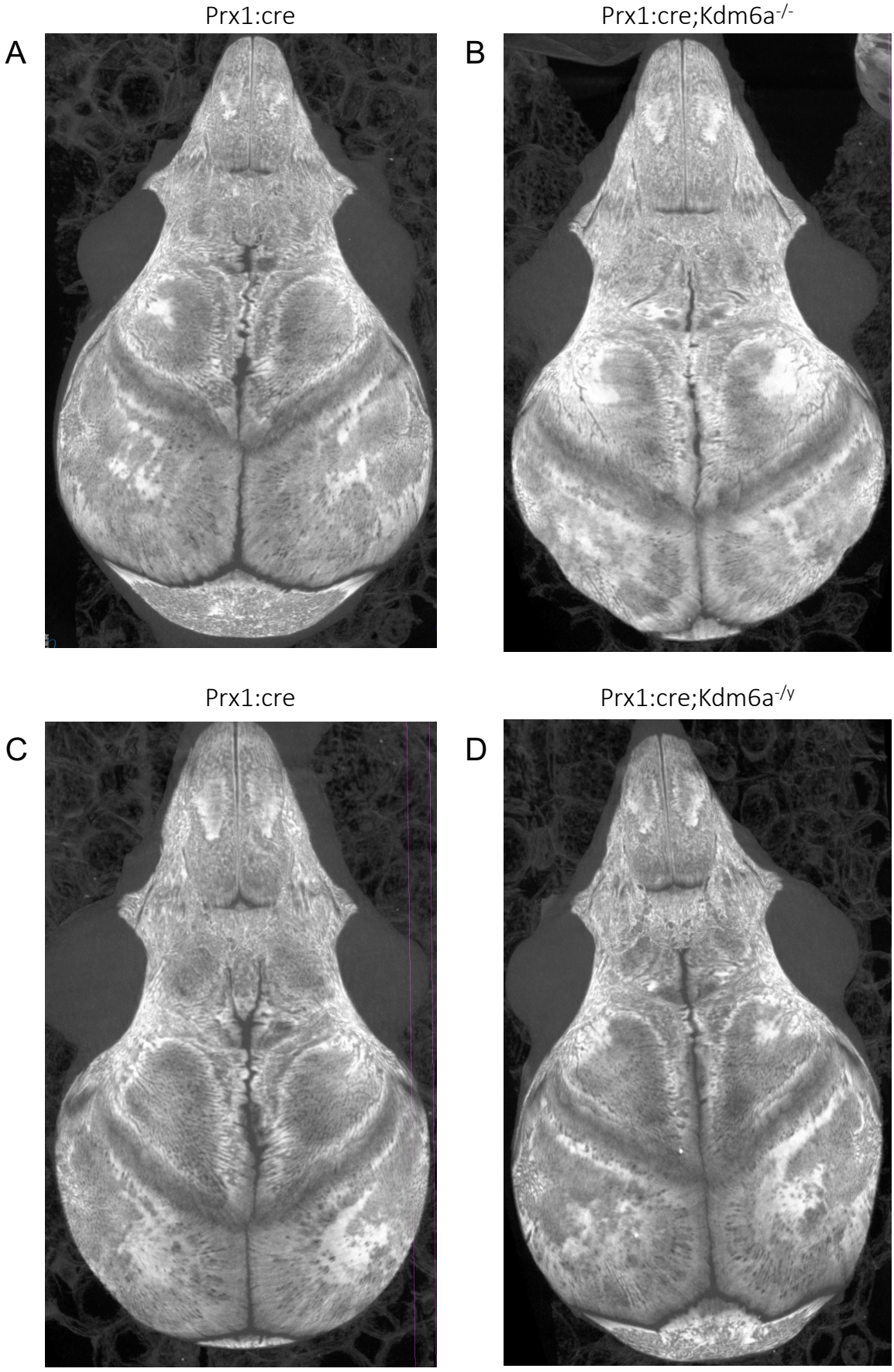
Prx1:cre
Prx1:cre;Kdm6a-/-
A
B
Prx1:cre
Prx1:cre;Kdm6a-/y
C
D

Figure 5.2.3. P9 *Kdm6a*-knockout calvaria do not visually differ from *Prx1*:cre control. Representative CTVox images from an overhead view generated from Micro CT analysis of the whole calvaria from P9 female (A) *Prx1*:cre control and (B) *Prx1*:cre*;Kdm6a*$^{-/-}$ conditional knockout mice, and from P9 male (C) *Prx1*:cre control and (D) *Prx1*:cre*;Kdm6a*$^{-/y}$ conditional knockout mice.

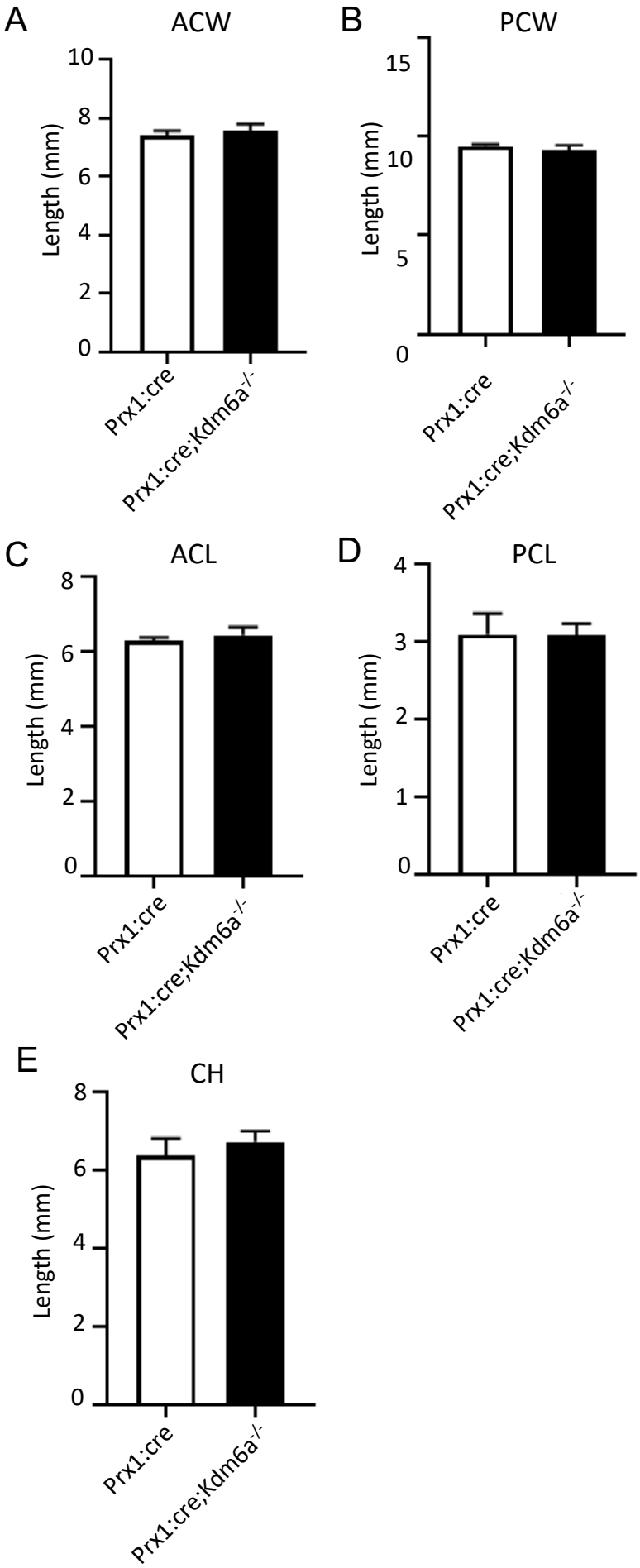
A
ACW
Length (mm)
10
8
6
4
2
0
Prx1:cre
Prx1:cre;Kdm6a-/-
B
PCW
Length (mm)
15
10
5
0
Prx1:cre
Prx1:cre;Kdm6a-/-
C
ACL
Length (mm)
8
6
4
2
0
Prx1:cre
Prx1:cre;Kdm6a-/-
D
PCL
Length (mm)
4
3
2
1
0
Prx1:cre
Prx1:cre;Kdm6a-/-
E
CH
Length (mm)
8
6
4
2
0
Prx1:cre
Prx1:cre;Kdm6a-/-

Figure 5.2.4. Conditional knockout of *Kdm6a* does not affect the calvaria morphometry of P9 female mice. Micro CT images of P9 *Prx1*:cre;*Kdm6a*$^{-/-}$ female mouse skulls were converted to a 3D structure by MIMICS Suite and morphometric analysis of (A) the Anterior Calvaria Width (ACW), (B) the Posterior Calvaria Width (PCW), (C) the Anterior Calvaria Length (ACL), (D) the Posterior Calvaria Length (PCL) and (E) the Calvaria Height (CH), were quantitated, compared to *Prx1*:cre control. Data represent mean ± S. E, *$p \leq 0.05$, two-tailed, unpaired, student's t-test, n=6 per group.

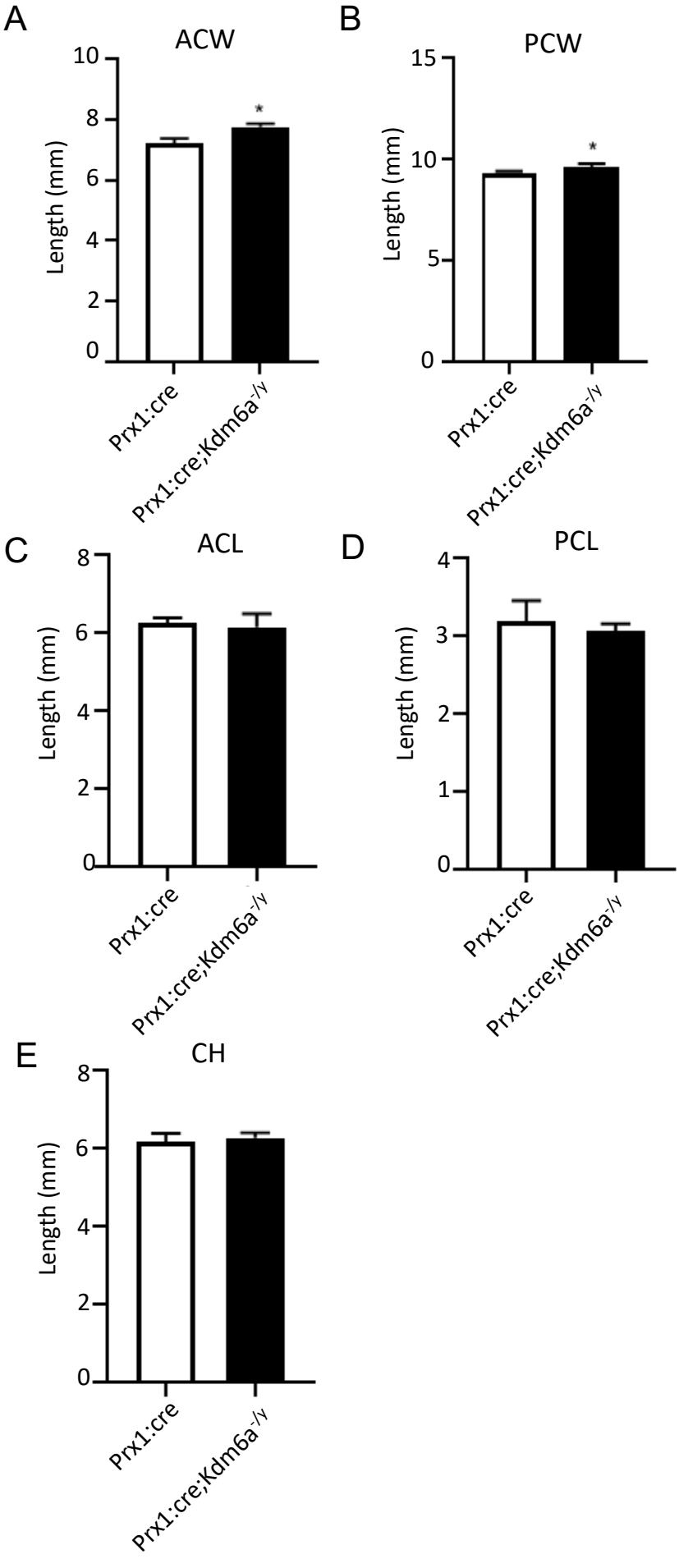
A
ACW
Length (mm)
10
8
6
4
2
0
*
Prx1:cre
Prx1:cre;Kdm6a-/y
B
PCW
Length (mm)
15
10
5
0
*
Prx1:cre
Prx1:cre;Kdm6a-/y
C
ACL
Length (mm)
8
6
4
2
0
Prx1:cre
Prx1:cre;Kdm6a-/y
D
PCL
Length (mm)
4
3
2
1
0
Prx1:cre
Prx1:cre;Kdm6a-/y
E
CH
Length (mm)
8
6
4
2
0
Prx1:cre
Prx1:cre;Kdm6a-/y

Figure 5.2.5. Conditional knockout of *Kdm6a* affects the calvaria width of P9 male mice compared to controls. Quantitative analysis of P9 *Prx1*:cre*;Kdm6a*$^{-/y}$ male (A) Anterior Calvaria Width (ACW), (B) Posterior Calvaria Width (PCW), (C) Anterior Calvaria Length (ACL), (D) Posterior Calvaria Length (PCL) and (E) Calvaria Height (CH) were generated from a 3D construct on the MIMICS software, compared to *Prx1*:cre control. Data represent mean ± S. E, *p ≤ 0.05, two-tailed, unpaired, student's t-test, n=6 per group.

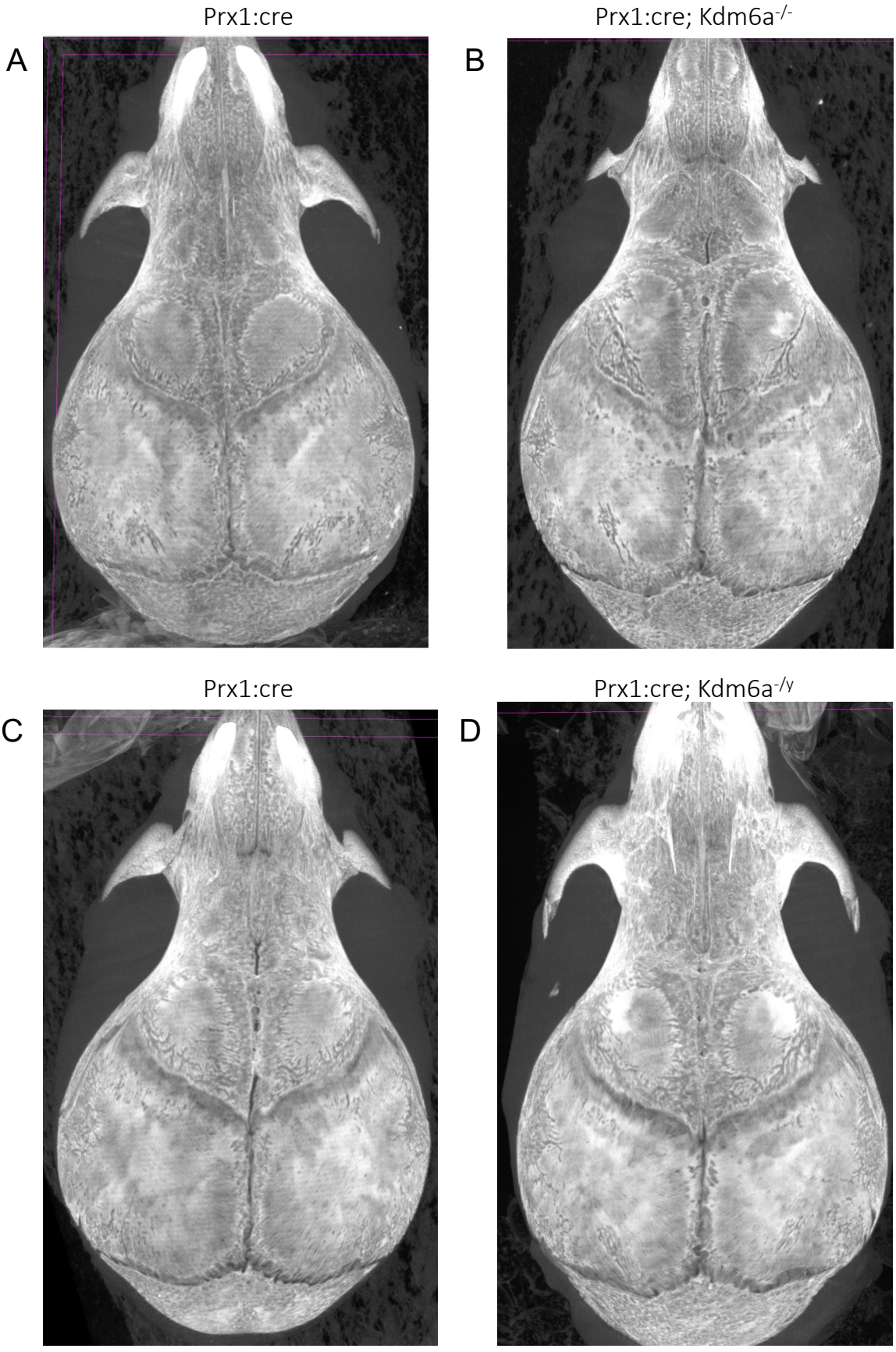
A
Prx1:cre
B
Prx1:cre; Kdm6a-/-
C
Prx1:cre
D
Prx1:cre; Kdm6a-/y

Figure 5.2.6. The visual morphometry of P15 *Kdm6a*-knockout calvaria do not differ from *Prx1*:cre control. Representative overhead images of the calvaria from P15 female (A) *Prx1*:cre control and (B) *Prx1*:cre*;Kdm6a*$^{-/-}$ knockout mice and from P15 male (C) *Prx1*:cre control and (D) *Prx1*:cre*;Kdm6a*$^{-/y}$ knockout mice were generated using CTVox software using reconstructed MicroCT scans.

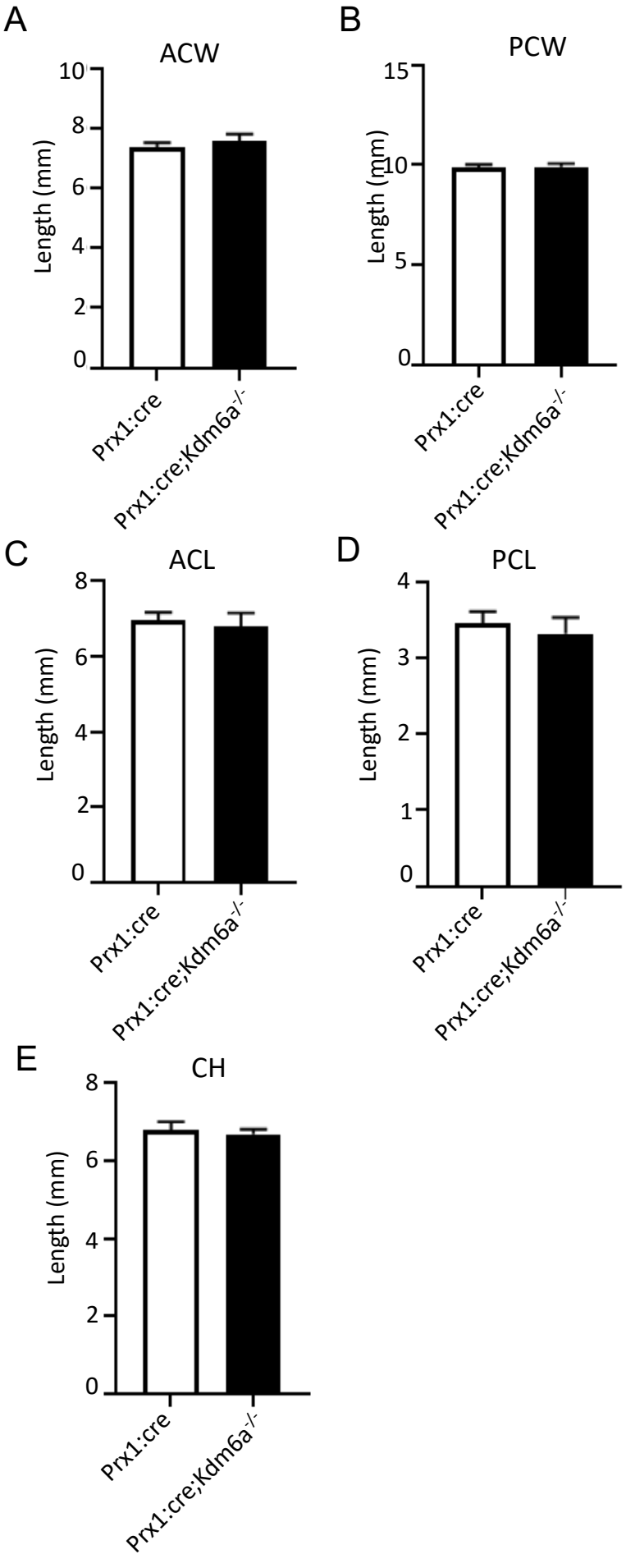
A
ACW
Length (mm)
10
8
6
4
2
0
Prx1:cre
Prx1:cre;Kdm6a-/-
B
PCW
Length (mm)
15
10
5
0
Prx1:cre
Prx1:cre;Kdm6a-/-
C
ACL
Length (mm)
8
6
4
2
0
Prx1:cre
Prx1:cre;Kdm6a-/-
D
PCL
Length (mm)
4
3
2
1
0
Prx1:cre
Prx1:cre;Kdm6a-/-
E
CH
Length (mm)
8
6
4
2
0
Prx1:cre
Prx1:cre;Kdm6a-/-

Figure 5.2.7. Conditional loss of *Kdm6a* does not affect the calvaria morphometry of P15 female mice. Three-dimensional Micro CT structure of P15 female *Prx1*:cre;*Kdm6a*$^{-/-}$ calvaria were generated by MIMICS software, and morphometric analysis of (A) the anterior calvaria width (ACW), (B) the Posterior Calvaria Width (PCW), (C) the Anterior Calvaria Length (ACL), (D) the Posterior Calvaria Length (PCL) and (E) the Calvaria Height (CH), were quantitated and compared to *Prx1*:cre control. Data represent mean ± S. E, *p ≤ 0.05, two-tailed, unpaired, student's t-test, n=6 per group.

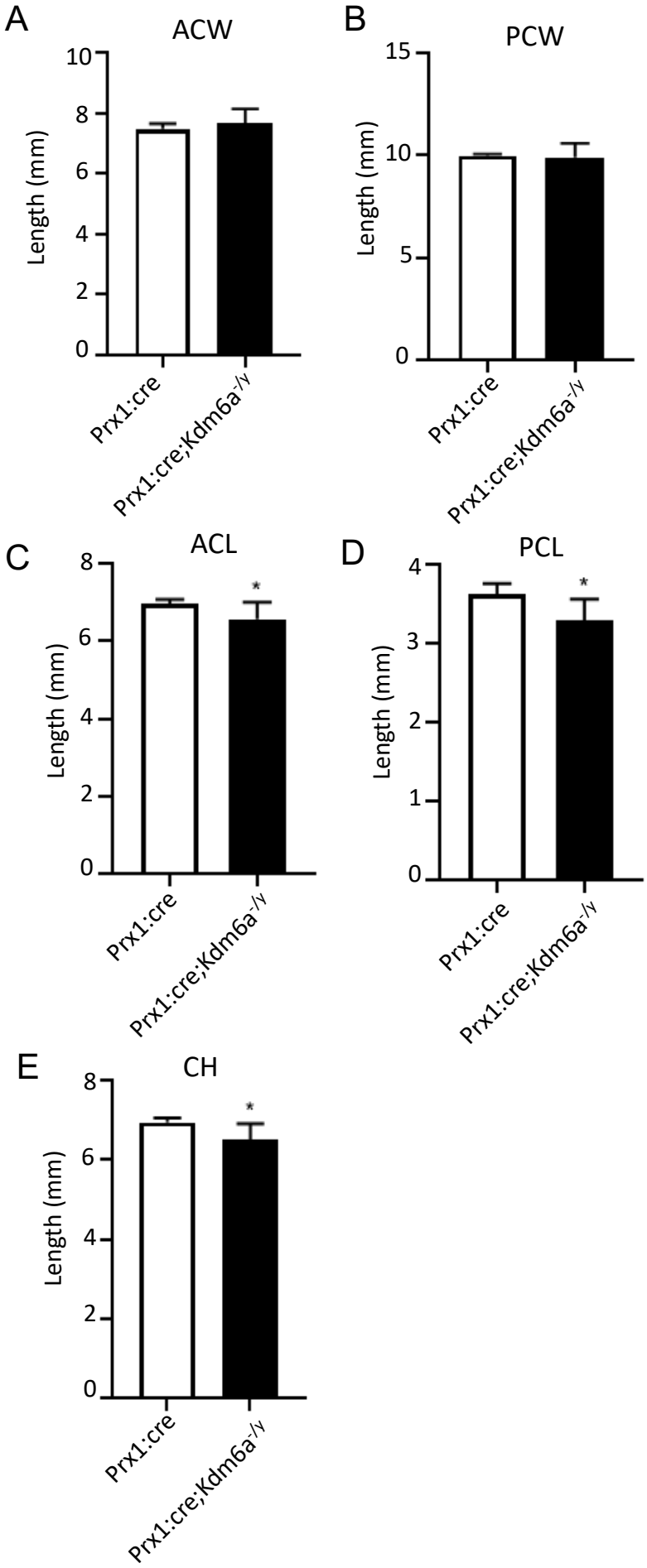
A
ACW
Length (mm)
10
8
6
4
2
0
Prx1:cre
Prx1:cre;Kdm6a-/y
B
PCW
Length (mm)
15
10
5
0
Prx1:cre
Prx1:cre;Kdm6a-/y
C
ACL
Length (mm)
8
6
4
2
0
*
Prx1:cre
Prx1:cre;Kdm6a-/y
D
PCL
Length (mm)
4
3
2
1
0
*
Prx1:cre
Prx1:cre;Kdm6a-/y
E
CH
Length (mm)
8
6
4
2
0
*
Prx1:cre
Prx1:cre;Kdm6a-/y

Figure 5.2.8. Conditional Kdm6a loss changes the calvaria length and height of P15 male compared to control. Quantitative analysis by MIMICS on Micro CT images of (A) the Anterior Calvaria Width (ACW), (B) the Posterior Calvaria Width (PCW), (C) the Anterior Calvaria Length (ACL), (D) the Posterior Calvaria Length (PCL) and (E) the Calvaria Height (CH) of 15-days-old *Prx1*:cre;*Kdm6a*$^{-/y}$ compared to *Prx1*:cre control. Data represent mean ± S. E, *p ≤ 0.05, two-tailed, unpaired, student's t-test, n=6 per group.

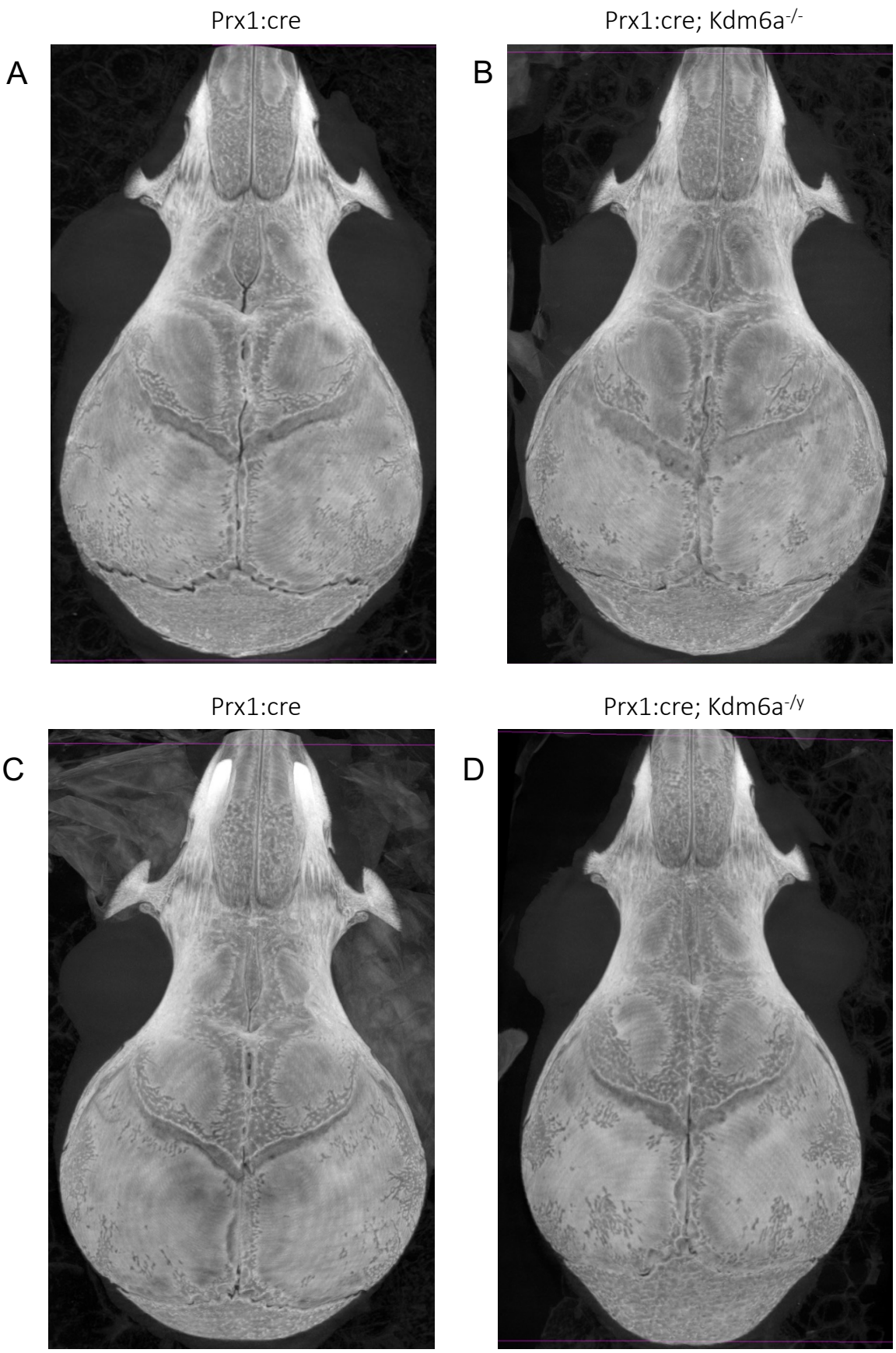
Prx1:cre
Prx1:cre; Kdm6a-/-
A
B
Prx1:cre
Prx1:cre; Kdm6a-/y
C
D

Figure 5.2.9. The calvaria of P25 *Kdm6a*-knockout mice are not visually different from *Prx1*:cre control calvaria. Representative overhead CTVox images of reconstructed MicroCT scans of the calvaria from P25 female (A) *Prx1*:cre control and (B) *Prx1*:cre;*Kdm6a*$^{-/-}$ knockout mice and from P25 (C) *Prx1*:cre control and (D) *Prx1*:cre;*Kdm6a*$^{-/y}$ knockout mice.

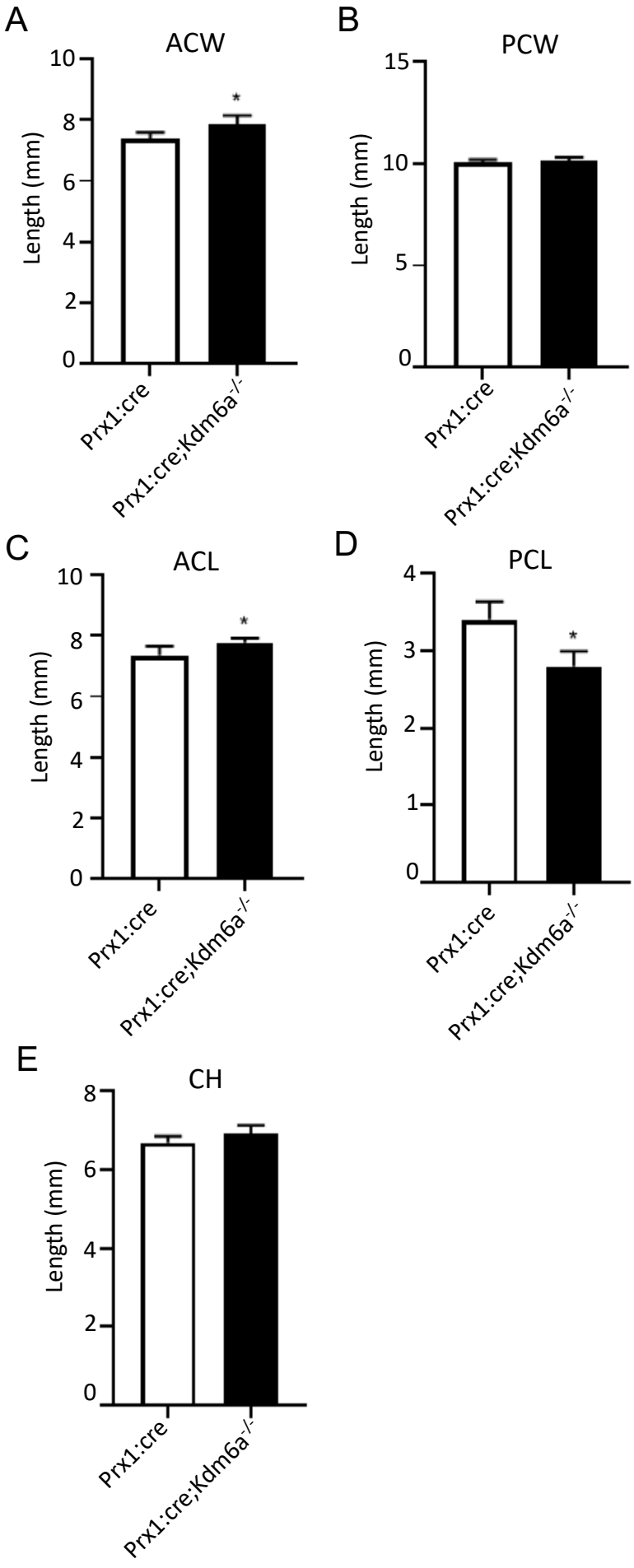
A
ACW
Length (mm)
10
8
6
4
2
0
*
Prx1:cre
Prx1:cre;Kdm6a-/-
B
PCW
Length (mm)
15
10
5
0
Prx1:cre
Prx1:cre;Kdm6a-/-
C
ACL
Length (mm)
10
8
6
4
2
0
*
Prx1:cre
Prx1:cre;Kdm6a-/-
D
PCL
Length (mm)
4
3
2
1
0
*
Prx1:cre
Prx1:cre;Kdm6a-/-
E
CH
Length (mm)
8
6
4
2
0
Prx1:cre
Prx1:cre;Kdm6a-/-

Figure 5.2.10. Loss of *Kdm6a* within the suture mesenchyme changes the calvaria width and length of P25 female mice. Reconstructed Micro CT images of P25 *Prx1*:cre *Kdm6a*$^{-/-}$ female were converted to a 3D structure by MIMICS Suite software. Quantitative morphometric analysis of (A) the Anterior Calvaria Width (ACW), (B) the Posterior Calvaria Width (PCW), (C) the Anterior Calvaria Length (ACL), (D) the Posterior Calvaria Length (PCL) and (E) the Calvaria Height (CH) compared to *Prx1*:cre control were generated using MIMICS, according to established calvaria landmarks. Data represent mean ± S. E, *$p \leq 0.05$, two-tailed, unpaired, student's t-test, n=6 per group.

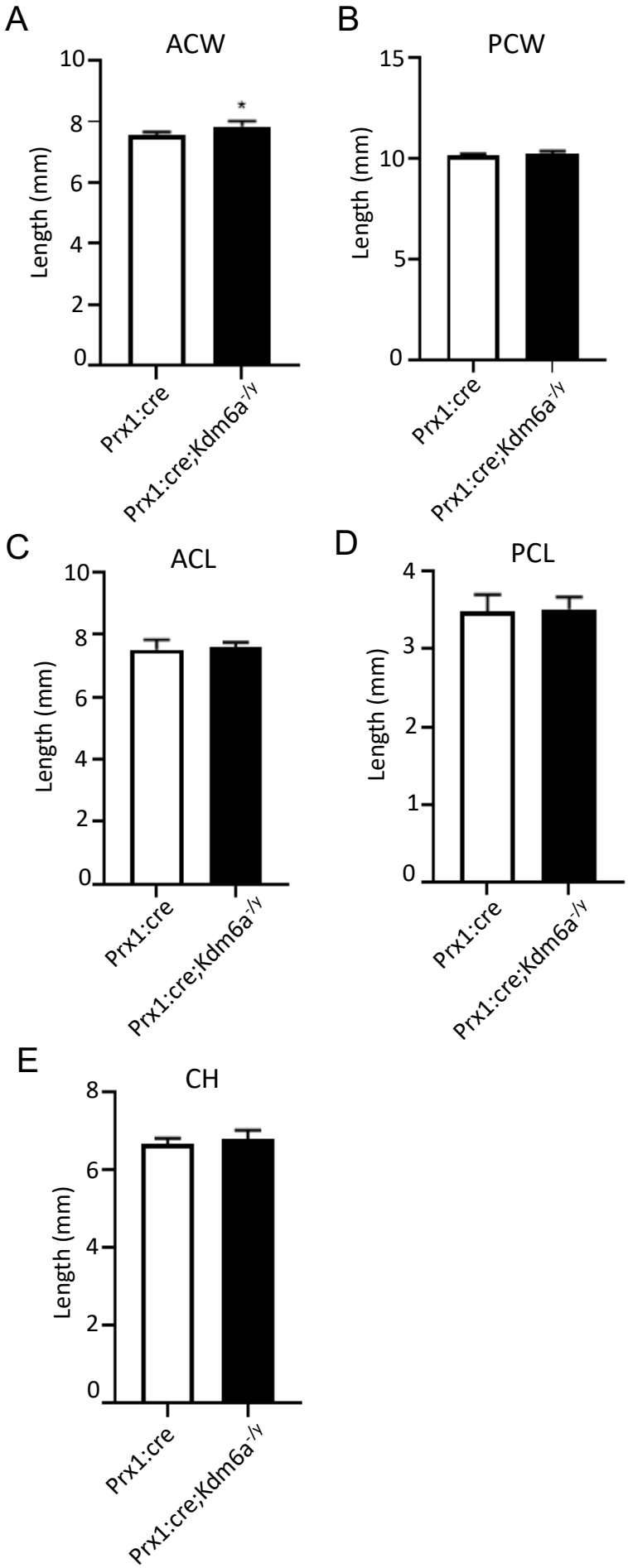
A
ACW
Length (mm)
10
8
6
4
2
0
*
Prx1:cre
Prx1:cre;Kdm6a-/y
B
PCW
Length (mm)
15
10
5
0
Prx1:cre
Prx1:cre;Kdm6a-/y
C
ACL
Length (mm)
10
8
6
4
2
0
Prx1:cre
Prx1:cre;Kdm6a-/y
D
PCL
Length (mm)
4
3
2
1
0
Prx1:cre
Prx1:cre;Kdm6a-/y
E
CH
Length (mm)
8
6
4
2
0
Prx1:cre
Prx1:cre;Kdm6a-/y

Figure 5.2.11. Conditional Kdm6a loss changes the calvaria width of P25 male mice compared to *Prx1:cre* control. Morphometric quantitative analysis with MIMICS software of (A) the Anterior Calvaria Width (ACW), (B) the Posterior Calvaria Width (PCW), (C) the Anterior Calvaria Length (ACL), (D) the Posterior Calvaria Length (PCL) and (E) the Calvaria Height (CH) on reconstructed Micro CT scans of P25 *Prx1*:cre control and *Prx1*:cre;*Kdm6a*$^{-/y}$ mice. Data represent mean ± S. E, *p ≤ 0.05, two-tailed, unpaired, student's t-test, n=6 per group.

Table 5.2.1. Loss of *Kdm6a* alters the calvaria width of P9 male mice. Quantitative analysis of P9 female *Prx1:cre;Kdm6a*$^{-/-}$ and male *Prx1:cre;Kdm6a*$^{-/y}$ (A) anterior calvaria width (ACW), (B) Posterior Calvaria Width (PCW), (C) Anterior Calvaria Length (ACL), (D) Posterior Calvaria Length (PCL) and (E) Calvaria Height (CH), compared to *Prx1:cre* control. Data represent asterisk (*) as statistically significant value with $p \leq 0.05$ and dash (-) as not statistically significant value, based on two-tailed, unpaired, student's t-test, n=6 per group.

Morphometric Landmarks	**ACW**	**PCW**	**ACL**	**PCL**	**CH**
Prx1:cre;*Kdm6a*$^{-/-}$	-	-	-	-	-
Prx1:cre;*Kdm6a*$^{-/y}$	*	*	-	-	-

Table 5.2.2. Loss of Kdm6a alters the calvaria length of P15 male mice. Quantitative analysis of P9 female *Prx1*:cre*;Kdm6a*$^{-/-}$ and male *Prx1*:cre*;Kdm6a*$^{-/y}$ (A) anterior calvaria width (ACW), (B) Posterior Calvaria Width (PCW), (C) Anterior Calvaria Length (ACL), (D) Posterior Calvaria Length (PCL) and (E) Calvaria Height (CH), compared to control. Data represent asterisk (*) as statistically significant value with $p \leq 0.05$ and dash (-) as not statistically significant value, based on two-tailed, unpaired, student's t-test, n=6 per group.

Morphometric Landmarks	**ACW**	**PCW**	**ACL**	**PCL**	**CH**
*Prx1:*cre;*Kdm6a*$^{-/-}$	-	-	-	-	-
Prx1:cre;*Kdm6a*$^{-/y}$	-	-	*	*	*

Table 5.2.3. Loss of Kdm6a alters the calvaria shape of P25 female and male mice. Quantitative analysis of P9 female *Prx1*:Cre*;Kdm6a*$^{-/-}$ and male *Prx1*:Cre*;Kdm6a*$^{-/y}$ (A) anterior calvaria width (ACW), (B) Posterior Calvaria Width (PCW), (C) Anterior Calvaria Length (ACL), (D) Posterior Calvaria Length (PCL) and (E) Calvaria Height (CH), compared to *Prx1*:cre control. Data represent asterisk (*) as statistically significant value with $p \leq 0.05$ and dash (-) as not statistically significant value, based on two-tailed, unpaired, student's t-test, n=6 per group.

Morphometric Landmarks	**ACW**	**PCW**	**ACL**	**PCL**	**CH**
Prx1:cre;*Kdm6a*$^{-/-}$	*	-	*	*	-
Prx1:cre;*Kdm6a*$^{-/y}$	*	-	-	-	-

5.2.3 Kdm6a is not essential in early suture and calvarial bone formation but promotes late suture development and bone formation in female mice.

The present chapter investigated the effects of *Kdm6a* loss on the formation of the posterior interfrontal (PIF) suture as the only naturally fusing calvarial suture in wild type mice, by quantitating the volume and thickness of the parietal bones surrounding the suture area. The percentages of bone volume and bone surface area of the suture regions were analysed using Micro-CT to assess the role of Kdm6a at the start of PIF endocranial suture ossification (P9), at fusion completion (P15) and after suture fusion (P25). The ectocranial suture remains open throughout adulthood. The levels of bone volume and surface area at P9 and P15 mice were similar between FKO and MKO and age and gender-matched *Prx1*:cre controls (Figure 5.2.12 & 5.2.13, Figure 5.2.14 & 5.2.15). However, in P25 FKO mice, the PIF suture fusion points were reduced, and the bone volume and surface area were significantly decreased compared to *Prx1*:cre controls (Figure 5.2.16). On the other hand, the suture formation appeared accelerated in P25 MKO mice, and the calvarial bone volume and surface levels were elevated compared to *Prx1*:cre controls (Figure 5.2.17). These results further confirmed that the effects of *Kdm6a* knockout differ between FKO and MKO mice.

Further studies assessed the cellular composition of P25 PIF sutures by staining coronal sections of the calvaria with Movat's Pentachrome stain, that identifies nuclei and elastic fibres in black, muscle fibres in red, collagen fibres in yellow, mucins produced by epithelial cells in bluish green and mineralised bone in red. The staining displayed an open and heterogenous cell population within the suture mesenchyme on the endocranial and ectocranial sites of the PIF suture in FKO mice, whereas fused endocranial sutures were observed in *Prx1*:cre control sections. On the other hand, both the PIF sutures of MKO and

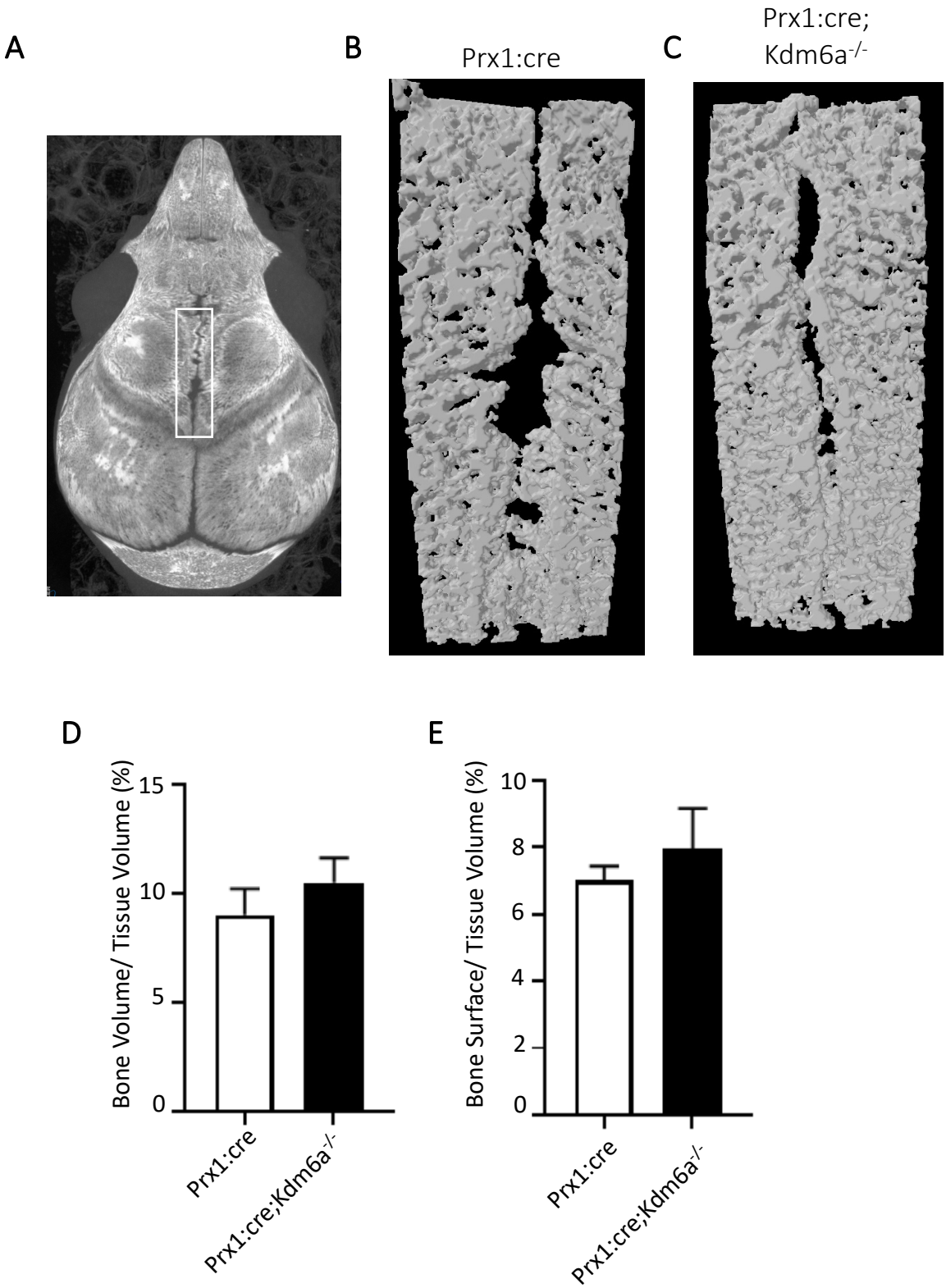
A
B
Prx1:cre
C
Prx1:cre;
Kdm6a-/-
D
Bone Volume/ Tissue Volume (%)
15
10
5
0
Prx1:cre
Prx1:cre;Kdm6a-/-
E
Bone Surface/ Tissue Volume (%)
10
8
6
4
2
0
Prx1:cre
Prx1:cre;Kdm6a-/-

Figure 5.2.12. *Kdm6a* is not essential in maintaining the calvaria bone density and surface area of the posterior interfrontal suture in P9 female mice. (A) The Region of Interest (ROI) covering the posterior interfrontal suture region of P9 female mice was selected in the CTan MicroCT analysis software, and indicated with the white rectangular box. Representative 3D volumes of the ROI generated by CTVol software of (B) *Prx1:cre* control and (C) *Prx1*:*cre*;*Kdm6a*$^{-/-}$ conditional knockout mice at P9. Quantitative analysis using an optimised threshold of the (D) bone volume and (E) bone surface normalised to tissue volume of the ROI of conditionally knockout female mice compared to control. Data represent mean ± S. E, *$p \leq 0.05$, two-tailed, unpaired, student's t-test, n=6 per group.

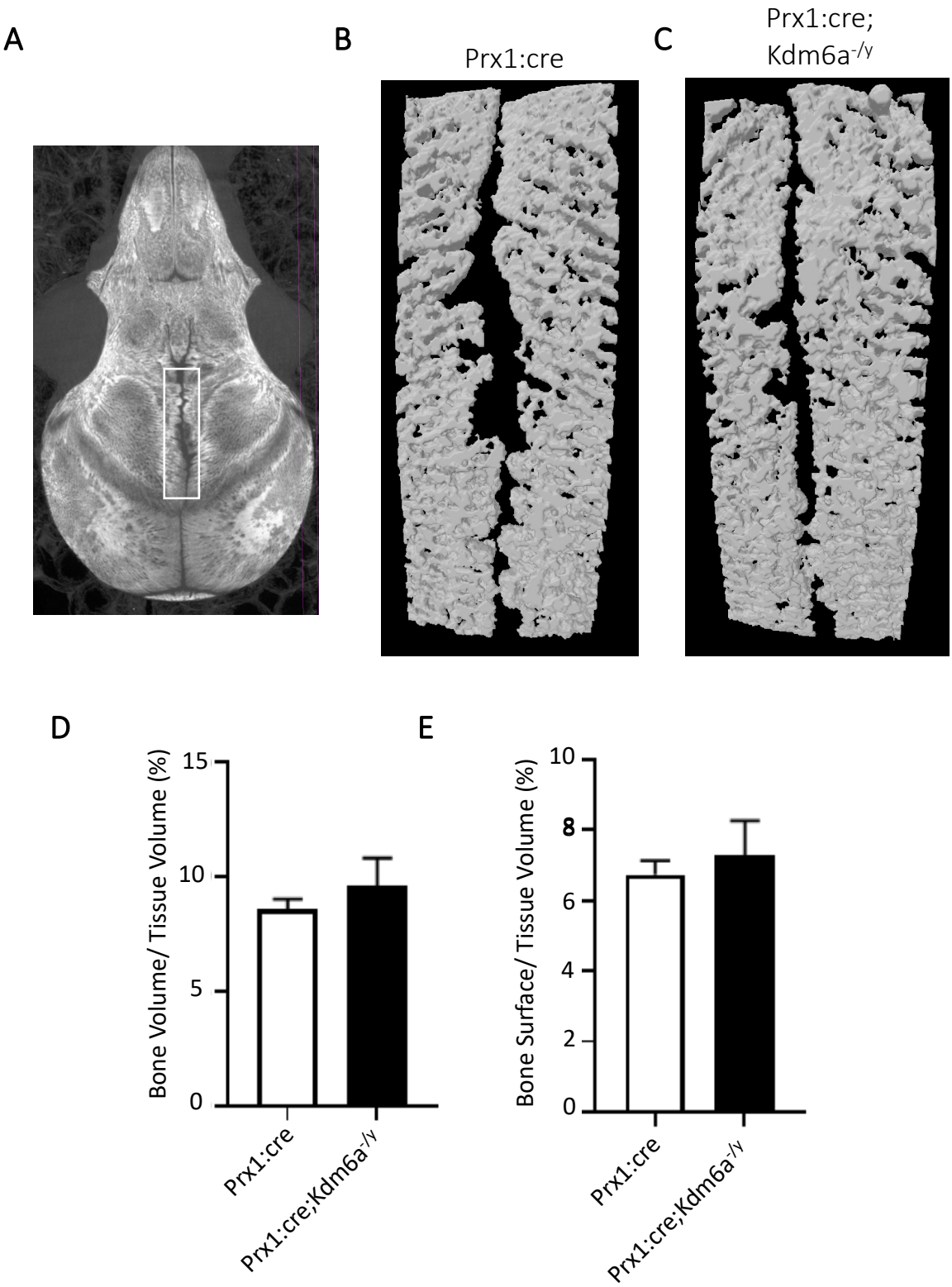
A
B
Prx1:cre
C
Prx1:cre;
Kdm6a-/y
D
Bone Volume/ Tissue Volume (%)
15
10
5
0
Prx1:cre
Prx1:cre;Kdm6a-/y
E
Bone Surface/ Tissue Volume (%)
10
8
6
4
2
0
Prx1:cre
Prx1:cre;Kdm6a-/y

Figure 5.2.13. *Kdm6a* is not essential in maintaining the calvaria bone density and surface area of the posterior interfrontal suture in P9 male mice. (A) The Region of Interest (ROI) indicated with the white rectangular box was selected on the posterior interfrontal suture region of P9 male mice using the CTan MicroCT analysis software. Representative 3D volumes of the ROI generated by CTVol software of the ROI of male (B) *Prx1*:cre control and (C) *Prx1*:cre;*Kdm6a*$^{-/y}$ conditional knockout mice. Quantitative analysis of the (D) bone volume and (E) bone surface normalised to tissue volume of the ROI of conditionally knockout male mice compared to control. Data represent mean ± S. E, *$p \leq 0.05$, two-tailed, unpaired, student's t-test, n=6 per group.

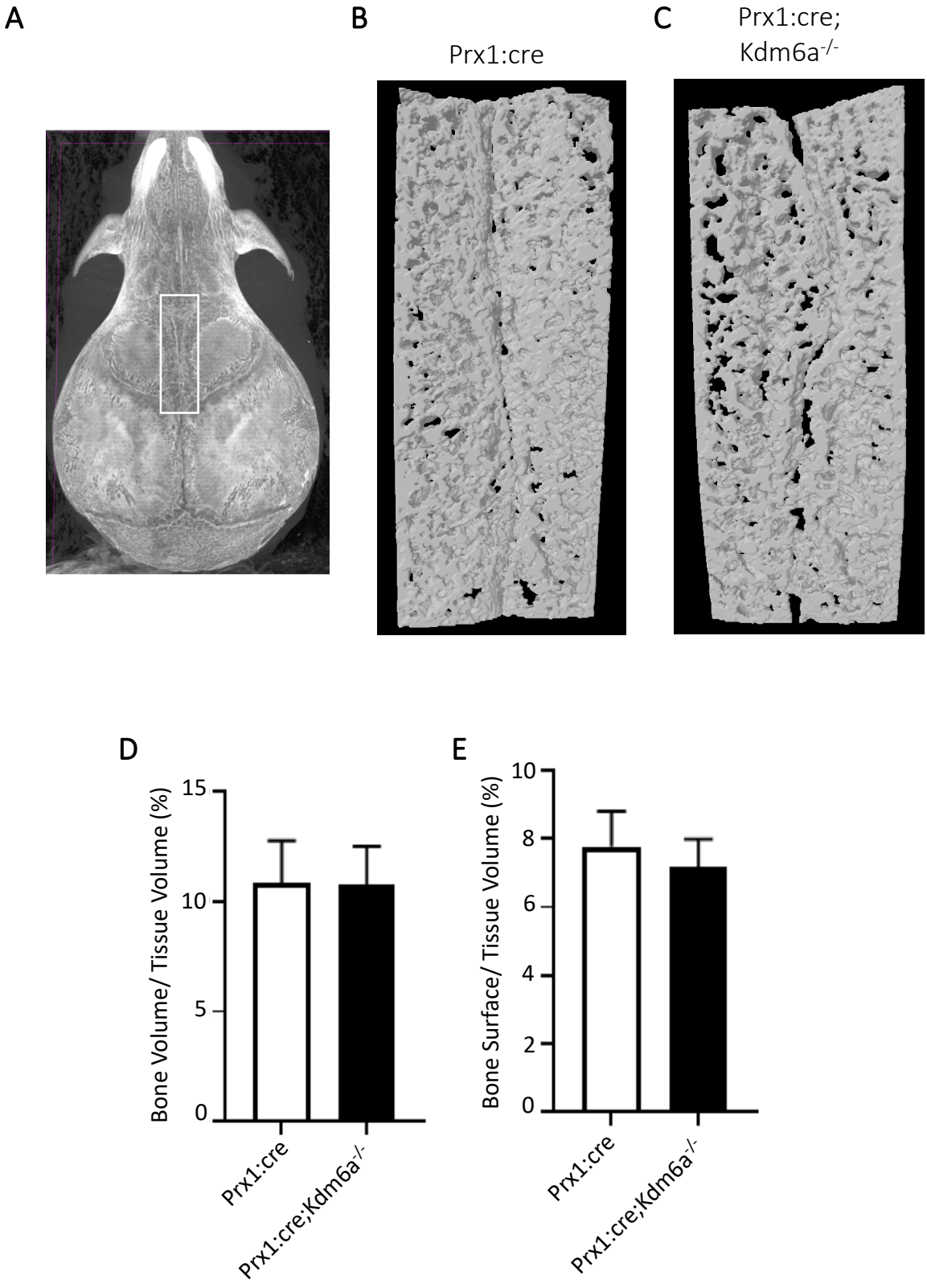
A
B
Prx1:cre
C
Prx1:cre;
Kdm6a-/-
D
Bone Volume/ Tissue Volume (%)
15
10
5
0
Prx1:cre
Prx1:cre;Kdm6a-/-
E
Bone Surface/ Tissue Volume (%)
10
8
6
4
2
0
Prx1:cre
Prx1:cre;Kdm6a-/-

Figure 5.2.14. *Kdm6a* is not essential in maintaining the calvaria bone density and surface area of the posterior interfrontal suture in P15 female mice. (A) The Region of Interest (ROI) of the posterior interfrontal suture of P15 female mice was created in CTan software, and indicated with the white rectangular box. Representative 3D volumes of the ROI generated by CTVol software of (B) *Prx1:cre* control and (C) *Prx1:cre;Kdm6a*$^{-/-}$ conditional knockout mice at P15. Quantitative analysis using an optimised threshold of the (D) bone volume and (E) bone surface normalised to tissue volume of the ROI of conditionally knockout female mice compared to control. Data represent mean ± S. E, *$p \leq 0.05$, two-tailed, unpaired, student's t-test, n=6 per group.

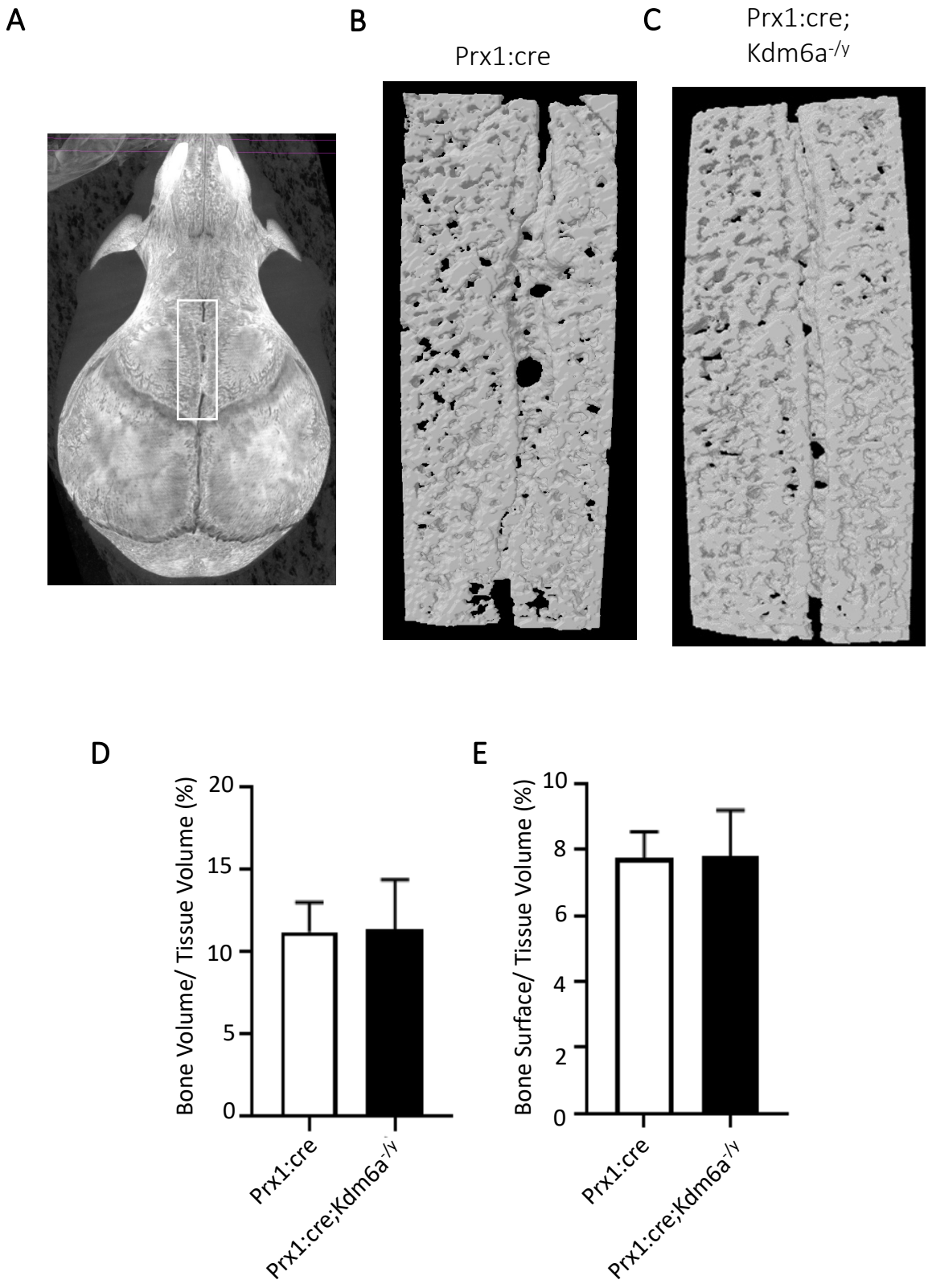
A
B
Prx1:cre
C
Prx1:cre;
Kdm6a-/y
D
Bone Volume/ Tissue Volume (%)
20
15
10
5
0
Prx1:cre
Prx1:cre;Kdm6a-/y
E
Bone Surface/ Tissue Volume (%)
10
8
6
4
2
0
Prx1:cre
Prx1:cre;Kdm6a-/y

Figure 5.2.15. *Kdm6a* is not essential in maintaining the calvaria bone density and surface area of the posterior interfrontal suture in P15 male mice. (A) The Region of Interest (ROI) indicated with the white rectangular box was selected to cover the posterior interfrontal suture area of P15 male mice using the CTan MicroCT analysis software. Representative 3D volumes of the ROI generated by CTVol software of the ROI of male (B) *Prx1:cre* control and (C) *Prx1:cre;Kdm6a*$^{-/y}$ conditional knockout mice. Quantitative analysis on CTan software of the (D) bone volume and (E) bone surface were normalised to tissue volume of the ROI of conditionally knockout male mice compared to control. Data represent mean ± S. E, *$p \leq 0.05$, two-tailed, unpaired, student's t-test, n=6 per group.

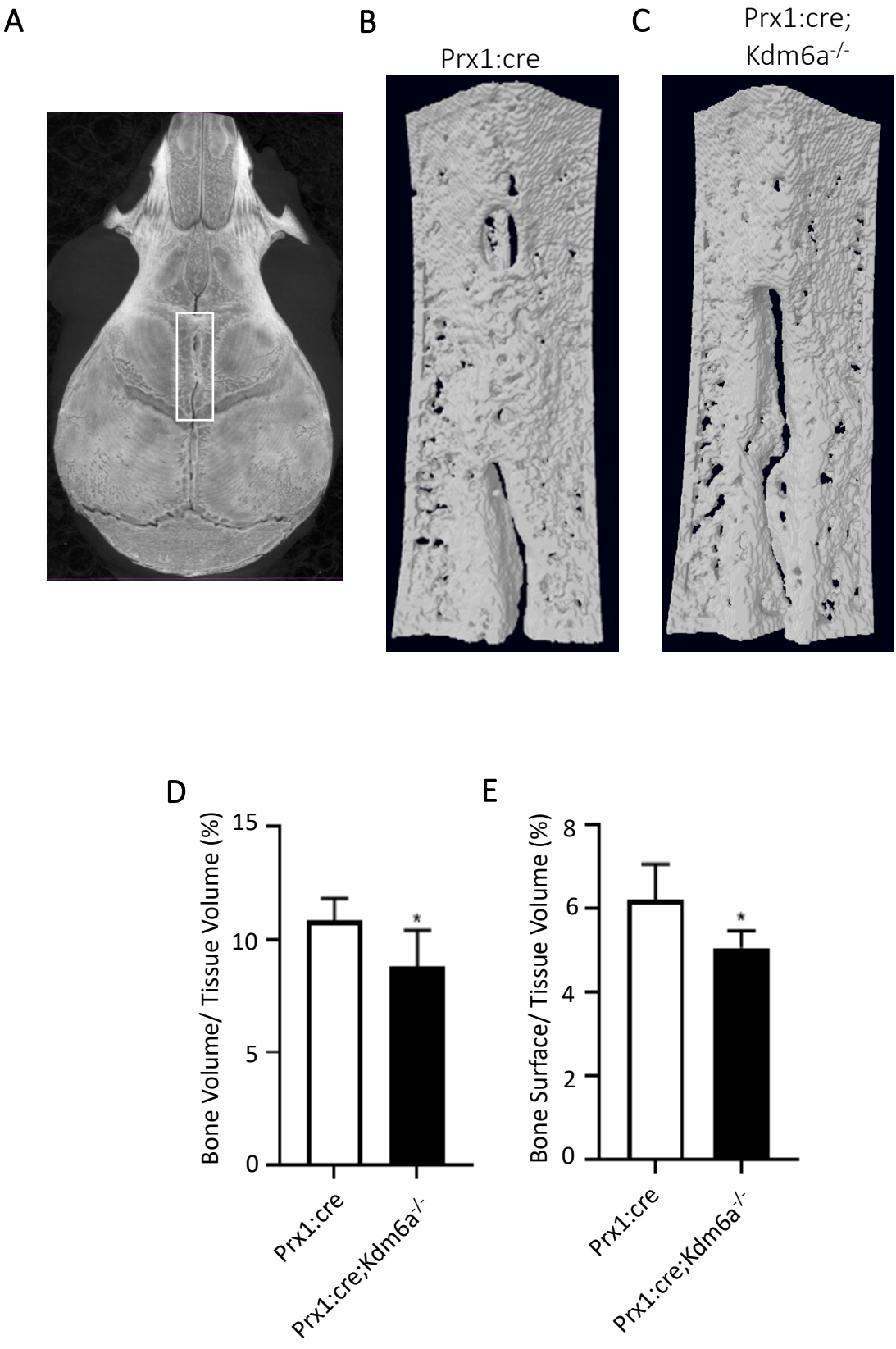
A
B
Prx1:cre
C
Prx1:cre;
Kdm6a-/-
D
Bone Volume/ Tissue Volume (%)
15
10
5
0
*
Prx1:cre
Prx1:cre;Kdm6a-/-
E
Bone Surface/ Tissue Volume (%)
8
6
4
2
0
*
Prx1:cre
Prx1:cre;Kdm6a-/-

Figure 5.2.16. *Kdm6a* promotes posterior interfrontal suture bone formation in P25 female mice. (A) The Region of Interest (ROI) of the posterior interfrontal suture area of P25 female mice was selected in CTan software, and indicated with the white rectangular box. Representative 3D volumes of the ROI generated by CTVol software of (B) *Prx1:cre* control and (C) *Prx1:cre;Kdm6a*$^{-/-}$ conditional knockout mice at P25. Quantitative analysis of the (D) bone volume and (E) bone surface normalised to tissue volume of the ROI using an optimised threshold in CTan of conditionally knockout female mice compared to female control. Data represent mean ± S. E, *$p \leq 0.05$, two-tailed, unpaired, student's t-test, n=6 per group.

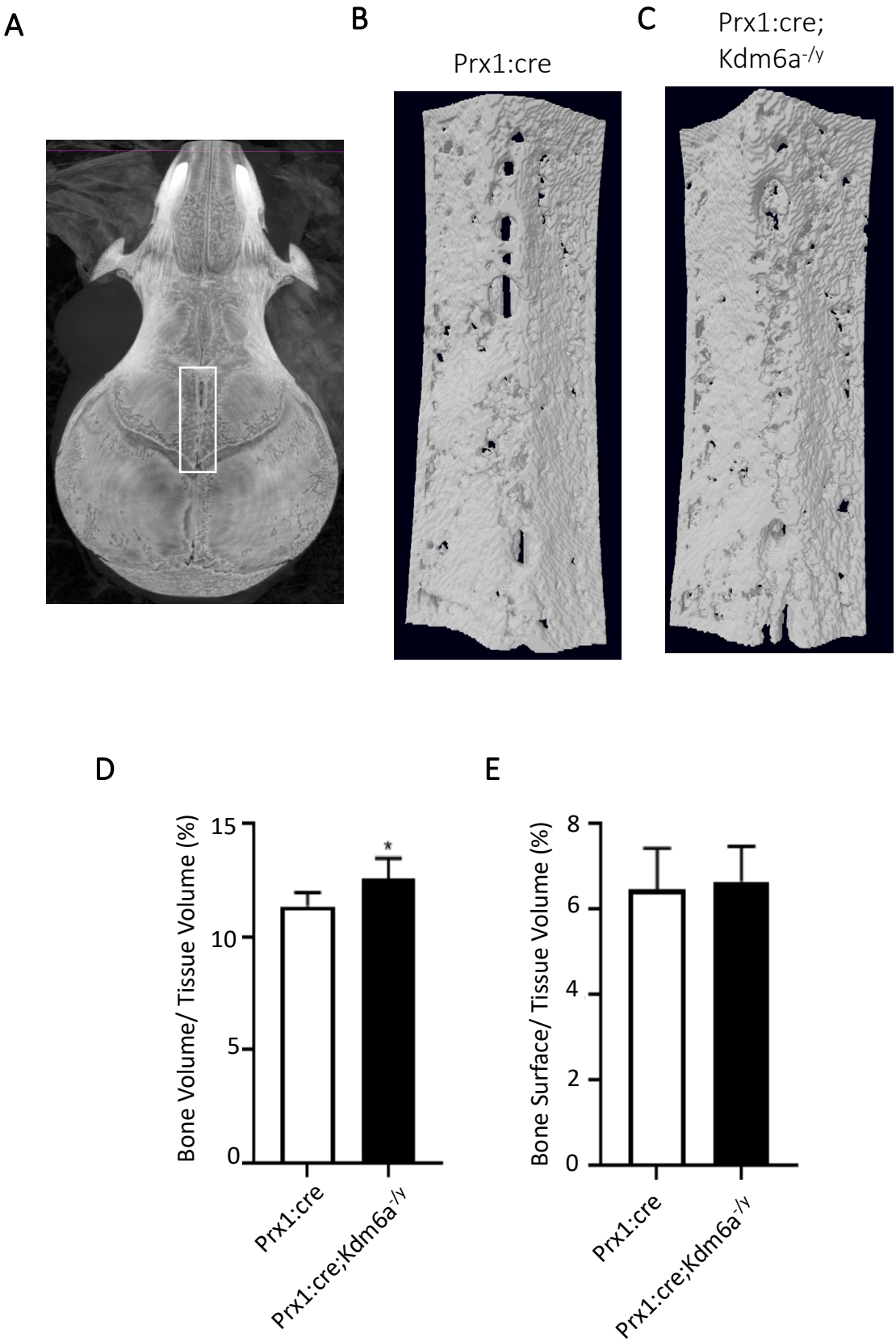
A
B
Prx1:cre
C
Prx1:cre;
Kdm6a-/y
D
Bone Volume/ Tissue Volume (%)
15
10
5
0
*
Prx1:cre
Prx1:cre;Kdm6a-/y
E
Bone Surface/ Tissue Volume (%)
8
6
4
2
0
Prx1:cre
Prx1:cre;Kdm6a-/y

Figure 5.2.17. *Kdm6a* loss in suture mesenchyme promotes posterior interfrontal suture bone formation in P25 male mice. (A) The Region of Interest (ROI) of the posterior interfrontal suture area of P25 male mice was selected in CTan software, and indicated with the white rectangular box. Representative 3D volumes of the ROI generated by CTVol software of (B) *Prx1:cre* control and (C) *Prx1:cre;Kdm6a*$^{-/y}$ conditional knockout mice at P25. Quantitative analysis of the (D) bone volume and (E) bone surface normalised to tissue volume of the ROI using an optimised threshold in CTan of conditionally knockout male mice compared to male control. Data represent mean ± S. E, *$p \leq 0.05$, two-tailed, unpaired, student's t test, n=6 per group.

Prx1:cre control showed total fusion of the endocranial PIF sutures, further suggesting a less severe effect of *Kdm6a* loss in MKO mice (Figure 5.2.18).

Since the calvarial bones forming the skull vault are derived from the MPC within the suture mesenchyme, it is hypothesised that the loss of *Kdm6a* in this population would affect the formation and maturation of the parietal bones surrounding the PIF sutures. To compare the amount of mineralised calvarial bones in P25 Kdm*6a* KO and *Prx1*:cre control mice, Masson's Trichrome staining, that identifies mineralised bone, muscle fibres and erythrocytes in red, collagen fibres in blue, and nuclei in black, was performed. The data showed significantly reduced mineralised bone formation and thickness in FKO, but not in MKO (Figure 5.2.19 & 5.2.20). These results provided confirmation that *Kdm6a* knockout affected the mineralisation of parietal bones in FKO mice differently than in MKO mice, suggesting a possible compensation from another member of the Kdm6 family.

5.2.4 Conditional loss of *Kdm6a* expression suppresses osteogenic differentiation capacity in mouse calvarial cells.

To investigate the underlying mechanisms of the reduction in calvarial bone formation and mineralisation, the effects of *Kdm6a* conditional knockout on cultured calvarial cells extracted from FKO and MKO mice were assessed. The calvarial cells were cultured in osteogenic inductive media for 7 days and their osteogenic differentiation capacity was analysed. The FKO cells exhibited a reduction in the number of Alkaline Phosphatase stained cells and diminished gene expression levels of *Runx2* and *Alkaline Phosphatase* compared to female *Prx1*:cre control cells, whereas MKO cells exhibited an increase in osteogenic associated markers (Figure 5.2.21 & 5.2.22). Therefore, suppression of early and late osteogenic differentiation capacity in FKO calvarial cells led to the inhibition of suture

Prx1:cre

A

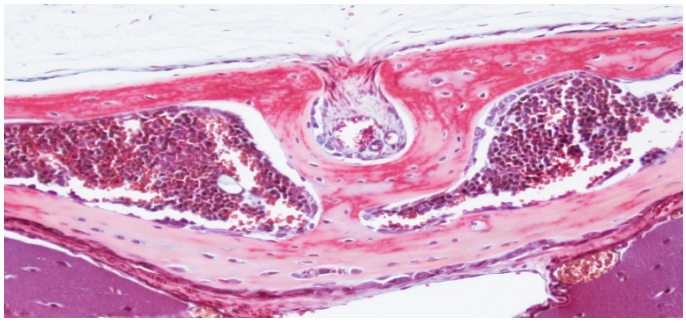

Prx1:cre;Kdm6a$^{-/-}$

B

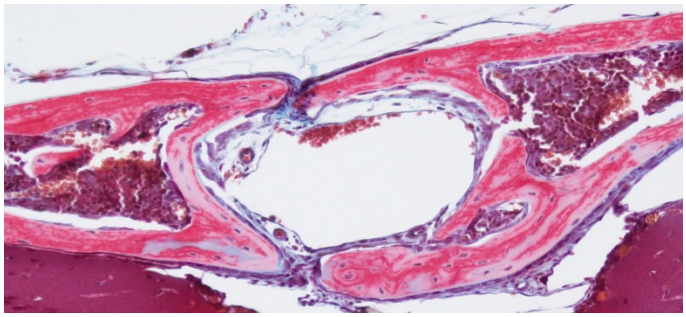

Prx1:cre

C

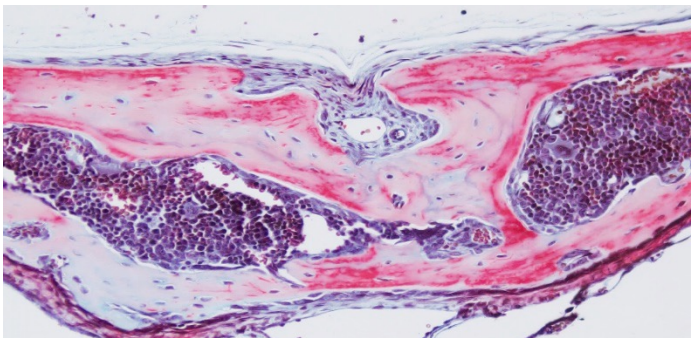

Prx1:cre;Kdm6a$^{-/y}$

D

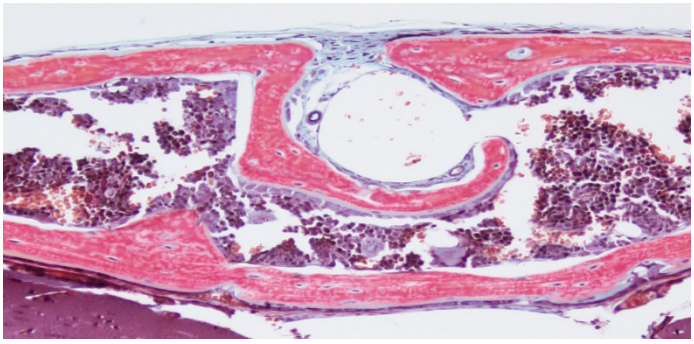

Figure 5.2.18. Loss of *Kdm6a* within the suture mesenchyme delays posterior interfrontal suture fusion in female mice, but not in male. Coronal sections of the posterior interfrontal sutures of fixed calvaria extracted from P25 mice were stained with Movat's Pentachrome. Representative histology images of (A) *Prx1:cre* female control, (B) *Prx1:cre*;*Kdm6a*$^{-/-}$, (C) *Prx1:cre* male control, and (D) *Prx1:cre;Kdm6a*$^{-/y}$ conditional Kdm6a knockout mice.

A

Prx1:cre

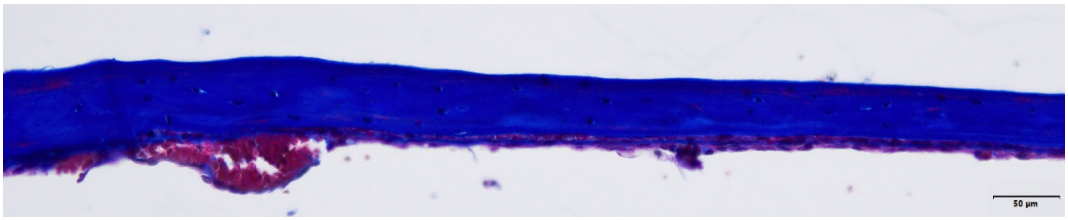

Prx1:cre;Kdm6a$^{-/-}$

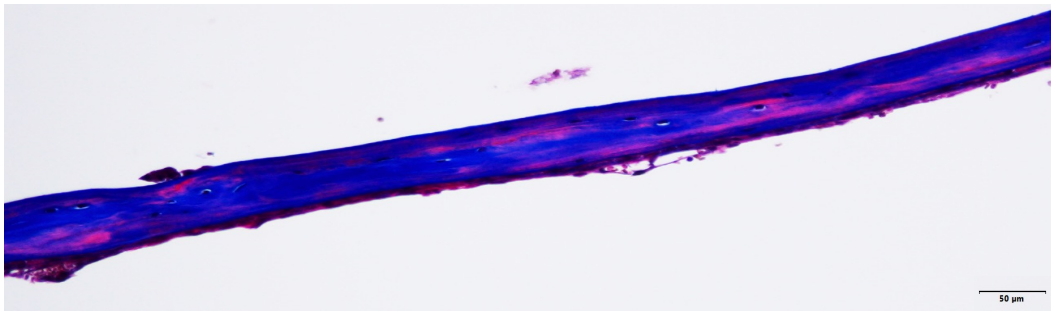

B

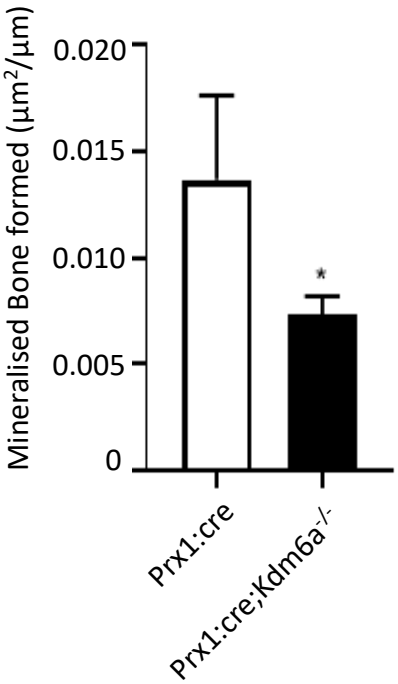

C

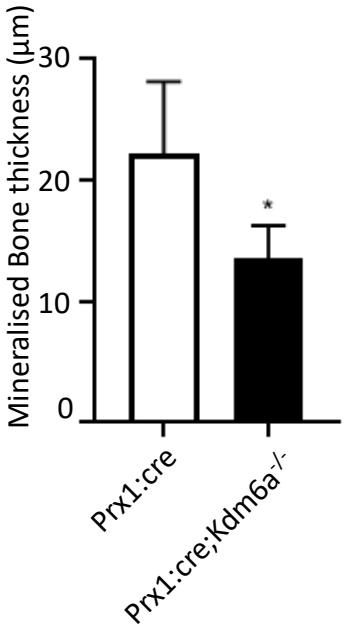

Figure 5.2.19. *Kdm6a* promotes mineralisation of calvaria bone in female mice. Calvarial bones extracted from P25 female mice were fixed, coronally sectioned and stained with Masson's Trichrome. Representative images of calvarial bones from (A) female *Prx1:cre* control and *Prx1:cre;Kdm6a*$^{-/-}$ mice displayed the blue stain as mineralised bone and the red stain as unmineralised osteoid. Images captured at 400X magnification with scale bar = 100μm. Histomorphometric analysis of (B) mineralised bone formed and (C) bone thickness of *Prx1:cre* control and conditional knockout calvarial bones were quantitated using Osteomeasure software. Data represent mean ± S.E. expression, *p≤ 0.05, two-tailed, unpaired, student's t-test, n=6 per group.

A

Prx1:cre

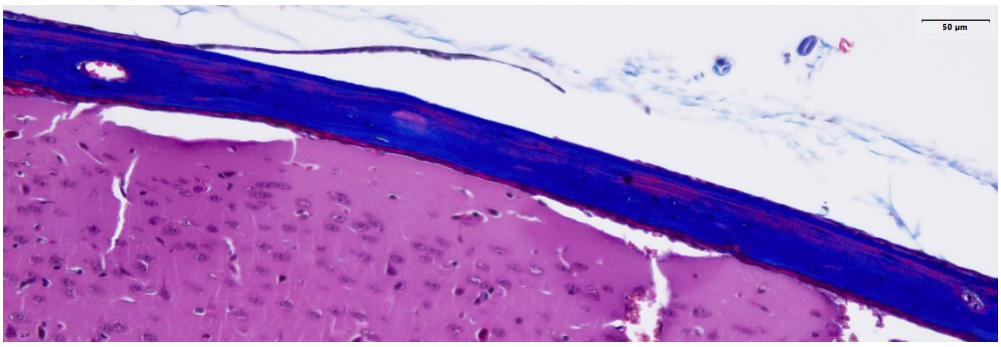

Prx1:cre;Kdm6a$^{-/y}$

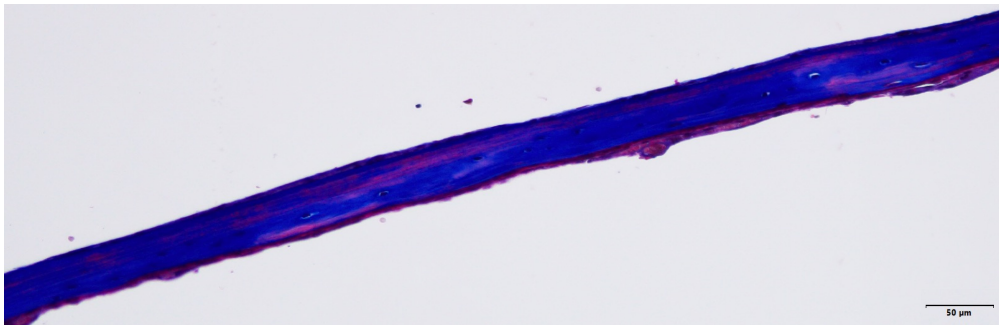

B

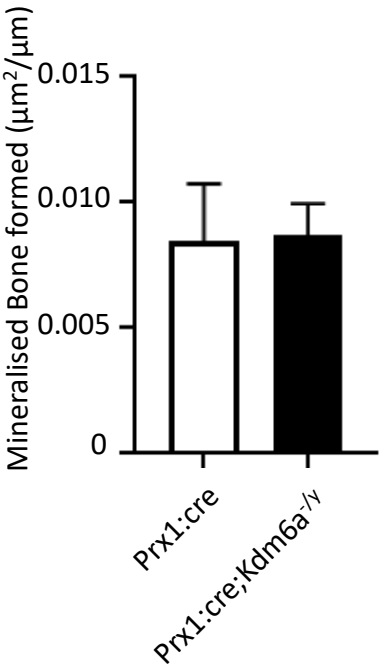

C

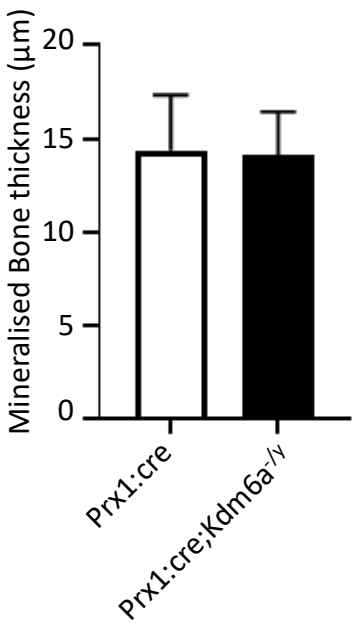

Figure 5.2.20. Conditional loss of *Kdm6a* does not affect mineralisation rate in male calvaria bone. (A) Representative images of calvarial bones from male *Prx1*:cre control and *Prx1:cre*;*Kdm6a*$^{-/y}$ mice, stained with Masson's Trichrome. The blue stain represents mineralised bone and the red stained represents unmineralised osteoid. Images captured at 400X magnification with scale bar = 100μm. Histomorphometric analysis with Osteomeasure software of (B) mineralised bone formed and (C) bone thickness of male *Prx1:cre* control and conditional knockout calvarial bones. Data represent mean ± S.E. expression, *p≤ 0.05, two-tailed, unpaired, student's t-test, n=6 per group.

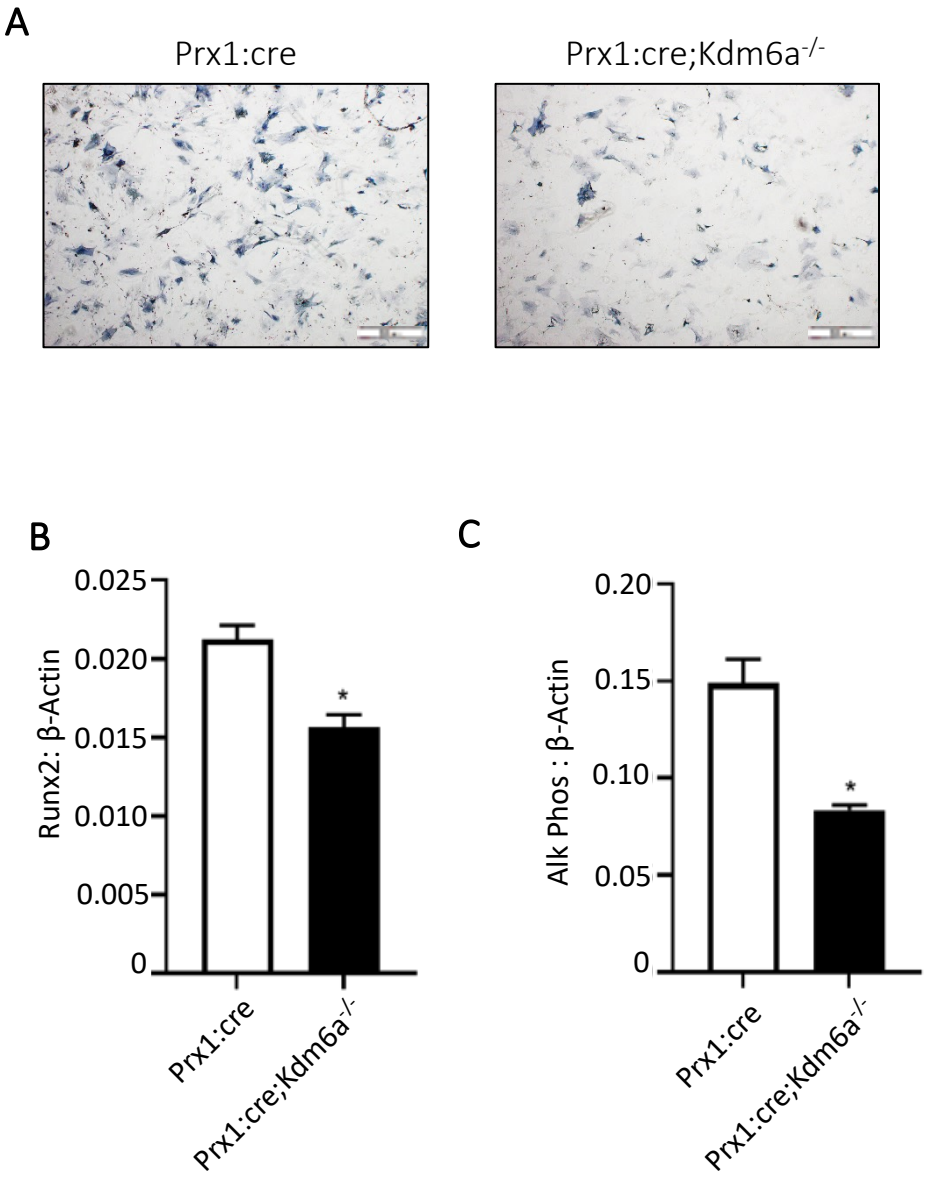
A
Prx1:cre
Prx1:cre;Kdm6a-/-
B
Runx2: β-Actin
0.025
0.020
0.015
0.010
0.005
0
*
Prx1:cre
Prx1:cre;Kdm6a-/-
C
Alk Phos : β-Actin
0.20
0.15
0.10
0.05
0
*
Prx1:cre
Prx1:cre;Kdm6a-/-

Figure 5.2.21. *Kdm6a* promotes osteogenic differentiation of female calvarial cells. (A) Representative images of Alkaline Phosphatase staining of calvarial cells extracted from female *Prx1:cre* control and *Prx1:cre*;*Kdm6a*$^{-/-}$ mice, following 1 week of osteogenic induction. Real-time qPCR analysis of (B) *Runx2* and (C) *Alkaline Phosphatase* (Alk Phos) in calvarial cells from female *Prx1:cre*;*Kdm6a*$^{-/-}$ compared to cells from *Prx1:cre* control, under osteogenic inductive conditions. Data represent mean gene expression levels normalised to *β-Actin* ± S.E. expression, *p≤ 0.05, two-tailed, unpaired, student's t-test, n=3 per group.

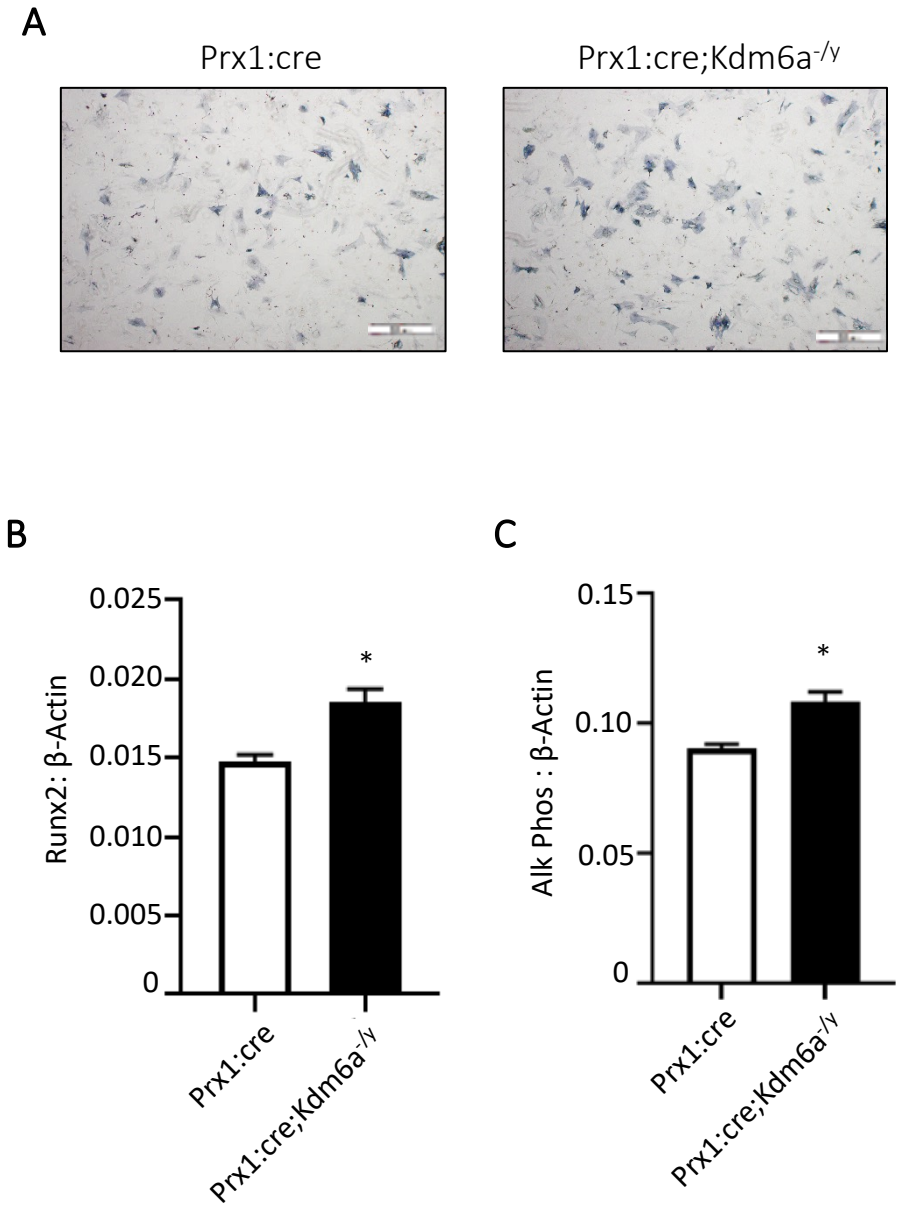
A
Prx1:cre
Prx1:cre;Kdm6a-/y
B
Runx2: β-Actin
0.025
0.020
0.015
0.010
0.005
0
*
Prx1:cre
Prx1:cre;Kdm6a-/y
C
Alk Phos : β-Actin
0.15
0.10
0.05
0
*
Prx1:cre
Prx1:cre;Kdm6a-/y

Figure 5.2.22. Conditional loss of *Kdm6a* upregulates osteogenic differentiation in male calvarial cells. (A) Representative images of Alkaline Phosphatase staining of *Prx1:cre;Kdm6a*$^{-/y}$ calvarial cells compared to cells from male *Prx1:cre* control, following 1 week of osteogenic induction. Real-time qPCR analysis of (B) *Runx2* and (C) *Alkaline Phosphatase* (Alk Phos) in calvarial cells extracted from male *Prx1*:cre *Kdm6a*$^{-/y}$, compared to cells from *Prx1:cre* control, under osteogenic inductive conditions. Data represent mean gene expression levels normalised to *β-Actin* ± S.E. expression, *p≤ 0.05, two-tailed, unpaired, student's t-test, n=3 per group.

fusion and calvarial bone formation *in vivo*. However, this was not observed in MKO calvarial cells further supporting the hypothesis of overcompensation activity by the male-specific Kdm6 family member, Kdm6c.

5.2.5 Overcompensation of the other members of the Kdm6 family is identified in Kdm6a MKO calvarial cells.

With the aim of identifying overcompensation by other Kdm6 family members following *Kdm6a* knockout, the gene expression levels of *Kdm6b*, a histone demethylase homolog and *Kdm6c*, a demethylase-inactive Y-linked enzyme, were quantified by qPCR analyses. In FKO calvarial cells, there was no significant overcompensation by *Kdm6b*, which was associated with lower expression levels of *Ezh2* (Figure 5.2.23). Supportive studies showed elevated levels of the epigenetic inhibitory mark, H3K27me3, on osteogenic genes, *Runx2* and *Alkaline Phosphatase*, in extracted chromatin from FKO calvarial cells cultured in osteogenic-inductive media, using ChIP analyses (Figure 5.2.25). The results demonstrated that higher levels of the inhibitory mark on *Runx2* and *Alkaline Phosphatase* promoter transcription start sites (TSS) suggested effective inhibition of osteogenic gene expression levels.

On the other hand, a significant upregulation of both *Kdm6b* and *Kdm6c* gene expression levels were identified in MKO calvarial cells, suggesting overcompensation by both lysine demethylase and demethylase-inactive enzymes (Figure 5.2.24). In addition, increased expression of *Ezh2* was observed, which correlated to the supressed expression of histone demethylase, *Kdm6a*. Interestingly, the H3K27me levels on *Alkaline Phosphatase* and *Runx*2 TSS were elevated, in contrast with the upregulated osteogenic differentiation capacity seen in MKO calvarial cells (Figure 5.2.25). Taken together, these results suggested

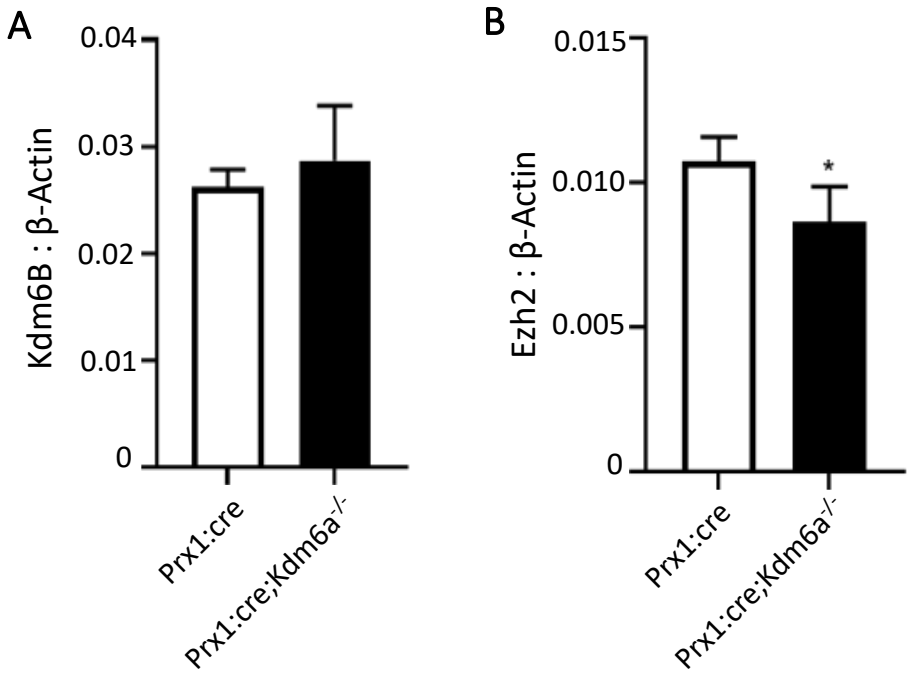
A
Kdm6B : β-Actin
0.04
0.03
0.02
0.01
0
Prx1:cre
Prx1:cre;Kdm6a-/-
B
Ezh2 : β-Actin
0.015
0.010
0.005
0
*
Prx1:cre
Prx1:cre;Kdm6a-/-

Figure 5.2.23. Female *Kdm6a* knocked-out calvarial cells exhibit differential expression of histone demethylase, *Kdm6b*, and histone methyltransferase, *Ezh2*. Gene expression levels of (A) *Kdm6b* and (B) *Ezh2* in calvarial cells extracted from female *Prx1:cre* and *Prx1:cre*;*Kdm6a*$^{-/-}$ mice, cultured in growth media, were analysed with real-time qPCR and normalised to *β-Actin.* Data represent mean ± S.E. expression, *p≤ 0.05, two-tailed, unpaired, student's t-test, n=3 per group.

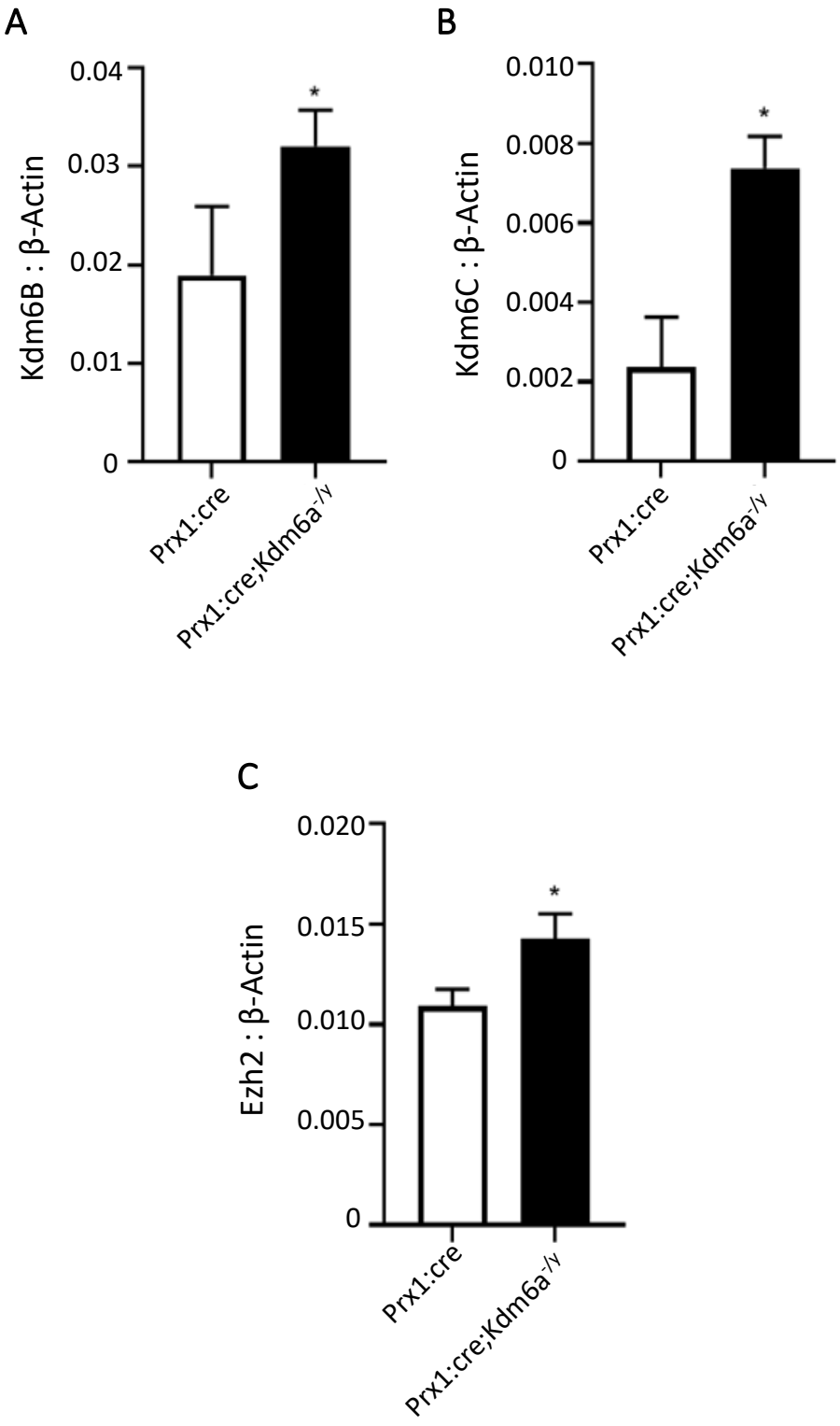
A
Kdm6B : β-Actin
0.04
0.03
0.02
0.01
0
*
Prx1:cre
Prx1:cre;Kdm6a-/Y
B
Kdm6C : β-Actin
0.010
0.008
0.006
0.004
0.002
0
*
Prx1:cre
Prx1:cre;Kdm6a-/Y
C
Ezh2 : β-Actin
0.020
0.015
0.010
0.005
0
*
Prx1:cre
Prx1:cre;Kdm6a-/Y

Figure 5.2.24. Male *Kdm6a* knocked-out calvarial cells exhibit differential expression of histone demethylases, *Kdm6b,* and male-specific, *Kdm6c*, and histone methyltransferase, *Ezh2*. Real-time qPCR analysis of gene expression levels of (A) *Kdm6b*, (B) *Kdm6c* and (C) *Ezh2* in calvarial cells cultured in growth media from male *Prx1:cre* and *Prx1:cre;Kdm6a*$^{-/y}$ calvarial cells, normalised to *β-Actin*. Data represent mean ± S.E. expression, *p≤ 0.05, two-tailed, unpaired, student's t-test, n=3 per group

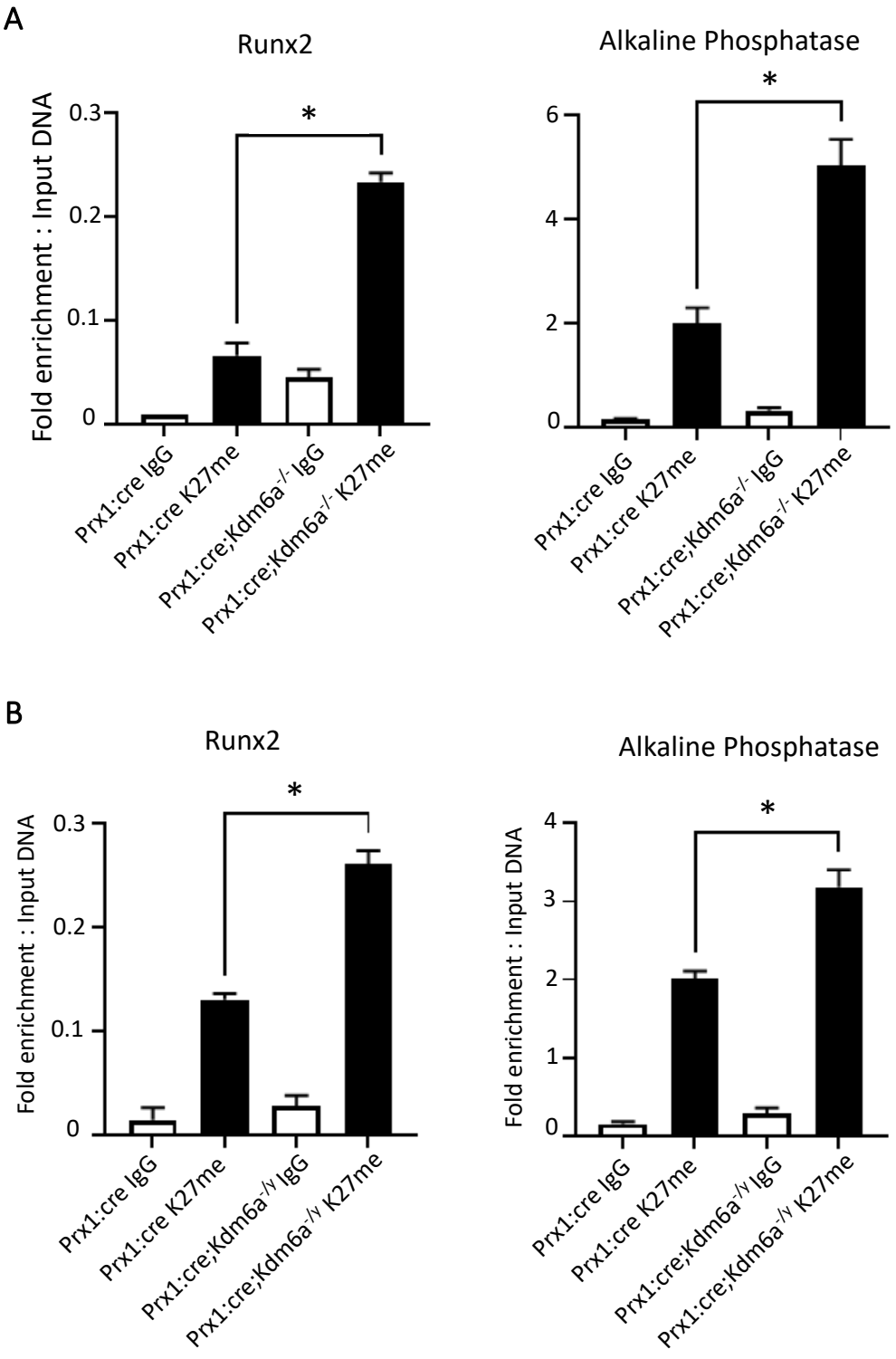
A
Runx2
Alkaline Phosphatase
Fold enrichment : Input DNA
0.3
0.2
0.1
0
6
4
2
*
Prx1:cre IgG
Prx1:cre K27me
Prx1:cre;Kdm6a-/- IgG
Prx1:cre;Kdm6a-/- K27me
B
Runx2
Alkaline Phosphatase
Fold enrichment : Input DNA
0.3
0.2
0.1
0
4
3
2
1
*
Prx1:cre IgG
Prx1:cre K27me
Prx1:cre;Kdm6a-/Y IgG
Prx1:cre;Kdm6a-/Y K27me

Figure 5.2.25. Loss of *Kdm6a* increases the level of histone repressive mark on osteogenic gene promoters in calvarial cells. Chromatin immunoprecipitation (ChIP) analysis of H3K27me3 levels on the transcriptional start sites of *Runx2* and *Alkaline Phosphatase* (Alk Phos) in calvarial cells from (A) female *Prx1:cre;Kdm6a*$^{-/-}$ and (B) male *Prx1:cre;Kdm6a*$^{-/y}$, compared to cells from sex-matched *Prx1:cre* control, under osteogenic inductive conditions. ChIP was performed using either IgG control antibody (IgG) or H3K27me3-specific antibody (K27me). Enriched genomic DNA was used to amplify the transcription start site of target genes. Data represent mean fold enrichment relative to input DNA ± S.E., *$p \leq 0.05$, One-way ANOVA with Tukey's multiple comparisons, n = 3 per group.

a role of demethylase-independent activity during osteogenic differentiation of calvarial cells, affecting the rate of suture fusion and calvarial bone formation.

Subsequently, FKO and MKO were crossed with *Twist-1*$^{del/+}$ mice to further analyse the effects of Kdm6a loss in alleviating premature suture fusion phenotype in SCS mouse model (Figure 5.2.26). However, this cross resulted in embryonic lethality.

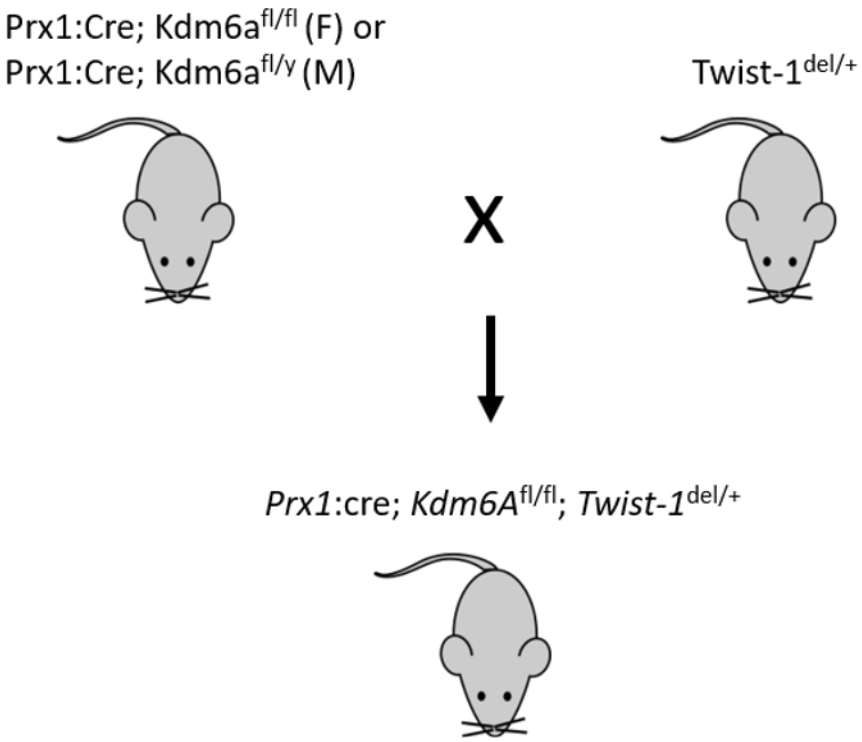
Prx1:Cre; Kdm6a$^{fl/fl}$ (F) or
Prx1:Cre; Kdm6a$^{fl/y}$ (M)
Twist-1$^{del/+}$
X
Prx1:cre; *Kdm6A*$^{fl/fl}$; *Twist-1*$^{del/+}$

Figure 5.2.26. *Kdm6a* conditional knockout model and *Twist-1*$^{del/+}$ cross breeding plan. Cross breeding flow chart of *Prx1*:cre*Kdm6a*-floxed mouse colony with *Twist-1*$^{del/+}$ mice, resulting in *Prx1:cre*;*Kdm6a*$^{fl/fl}$*;Twist-1*$^{del/+}$ female and *Prx1:cre*;*Kdm6a*$^{-/y}$*;Twist-1*$^{del/+}$ male mice.

5.3 Discussion

Prx-1-expressing stem cells have been previously identified within the suture mesenchyme and the limb skeletal bones in mice (Wilk et al. 2017). Thus, the present study utilised *Prx1*:cre driver for generating a *Kdm6a* conditional knockout mouse in early mesenchyme which includes the cranial sutures with the aim of further investigating the role of Kdm6a in suture determination and calvarial bone development. Firstly, the overall weight of *Prx1*:cre;*Kdm6a*$^{fl/fl}$ (FKO) and *Prx1*:cre;*Kdm6a*$^{fl/y}$ (MKO) mice with *Prx1*:cre control mice were compared. The reduced body weight of P25 FKO mice, while beyond the scope of the present thesis, warrants future investigations which will be performed to assess the effect of *Kdm6a* loss in *Prx-1*-expressing skeletal cells on skeletal bone formation and development. On the other hand, MKO mice showed comparable body weight with control mice throughout all the timepoints, suggesting that a less severe outcome in male mice would be observed in future studies. Furthermore, the present study analysed whether the loss of *Kdm6a* changed the calvarial morphometrics by utilising previously published morphometric landmarks on the MIMICS software (Perlyn et al. 2006; Richtsmeier, Baxter & Reeves 2000). These analyses demonstrated changes in the calvarial width in P9 and P25 MKO mice, calvarial length and height in 15-day-old MKO mice, and calvarial width and length in P25 FKO mice, compared to sex-matched *Prx1*:cre controls. The changes observed on cranial shape throughout mouse development suggested that Kdm6a plays a role in correct calvarial patterning. These observations are consistent with previous studies of the Kabuki Syndrome, a rare clinical condition caused by *KDM6A* deletion in the neural crest cells, where patients suffer from growth retardation, short stature and abnormal facial and cranial features (Faundes et al. 2021; Shpargel et al. 2017). This syndrome affects both males and females in equal frequencies, however, shorter stature is more frequently observed in males compared to female patients (Faundes et al. 2021). Interestingly, mutations in *KDM6C*

were not identified in Kabuki Syndrome mutation screening of male patients (Bögershausen et al. 2016). Furthermore, alterations in *KDM6B* gene are linked to neurodevelopmental disorders, including developmental delay, dysmorphic facial characteristics, and musculoskeletal deformities, including syndactyly.

To further investigate the role of Kdm6a in suture fusion, the present study focused on the only suture that fuses in wild type mice, the posterior interfrontal (PIF). This suture is one of the two sutures derived from the neural crest cells, the other being the sagittal suture, which closes between P13 and P15, where all other sutures remain open throughout the lifespan of mice, making it the most ideal suture for observing the effects of *Kdm6a* conditional knockout (Behr 2011; Cohen 1993; Jiang et al. 2002; Sahar, Longaker & Quarto 2005). The data showed significant reductions in both the bone volume and bone surface area of the PIF suture region in P25 FKO, but not in P9 and P15 FKO, which suggested that the role of Kdm6a in calvarial bone formation is essential in the late stage of suture development. This observation might be explained by the endochondral ossification pathway of PIF suture fusion, which incorporates chondrogenesis as a foundation for the ossification process (Sahar, Longaker & Quarto 2005).

The effects of the loss of *Kdm6a*, a promoter of osteogenesis, was observed following chondrogenesis completion, and at the peak of osteogenic differentiation at P15. In agreement, a previous study showed that neural crest-specific knockout of *Kdm6a* did not affect the cartilage formation and distribution (Shpargel et al. 2017). The effects of Kdm6a on osteogenic differentiation was further confirmed on the 3D representative images of the PIF region showing more bone void and less suture fusion points in P25 FKO compared to controls. Conversely, P25 MKO mice displayed an increase in bone volume, where higher bone density and more fusion points were observed. These multiple fusion points are

commonly initiated from the anterior region of the PIF suture during fusion of the endocranial site, where the ectocranial site remained open throughout adulthood. Furthermore, the PIF suture sections of P25 FKO displayed open sutures with heterogeneous cell population at the ectocranial and endocranial sites, whereas fused endocranial and opened ectocranial sutures were observed in *Prx1*:cre control mice and MKO mice. These observations suggested that the loss of *Kdm6a* in FKO resulted in enhanced phenotypic severity in the PIF sutures over MKO, which prompted a further investigation on the calvarial bones surrounding the PIF sutures. Of note, the severity of Kabuki Syndrome in female patients is highly variable compared to males, which could be due to the different levels of X-chromosome inactivation of *KDM6A* (Faundes et al. 2021; Lederer et al. 2012).

Further analyses of parietal bone maturation demonstrated a reduction in mineralised bone formed and bone thickness in FKO, whereas no changes were observed in MKO compared to controls. These results showed that loss of *Kdm6a* in the suture mesenchyme affected the maturation of the surrounding calvarial bones. This is aligned with previous studies which demonstrated that the calvarial bones, creating the skull vault, are derived from the suture mesenchyme (Doro, Grigoriadis & Liu 2017; Zhao 2015). Moreover, investigations into the rate of osteogenic differentiation on cultured calvarial cells *in vitro* found that the reduced mineralisation level seen in FKO *in vivo* were the consequences of suppression of early osteogenic gene expression (*Runx2* and *Osterix*) and late osteogenic gene expression (*Alkaline Phosphatase*) and activity. Conversely, *Runx2, Osterix* and *Alkaline Phosphatase* gene expression levels and *Alkaline Phosphatase* activity were upregulated in calvarial cells extracted from MKO. The contradictory effects on male mice when *Kdm6a* expression is reduced, suggested a potential redundancy of other members of the Kdm6 family. To investigate this, the gene expressions of other members of the Kdm6 family in FKO and MKO calvarial cells were quantified. The results showed significant overexpression of

Kdm6b, a homolog of *Kdm6a*, in MKO, compared with FKO. This suggested that Kdm6b might overcompensate for the loss of the histone demethylase activity of Kdm6a in MKO. Additionally, previous studies have shown that Kdm6b is a promoter of osteogenic differentiation of stromal cells via both its histone demethylase activity and chromatin remodelling function, independent from its demethylase activity (Yang, D et al. 2017; Ye et al. 2012; Zhang, FX, L.; Xu, L.; Xu, Q.; Karsenty, G.; Chen, C. D. 2015). The interesting differential effect of Kdm6a-loss between male and female on Kdm6b expression would need to be further explored using ChIP studies to identify sex-dependent regulators on the *Kdm6b* promotor. Furthermore, *Kdm6c*, a male-specific demethylase-dead homolog, was observed to be significantly upregulated, which suggested a further overcompensation in MKO mice. This ability of compensation by a demethylase-inactive enzyme suggested that osteogenic differentiation of calvarial stromal cells requires demethylase-independent Kdm6a activity, which is supported by a previous study in mouse neural crest cells (Shpargel et al. 2017). In this study, Kdm6c function was restricted to partial compensation of *Kdm6a* loss in neural crest cells. In addition, the expression of *Ezh2*, a histone methyltransferase, was upregulated as a response to the loss of the histone demethylase, *Kdm6a*, which could increase the level of H3K27me3 on osteogenic-promoting genes. Therefore, the phenotypes seen in MKO might be supported by both *Kdm6b* and *Kdm6c* redundancy and *Ezh2* upregulation. Further studies can include conditional knockout of *Kdm6b* and *Kdm6c* with *Prx1* driver to confirm the overcompensation activities of these enzymes. Alternatively, the use of *Gli1*:cre mice could be generated and crossed with *Kdm6a*$^{fl/fl}$, *Kdm6a*$^{fl/y}$, *Kdm6b*$^{fl/fl}$ or *Kdm6c*^{fl} mice to target Kdm6 loss on osteogenic mesenchymal progenitors in all skeletal sites, including the craniofacial, skull bones and vertebrae(Shi et al. 2017). Notably, *Gli-1*-positive stromal cell population covers the majority of the suture mesenchyme niche which includes *Prx-1*-expressing subsets (Doro, Grigoriadis & Liu 2017). Thus, while greater effects might be observed in *Gli1*:cre knockout mice, mouse viability might be decreased.

In the present study, the levels of the epigenetic repressive mark, H3K27me3, on the genic promotor region of osteogenic genes, *Runx2* and *Alkaline Phosphatase*, were compared between FKO and MKO mice. The results showed that FKO displayed an upregulation of H3K27me3 marks on both *Runx2* and *Alkaline Phosphatase*, which correlated with the downregulation of the expression levels of these genes and the suppression of osteogenic differentiation *in vitro* and calvarial bone formation *in vivo*. However, similar results were observed in MKO, which was unexpected. This suggests alternative roles of Kdm6a, including the possibility of congregating cofactors responsible for placing activating marks, such as H3K4me3 on osteogenic genes. This alternative function is supported by previous studies which identified that KDM6A and KMT2D or MLL2, an H3K4me3 lysine methyltransferase, co-exist as a part of a protein complex (Shpargel et al. 2017). H3K4me3 marks are associated with transcription activation and known to be present at the genic region of master regulatory genes at the same temporal and spatial space as H3K27me3 marks, creating bivalent promoters to provide timely switch between gene activation and repression. The balance between these epigenetic marks determines the recruitment of RNA Polymerase II to initiate gene transcription. Therefore, further studies utilising ChIP and co-immunoprecipitation assays are required to analyse the levels of H3K4me3 and RNA Polymerase II transcription complex on the promotors of osteogenic genes to determine the activity state of these genes.

The present chapter demonstrated a delay in PIF suture development and bone maturation in FKO mice, whereas contradictory phenotypes presented in MKO mice. The subsequent hypothesis was that the crossing of the *Kdm6a* suture-specific knockout female mice with *Twist-1*$^{del/+}$ heterozygous male mice would relieve the craniosynostosis phenotypes observed in female *Twist-1*$^{del/+}$ mutant mice. However, the loss of *Kdm6a* within the suture niches and

skeletal stromal cells, together with the systemic haploinsufficiency of *Twist-1* resulted in embryonically lethal offspring. Therefore, future studies could include a Tamoxifen-inducible system of cre recombinase and estrogen receptor fusion protein with postnatal activation to avoid embryonic mortality (Kim, H et al. 2018).

In conclusion, the present chapter has provided further evidence of the essential role of Kdm6a in correct calvarial suture development. The comparison between FKO and MKO presented an insight into a demethylase-independent role of Kdm6a in calvarial cell differentiation. Taken all together, Kdm6a and Kdm6b could be considered as novel pharmacological targets for SCS, and perhaps other syndromic and sporadic non-syndromic craniosynostosis.

Chapter 6: Discussion

6.1 Discussion

Previous evidence in the literature demonstrated that the proliferative and immature state of the suture MPC population is maintained by *TWIST-1* gene during development to preserve suture patency, where its osteogenic differentiation capacity is stimulated by osteogenic-promoting genes, such as *RUNX2*, *Osterix* and *Alkaline Phosphatase*, during suture fusion in adult calvaria. However, loss-of-function mutation of *TWIST-1* can lead to premature osteogenesis of the MPC population within the suture resulting in craniosynostosis, which may manifest as a part of a syndrome (Beederman, MF, E. M.; Reid, R. R. 2014; Cakouros, DI, S.; Cooper, L.; Zannettino, A.; Anderson, P.; Glackin, C.; Gronthos, S. 2012; el Ghouzzi, VLM, M.; Perrin-Schmitt, F.; Lajeunie, E.; Benit, P.; Renier, D.; Bourgeois, P.; Bolcato-Bellemin, A. L.; Munnich, A.; Bonaventure, J. 1997; Isenmann 2009; Lenton et al. 2005; Nacamuli et al. 2003; Yousfi et al. 2001; Zhao 2015). The present thesis focuses on Saethre-Chotzen Syndrome or SCS, the second most common syndromic form of craniosynostosis. Patients with SCS exhibit facial and limb deformities in addition to premature coronal suture fusion (Anderson et al. 1996; Gallagher, Ratisoontorn & Cunningham 1993). Recent studies revealed that the molecular factors regulating MPC proliferation and differentiation include epigenetic regulators, which have previously been shown to affect craniosynostosis occurrence and phenotypic severity. Notably, the *TWIST-1* gene has been shown to suppress osteogenic potential of MPC by promoting a histone methyltransferase, EZH2, which has a role in calvarial and skeletal development by placing the repressive H3K27me3 mark on osteogenic TSS (Cakouros, DI, S.; Cooper, L.; Zannettino, A.; Anderson, P.; Glackin, C.; Gronthos, S. 2012). Our laboratory has reported that EZH2 is found to co-localise with histone demethylases, KDM6A and KDM6B which remove the H3K27me3 marks from osteogenic genes creating a prompt epigenetic switch, essential for robust gene transcription or suppression (Hemming, SC, D.; Isenmann, S.; Cooper, L.; Menicanin, D.; Zannettino, A.; Gronthos, S. 2014). Chapter 3 showed that the expression of histone demethylases, *KDM6A*

and *KDM6B*, is upregulated in calvarial cells extracted from SCS patients and SCS mouse model, *Twist-1*$^{del/+}$ heterozygous mice, where upregulated osteogenic potential is observed. Knock down of *Kdm6a* and *Kdm6b* expression resulted in suppression of early and late osteogenic capacity of *Twist-1*$^{del/+}$ calvarial cells. This chapter supported the hypothesis that Kdm6a and Kdm6b may serve as novel targets to treat craniosynostosis in *Twist-1*$^{del/+}$ mice and potentially SCS patients. In the clinical settings, GSK-J4 treatment could be supplemented during the first calvarial remodeling surgery with the aim to prevent subsequent surgeries often required for SCS patients and other syndromic craniosynostosis patients. Alternatively, subcutaneous delivery of GSK-J4 onto the affected suture sites could be potentially introduced to eliminate invasive approaches completely. However, further investigations on rate-controlled delivery systems and the systemic toxicity effects from GSK-J4 treatment *in vivo* are fundamental in the clinical progression of the present study.

Currently, the treatment for craniosynostosis involves invasive cranial surgery, which is associated with various post-operative complications. Therefore, research on alternative minimally invasive treatments is necessary. Recent studies have demonstrated the potential of pharmacological targeting of various molecular factors to treat craniosynostosis. However, the rarity of craniosynostosis cases and the established current treatments have delayed the progression of these alternative methods to the clinical settings. Previous studies by our laboratory were the first to investigate the use of a Twist-1 target to suppress calvarial bone formation in an organotypic *ex vivo* model extracted from *Twist-1*$^{del/+}$ mice (Camp, E et al. 2018). This study showed that molecular inhibition can serve as a potential treatment to treat craniosynostosis in SCS. However, until now, no studies have investigated epigenetic enzymes as targets for treating craniosynostosis in SCS. Chapter 4 showed that local inhibition of Kdm6a and Kdm6b enzymatic activities with a pharmacological inhibitor, GSK-J4, prevented premature suture fusion in P20 *Twist-1*$^{del/+}$ mice and reduced

mineralisation potential of *Twist-1*$^{del/+}$ calvarial cells. This timepoint was selected to represent post-premature suture fusion in *Twist-1*$^{del/+}$ mice, which occurs between P9 to P15. During normal development, mouse calvarial sutures stay open throughout their lifespans and therefore, further investigation into mature aged *Twist-1*$^{del/+}$ mice following GSK-J4 treatment is required to understand the stability of this pharmacological intervention. In SCS patients, premature coronal suture fusion generally occurs before 1 year of age, which is approximately equal to P9 in mice, suggesting that GSK-J4 treatment may delay premature fusion beyond this period during mice as well as human development. This was achieved by blocking the histone demethylase capacity of Kdm6a and Kdm6b and in turn, increased the H3K27me3 levels at the TSS of osteogenic genes. Of note, Kdm6a and Kdm6b possess histone demethylase-independent activities capable of inducing general chromatin remodeling allowing for gene expression initiation during mouse skeletal development (Shpargel et al. 2017; Wang, C et al. 2012). Therefore, knockout of *Kdm6a* and/or *Kdm6b* genes within the suture mesenchyme was hypothesised to result in a more significant impact in the suture patency during mouse development.

The effects of *Kdm6b* knockout on mouse sutures and calvarial bone development has been previously reported, including open sutures and suppressed calvarial bone maturation(Zhang, FX, L.; Xu, L.; Xu, Q.; Karsenty, G.; Chen, C. D. 2015). On the other hand, previous study on *Kdm6a*-null mice focused on neural crest and heart development defects, revealed that *Kdm6a* loss in both X-chromosomes led to embryonic lethality in homozygous female mice, where *Kdm6c* compensation from the Y-chromosome in hemizygous male mice was capable to compensate *Kdm6a* loss (Shpargel et al. 2012; Welstead et al. 2012). Therefore, Chapter 5 of the present thesis generated, for the first time, a conditional knockout of *Kdm6a* within the suture mesenchyme and skeletal bones, using a *Prx-1* driver, to further confirm the role of Kdm6a in suture and calvarial bone formation

during female and male mouse development. The initial comparison of the weight between *Prx1*:cre*;Kdm6a*$^{-/-}$ (FKO) and *Prx1*:cre*;Kdm6a*$^{-/y}$ (MKO) mice suggested that Kdm6a is essential during late skeletal development of FKO mice, but not in MKO mice. Furthermore, prevention of PIF endocranial suture fusion, suppression of calvarial cell osteogenic differentiation and reduction of bone volume and surface area of the parietal bones surrounding PIF were observed in the late-stage suture development of FKO (P25), but not during MKO development. The late-stage response of *Kdm6a* loss seen in FKO is potentially related to the endochondral ossification process of calvarial bone formation, where the early-stage is mediated by cartilage scaffolds. This observation further confirmed Kdm6a role in osteogenesis, but not in chondrogenesis.

The differential results between sexes of *Kdm6a* knockout mice prompted an investigation on the expression levels of other *Kdm6* members, including *Kdm6a* homolog, *Kdm6b*, and the demethylase-inactive Y-linked member, *Kdm6c*, in *Kdm6a* knockout mice. Comparable levels of *Kdm6b* was observed in FKO and *Prx1*:cre control calvarial cells, whereas upregulation of both *Kdm6b* and *Kdm6c* expression were discovered in MKO calvarial cells. These results further corroborated the role of Kdm6b in osteogenic differentiation in MPC and the overcompensation capability of Kdm6c in MKO. Furthermore, elevated levels of the H3K27me3 mark on osteogenic genes in FKO and MKO calvarial cells supported the suppression of osteogenic differentiation detected in FKO; however, contradicting the increased osteogenic capacity in MKO. This observation proposed that an increased level of the activating mark, H3K4me3, which is often co-localised with the H3K27me3 mark, are located on osteogenic gene promoters in MKO, providing a docking site for RNA Pol II. Therefore, further studies on the levels of activating epigenetic marks on osteogenic TSS in calvarial cells from FKO and MKO are necessary to confirm the transcription activity of

osteogenic genes following *Kdm6a* knockout. Furthermore, this study is the first such study identifying epigenetic enzymes involved in craniosynostosis.

6.2 Future Directions

6.2.1 Rate-controlled delivery system for GSK-J4 subcutaneous treatment *in vivo*

The present thesis highlights that Kdm6a and Kdm6b possess critical roles in the aberrant osteogenic differentiation seen in the SCS mouse model, *Twist-1*$^{del/+}$ mice, and that a localised therapeutic strategy targeting Kdm6a and Kdm6b demethylase activity using a pharmacological inhibitor, GSK-J4, with 2μM concentration is effective to prevent coronal craniosynostosis of *Twist-1*$^{del/+}$ mice. This study utilised a resorbable collagen sponge, Collacote^{TM}, as GSK-J4 delivery method. However, the primary limitation of this approach involves the uncontrolled release of GSK-J4 onto the coronal sutures. To address this, further pre-clinical studies using rate-controlled delivery system; such as Titania-nanotube based protein (Bariana et al. 2017) and mesoporous silica nanoparticles (Finlay 2015; Yokota et al. 2014), are warranted to potentially lower the required concentration of GSK-J4.

6.2.2 Systemic toxicity analyses following GSK-J4 local treatment *in vivo*

Initial histological analyses on the brain tissue of GSK-J4-treated calvaria displayed comparable structure with control DMSO-treated calvaria. Additional key toxicity studies from the start of treatment to adulthood, including weight comparison, serum analyses and histopathology studies, are required to ensure the short- and long-term safety of GSK-J4 subcutaneous therapy. Overall, Chapter 3 and 4 demonstrated that both Kdm6a and Kdm6b serve as efficient novel targets to prevent syndromic craniosynostosis and that GSK-J4 treatment could provide an alternative to the minimally invasive approach for SCS patients.

6.2.3 Chondrogenic analyses of PIF suture and calvarial bone formation in *Kdm6a* conditional knockout mouse model

In Chapter 5, conditional knockout of *Kdm6a* confirmed the role of Kdm6a as an osteogenic promoter, during suture fusion and calvarial bone endochondral ossification. Additional experiments to investigate the effects of Kdm6a during the chondrogenesis stage of calvarial bone maturation would include analyses on the expression levels of *Sox9* and *Collagen Type II*, using qPCR and immunohistological analyses within the PIF sutures of *Kdm6a* conditional knockout mouse model at P9 and P15, which represent pre-osteogenic differentiation timepoints. Additionally, Movat's pentachrome will be used on calvarial fixed sections of P9 and P15 *Kdm6a* conditional knockout mice to visually analyse collagen fibres formation from chondrocytes which would be observed as yellow dye.

6.2.4 Generation of *Prx1*:cre; *Kdm6b*$^{fl/fl}$ and *Prx1*:cre; *Kdm6c*^{fl} mice and utilisation of *Gli-1* as an alternative driver.

Furthermore, comparison between the sexes of the knockout model revealed overcompensation activities of *Kdm6b* and *Kdm6c* in male mice. Accordingly, future studies would include the generation of conditional knockout of *Kdm6b*$^{fl/fl}$ and *Kdm6c*^{fl} with *Prx-1* driver and subsequent generation of the double knockout model with *Prx1*:cre*;Kdm6a*$^{-/-}$ and *Prx1*:cre*;Kdm6a*$^{-/y}$ mice. Moreover, consideration of utilising *Gli-1*, a marker of a greater suture mesenchyme population, as a driver for the knockout models would be fundamental in achieving more significant phenotypical effects. Another key experiment to confirm the transcription activity of osteogenic genes in calvarial cells of the conditional knockout mice include ChIP and Co-IP analyses on the levels of activating epigenetic markers, such as

H3K4me3, and RNA Polymerase II as the determining factor for transcription activities of osteogenic genes.

6.3 Concluding Remarks

The studies presented in this thesis identified *Kdm6a* and *Kdm6b* as novel molecular targets to suppress aberrant upregulation of osteogenic differentiation of SCS mouse calvarial cells. Further investigations revealed that local subcutaneous treatment of GSK-J4, which inhibits Kdm6a and Kdm6b epigenetic activities, effectively prevented coronal synostosis in SCS mouse model with minimal to no toxicity reactions. These results prompted a generation of *Kdm6a* conditional knockout mice, specifically within the suture mesenchyme and skeletal bones, with the aim to confirm Kdm6a role in the suture and calvarial bone formation during mouse development. This mouse model exhibited differential response to *Kdm6a* loss between sexes, where reduced bone formation and open suture were observed on the naturally fusing posterior interfrontal suture in female knockout mice, but not in male mice. Additionally, female knockout calvarial cells displayed suppressed osteogenic differentiation, whereas the contrary effects were observed in male knockout calvarial cells. Collectively, the present thesis demonstrated for the first time the potential alternative treatment to the current invasive approaches to treat craniosynostosis in SCS patients and other syndromic and non-syndromic craniosynostosis.

Chapter 7: References

1. Adamo, MA & Pollack, IF 2010, 'A single-center experience with symptomatic postoperative calvarial growth restriction after extended strip craniectomy for sagittal craniosynostosis', *J Neurosurg Pediatr*, vol. 5, no. 1, Jan, pp. 131-135.

2. Agger, K, Cloos, PA, Christensen, J, Pasini, D, Rose, S, Rappsilber, J, Issaeva, I, Canaani, E, Salcini, AE & Helin, K 2007, 'UTX and JMJD3 are histone H3K27 demethylases involved in HOX gene regulation and development', *Nature*, vol. 449, no. 7163, Oct 11, pp. 731-734.

3. Ahmed, H, Akbari, H, Emami, A & Akbari, MR 2017, 'Genetic Overview of Syndactyly and Polydactyly', *Plast Reconstr Surg Glob Open*, vol. 5, no. 11, Nov, p. e1549.

4. Alver, BH, Kim, KH, Lu, P, Wang, X, Manchester, HE, Wang, W, Haswell, JR, Park, PJ & Roberts, CW 2017, 'The SWI/SNF chromatin remodelling complex is required for maintenance of lineage specific enhancers', *Nat Commun*, vol. 8, Mar 6, p. 14648.

5. Anderson, P, M Hall, C, D Evans, R, D Hayward, R & M Jones, B 1996, *The hands in Saethre-Chotzen syndrome*, vol. 16.

6. Arthur, A, Panagopoulos, RA, Cooper, L, Menicanin, D, Parkinson, IH, Codrington, JD, Vandyke, K, Zannettino, AC, Koblar, SA, Sims, NA, Matsuo, K & Gronthos, S 2013, 'EphB4 enhances the process of endochondral ossification and inhibits remodeling during bone fracture repair', *J Bone Miner Res*, vol. 28, no. 4, Apr, pp. 926-935.

7. Bariana, M, Dwivedi, P, Ranjitkar, S, Kaidonis, JA, Losic, D & Anderson, PJ 2017, 'Biological response of human suture mesenchymal cells to Titania nanotube-based implants for advanced craniosynostosis therapy', *Colloids Surf B Biointerfaces*, vol. 150, Feb 1, pp. 59-67.

8. Beederman, M, Lamplot, JD, Nan, G, Wang, J, Liu, X, Yin, L, Li, R, Shui, W, Zhang, H, Kim, SH, Zhang, W, Zhang, J, Kong, Y, Denduluri, S, Rogers, MR, Pratt, A, Haydon, RC, Luu, HH, Angeles, J, Shi, LL & He, TC 2013, 'BMP signaling in mesenchymal stem cell differentiation and bone formation', *J Biomed Sci Eng*, vol. 6, no. 8a, Aug, pp. 32-52.

9. Beederman, MF, E. M.; Reid, R. R. 2014, 'Molecular basis of cranial suture biology and disease: Osteoblastic and osteoclastic perspectives', *Genes Dis*, vol. 1, no. 1, Sep, pp. 120-125.

10. Behr, BL, M. T.; Quarto, N. 2011, 'Craniosynostosis of coronal suture in twist1 mice occurs through endochondral ossification recapitulating the physiological closure of posterior frontal suture', *Front Physiol*, vol. 2, p. 37.

11. Benyoucef, A, Palii, CG, Wang, C, Porter, CJ, Chu, A, Dai, F, Tremblay, V, Rakopoulos, P, Singh, K, Huang, S, Pflumio, F, Hebert, J, Couture, JF, Perkins, TJ, Ge,

K, Dilworth, FJ & Brand, M 2016, 'UTX inhibition as selective epigenetic therapy against TAL1-driven T-cell acute lymphoblastic leukemia', *Genes Dev*, vol. 30, no. 5, Mar 01, pp. 508-521.

12. Berger, SL, Kouzarides, T, Shiekhattar, R & Shilatifard, A 2009, 'An operational definition of epigenetics', *Genes Dev*, vol. 23, no. 7, Apr 01, pp. 781-783.

13. Bergquist, CS, Nauta, AC, Selden, NR & Kuang, AA 2016, 'Age at the Time of Surgery and Maintenance of Head Size in Nonsyndromic Sagittal Craniosynostosis', *Plast Reconstr Surg*, vol. 137, no. 5, May, pp. 1557-1565.

14. Berletch, JB, Deng, X, Nguyen, DK & Disteche, CM 2013, 'Female bias in Rhox6 and 9 regulation by the histone demethylase KDM6A', *PLoS Genet*, vol. 9, no. 5, May, p. e1003489.

15. Bialek, P, Kern, B, Yang, X, Schrock, M, Sosic, D, Hong, N, Wu, H, Yu, K, Ornitz, DM, Olson, EN, Justice, MJ & Karsenty, G 2004, 'A twist code determines the onset of osteoblast differentiation', *Dev Cell*, vol. 6, no. 3, Mar, pp. 423-435.

16. Bildsoe, H, Fan, X, Wilkie, EE, Ashoti, A, Jones, VJ, Power, M, Qin, J, Wang, J, Tam, PPL & Loebel, DAF 2016, 'Transcriptional targets of TWIST1 in the cranial mesoderm regulate cell-matrix interactions and mesenchyme maintenance', *Dev Biol*, vol. 418, no. 1, Oct 1, pp. 189-203.

17. Bildsoe, H, Loebel, DA, Jones, VJ, Chen, YT, Behringer, RR & Tam, PP 2009, 'Requirement for Twist1 in frontonasal and skull vault development in the mouse embryo', *Dev Biol*, vol. 331, no. 2, Jul 15, pp. 176-188.

18. Bin Alamer, O, Jimenez, AE & Azad, TD 2021, 'Single-suture craniosynostosis and the epigenome: current evidence and a review of epigenetic principles', *Neurosurg Focus*, vol. 50, no. 4, Apr, p. E10.

19. Bögershausen, N, Gatinois, V, Riehmer, V, Kayserili, H, Becker, J, Thoenes, M, Simsek-Kiper, P, Barat-Houari, M, Elcioglu, NH, Wieczorek, D, Tinschert, S, Sarrabay, G, Strom, TM, Fabre, A, Baynam, G, Sanchez, E, Nürnberg, G, Altunoglu, U, Capri, Y, Isidor, B, Lacombe, D, Corsini, C, Cormier-Daire, V, Sanlaville, D, Giuliano, F, Le Quan Sang, KH, Kayirangwa, H, Nürnberg, P, Meitinger, T, Boduroglu, K, Zoll, B, Lyonnet, S, Tzschach, A, Verloes, A, Di Donato, N, Touitou, I, Netzer, C, Li, Y, Geneviève, D, Yigit, G & Wollnik, B 2016, 'Mutation Update for Kabuki Syndrome Genes KMT2D and KDM6A and Further Delineation of X-Linked Kabuki Syndrome Subtype 2', *Hum Mutat*, vol. 37, no. 9, Sep, pp. 847-864.

20. Brat, DJ 2018, '2 - Normal Brain Histopathology', in A Perry & DJ Brat (eds), *Practical Surgical Neuropathology: A Diagnostic Approach (Second Edition)*, Elsevier, pp. 19-37.

21. Burgos-Florez, FJ, Gavilan-Alfonso, ME & Garzon-Alvarado, DA 2016, 'Flat bones and sutures formation in the human cranial vault during prenatal development and infancy: A computational model', *J Theor Biol*, vol. 393, Mar 21, pp. 127-144.

22. Cakouros, D & Gronthos, S 2020, 'Epigenetic Regulators of Mesenchymal Stem/Stromal Cell Lineage Determination', *Curr Osteoporos Rep*, vol. 18, no. 5, Oct, pp. 597-605.

23. Cakouros, D, Hemming, S, Gronthos, K, Liu, R, Zannettino, A, Shi, S & Gronthos, S 2019, 'Specific functions of TET1 and TET2 in regulating mesenchymal cell lineage determination', *Epigenetics Chromatin*, vol. 12, no. 1, Jan 3, p. 3.

24. Cakouros, DI, S.; Cooper, L.; Zannettino, A.; Anderson, P.; Glackin, C.; Gronthos, S. 2012, 'Twist-1 induces Ezh2 recruitment regulating histone methylation along the Ink4A/Arf locus in mesenchymal stem cells', *Mol Cell Biol*, vol. 32, no. 8, Apr, pp. 1433-1441.

25. Camp, E, Anderson, PJ, Zannettino, ACW, Glackin, CA & Gronthos, S 2018, 'Tyrosine kinase receptor c-ros-oncogene 1 inhibition alleviates aberrant bone formation of TWIST-1 haploinsufficient calvarial cells from Saethre-Chotzen syndrome patients', *J Cell Physiol*, Apr 16.

26. Camp, EA, P. J.; Zannettino, A. C.; Gronthos, S. 2017, 'Tyrosine kinase receptor c-ros-oncogene 1 mediates TWIST-1 regulation of human mesenchymal stem cell lineage commitment', *Bone*, vol. 94, Jan, pp. 98-107.

27. Cao, R, Wang, L, Wang, H, Xia, L, Erdjument-Bromage, H, Tempst, P, Jones, RS & Zhang, Y 2002, 'Role of histone H3 lysine 27 methylation in Polycomb-group silencing', *Science*, vol. 298, no. 5595, Nov 1, pp. 1039-1043.

28. Carver, EAO, K. F.; Gridley, T. 2002, 'Craniosynostosis in Twist heterozygous mice: a model for Saethre-Chotzen syndrome', *Anat Rec*, vol. 268, no. 2, Oct 01, pp. 90-92.

29. Chen, ZF & Behringer, RR 1995, 'twist is required in head mesenchyme for cranial neural tube morphogenesis', *Genes Dev*, vol. 9, no. 6, Mar 15, pp. 686-699.

30. Cohen, MM 1993, 'Sutural biology and the correlates of craniosynostosis', *Am J Med Genet*, vol. 47.

31. Connerney, J, Andreeva, V, Leshem, Y, Muentener, C, Mercado, MA & Spicer, DB 2006, 'Twist1 dimer selection regulates cranial suture patterning and fusion', *Dev Dyn*, vol. 235, no. 5, May, pp. 1345-1357.

32. Dai, J, Yu, D, Wang, Y, Chen, Y, Sun, H, Zhang, X, Zhu, S, Pan, Z, Heng, BC, Zhang, S & Ouyang, H 2017, 'Kdm6b regulates cartilage development and homeostasis through anabolic metabolism', *Ann Rheum Dis*, vol. 76, no. 7, Jul, pp. 1295-1303.

33. De Santa, F, Totaro, MG, Prosperini, E, Notarbartolo, S, Testa, G & Natoli, G 2007, 'The histone H3 lysine-27 demethylase Jmjd3 links inflammation to inhibition of polycomb-mediated gene silencing', *Cell*, vol. 130, no. 6, Sep 21, pp. 1083-1094.

34. Di Pietro, L, Barba, M, Prampolini, C, Ceccariglia, S, Frassanito, P, Vita, A, Guadagni, E, Bonvissuto, D, Massimi, L, Tamburrini, G, Parolini, O & Lattanzi, W 2020, 'GLI1 and AXIN2 Are Distinctive Markers of Human Calvarial Mesenchymal Stromal Cells in Nonsyndromic Craniosynostosis', *Int J Mol Sci*, vol. 21, no. 12, Jun 19.

35. Dong, YF, Soung do, Y, Chang, Y, Enomoto-Iwamoto, M, Paris, M, O'Keefe, RJ, Schwarz, EM & Drissi, H 2007, 'Transforming growth factor-beta and Wnt signals regulate chondrocyte differentiation through Twist1 in a stage-specific manner', *Mol Endocrinol*, vol. 21, no. 11, Nov, pp. 2805-2820.

36. Doro, DH, Grigoriadis, AE & Liu, KJ 2017, 'Calvarial Suture-Derived Stem Cells and Their Contribution to Cranial Bone Repair', *Front Physiol*, vol. 8, p. 956.

37. El Ghouzzi, V, Legeai-Mallet, L, Aresta, S, Benoist, C, Munnich, A, de Gunzburg, J & Bonaventure, J 2000, 'Saethre-Chotzen mutations cause TWIST protein degradation or impaired nuclear location', *Hum Mol Genet*, vol. 9, no. 5, Mar 22, pp. 813-819.

38. el Ghouzzi, VLM, M.; Perrin-Schmitt, F.; Lajeunie, E.; Benit, P.; Renier, D.; Bourgeois, P.; Bolcato-Bellemin, A. L.; Munnich, A.; Bonaventure, J. 1997, 'Mutations of the TWIST gene in the Saethre-Chotzen syndrome', *Nat Genet*, vol. 15, no. 1, Jan, pp. 42-46.

39. Farooq, S, Morton, J, Lloyd, M & Krishna, ST 2020, 'The Influence of Epigenetic Factors in Four Pairs of Twins With Non-Syndromic Craniosynostosis', *J Craniofac Surg*, vol. 31, no. 1, Jan/Feb, pp. 283-285.

40. Faundes, V, Goh, S, Akilapa, R, Bezuidenhout, H, Bjornsson, HT, Bradley, L, Brady, AF, Brischoux-Boucher, E, Brunner, H, Bulk, S, Canham, N, Cody, D, Dentici, ML, Digilio, MC, Elmslie, F, Fry, AE, Gill, H, Hurst, J, Johnson, D, Julia, S, Lachlan, K, Lebel, RR, Byler, M, Gershon, E, Lemire, E, Gnazzo, M, Lepri, FR, Marchese, A, McEntagart, M, McGaughran, J, Mizuno, S, Okamoto, N, Rieubland, C, Rodgers, J, Sasaki, E, Scalais, E, Scurr, I, Suri, M, van der Burgt, I, Matsumoto, N, Miyake, N, Benoit, V, Lederer, D & Banka, S 2021, 'Clinical delineation, sex differences, and genotype–phenotype correlation in pathogenic KDM6A variants causing X-linked Kabuki syndrome type 2', *Genetics in Medicine*, vol. 23, no. 7, 2021/07/01, pp. 1202-1210.

41. Finlay, JR, C. M.; Dong, J.; Zink, J. I.; Tamanoi, F.; Glackin, C. A. 2015, 'Mesoporous silica nanoparticle delivery of chemically modified siRNA against TWIST1 leads to reduced tumor burden', *Nanomedicine*, vol. 11, no. 7, Oct, pp. 1657-1666.

42. Gallagher, ER, Ratisoontorn, C & Cunningham, ML 1993, 'Saethre-Chotzen Syndrome', in MP Adam, HH Ardinger, RA Pagon, SE Wallace, LJH Bean, K Stephens & A Amemiya (eds), *GeneReviews((R))*, University of Washington, Seattle. GeneReviews is a registered trademark of the University of Washington, Seattle, Seattle WA.

43. Garman, RH 2011, 'Histology of the central nervous system', *Toxicol Pathol*, vol. 39, no. 1, Jan, pp. 22-35.

44. Garrett, IR 2003, 'Assessing bone formation using mouse calvarial organ cultures', *Methods Mol Med*, vol. 80, pp. 183-198.

45. Ge, W, Shi, L, Zhou, Y, Liu, Y, Ma, GE, Jiang, Y, Xu, Y, Zhang, X & Feng, H 2011, 'Inhibition of osteogenic differentiation of human adipose-derived stromal cells by retinoblastoma binding protein 2 repression of RUNX2-activated transcription', *Stem Cells*, vol. 29, no. 7, Jul, pp. 1112-1125.

46. Goodnough, LH, Dinuoscio, GJ & Atit, RP 2016, 'Twist1 contributes to cranial bone initiation and dermal condensation by maintaining Wnt signaling responsiveness', *Dev Dyn*, vol. 245, no. 2, Feb, pp. 144-156.

47. Han, RH, Nguyen, DC, Bruck, BS, Skolnick, GB, Yarbrough, CK, Naidoo, SD, Patel, KB, Kane, AA, Woo, AS & Smyth, MD 2016, 'Characterization of complications associated with open and endoscopic craniosynostosis surgery at a single institution', *J Neurosurg Pediatr*, vol. 17, no. 3, Mar, pp. 361-370.

48. Hashizume, R, Andor, N, Ihara, Y, Lerner, R, Gan, H, Chen, X, Fang, D, Huang, X, Tom, MW, Ngo, V, Solomon, D, Mueller, S, Paris, PL, Zhang, Z, Petritsch, C, Gupta, N, Waldman, TA & James, CD 2014, 'Pharmacologic inhibition of histone demethylation as a therapy for pediatric brainstem glioma', *Nat Med*, vol. 20, no. 12, Dec, pp. 1394-1396.

49. Hemming, S, Cakouros, D, Codrington, J, Vandyke, K, Arthur, A, Zannettino, A & Gronthos, S 2017, 'EZH2 deletion in early mesenchyme compromises postnatal bone microarchitecture and structural integrity and accelerates remodeling', *Faseb j*, vol. 31, no. 3, Mar, pp. 1011-1027.

50. Hemming, SC, D.; Codrington, J.; Vandyke, K.; Arthur, A.; Zannettino, A.; Gronthos, S. 2017, 'EZH2 deletion in early mesenchyme compromises postnatal bone microarchitecture and structural integrity and accelerates remodeling', *Faseb j*, vol. 31, no. 3, Mar, pp. 1011-1027.

51. Hemming, SC, D.; Isenmann, S.; Cooper, L.; Menicanin, D.; Zannettino, A.; Gronthos, S. 2014, 'EZH2 and KDM6A act as an epigenetic switch to regulate mesenchymal stem cell lineage specification', *Stem Cells*, vol. 32, no. 3, Mar, pp. 802-815.

52. Hersh, DS, Hoover-Fong, JE, Beck, N, Dorafshar, AH & Ahn, ES 2017, 'Endoscopic surgery for patients with syndromic craniosynostosis and the requirement for additional open surgery', *J Neurosurg Pediatr*, vol. 20, no. 1, Jul, pp. 91-98.

53. Holmes, G, Zhang, L, Rivera, J, Murphy, R, Assouline, C, Sullivan, L, Oppeneer, T & Jabs, EW 2018, 'C-type natriuretic peptide analog treatment of craniosynostosis in a Crouzon syndrome mouse model', *PLoS One*, vol. 13, no. 7, p. e0201492.

54. Hong, SC, Y. W.; Yu, L. R.; Yu, H.; Veenstra, T. D.; Ge, K. 2007, 'Identification of JmjC domain-containing UTX and JMJD3 as histone H3 lysine 27 demethylases', *Proc Natl Acad Sci U S A*, vol. 104, no. 47, Nov 20, pp. 18439-18444.

55. Huang, Y, Meng, T, Wang, S, Zhang, H, Mues, G, Qin, C, Feng, JQ, D'Souza, RN & Lu, Y 2014, 'Twist1- and Twist2-haploinsufficiency results in reduced bone formation', *PLoS One*, vol. 9, no. 6, p. e99331.

56. Idriz, S, Patel, JH, Ameli Renani, S, Allan, R & Vlahos, I 2015, 'CT of Normal Developmental and Variant Anatomy of the Pediatric Skull: Distinguishing Trauma from Normality', *Radiographics*, vol. 35, no. 5, Sep-Oct, pp. 1585-1601.

57. Isenmann, SA, A.; Zannettino, A. C.; Turner, J. L.; Shi, S.; Glackin, C. A.; Gronthos, S. 2009, 'TWIST family of basic helix-loop-helix transcription factors mediate human mesenchymal stem cell growth and commitment', *Stem Cells*, vol. 27, no. 10, Oct, pp. 2457-2468.

58. Issaeva, I, Zonis, Y, Rozovskaia, T, Orlovsky, K, Croce, CM, Nakamura, T, Mazo, A, Eisenbach, L & Canaani, E 2007, 'Knockdown of ALR (MLL2) reveals ALR target genes and leads to alterations in cell adhesion and growth', *Mol Cell Biol*, vol. 27, no. 5, Mar, pp. 1889-1903.

59. Jiang, X, Iseki, S, Maxson, RE, Sucov, HM & Morriss-Kay, GM 2002, 'Tissue origins and interactions in the mammalian skull vault', *Dev Biol*, vol. 241.

60. Jimenez, DF, McGinity, MJ & Barone, CM 2018, 'Endoscopy-assisted early correction of single-suture metopic craniosynostosis: a 19-year experience', *J Neurosurg Pediatr*, Sep 28, pp. 1-14.

61. Johnson, D, Iseki, S, Wilkie, AO & Morriss-Kay, GM 2000, 'Expression patterns of Twist and Fgfr1, -2 and -3 in the developing mouse coronal suture suggest a key role for twist in suture initiation and biogenesis', *Mech Dev*, vol. 91, no. 1-2, Mar 01, pp. 341-345.

62. Katsianou, MA, Adamopoulos, C, Vastardis, H & Basdra, EK 2016, 'Signaling mechanisms implicated in cranial sutures pathophysiology: Craniosynostosis', *BBA Clin*, vol. 6, Dec, pp. 165-176.

63. Kim, H, Kim, M, Im, SK & Fang, S 2018, 'Mouse Cre-LoxP system: general principles to determine tissue-specific roles of target genes', *Lab Anim Res*, vol. 34, no. 4, Dec, pp. 147-159.

64. Kim, SY, Shin, HJ & Lim, SY 2017, 'Determining the fate of cranial sutures after surgical correction of non-syndromic craniosynostosis', *J Craniomaxillofac Surg*, Aug 19.

65. Knight, SJ, Anderson, VA, Spencer-Smith, MM & Da Costa, AC 2014, 'Neurodevelopmental outcomes in infants and children with single-suture craniosynostosis: a systematic review', *Dev Neuropsychol*, vol. 39, no. 3, pp. 159-186.

66. Kooistra, SM & Helin, K 2012, 'Molecular mechanisms and potential functions of histone demethylases', *Nat Rev Mol Cell Biol*, vol. 13, no. 5, Apr 4, pp. 297-311.

67. Kreiborg, S & Cohen, MM, Jr. 2010, 'Ocular manifestations of Apert and Crouzon syndromes: qualitative and quantitative findings', *J Craniofac Surg*, vol. 21, no. 5, Sep, pp. 1354-1357.

68. Krishnan, V, Bryant, HU & Macdougald, OA 2006, 'Regulation of bone mass by Wnt signaling', *J Clin Invest*, vol. 116.

69. Kruidenier, LC, C. W.; Cheng, Z.; Liddle, J.; Che, K.; Joberty, G.; Bantscheff, M.; Bountra, C.; Bridges, A.; Diallo, H.; Eberhard, D.; Hutchinson, S.; Jones, E.; Katso, R.; Leveridge, M.; Mander, P. K.; Mosley, J.; Ramirez-Molina, C.; Rowland, P.; Schofield, C. J.; Sheppard, R. J.; Smith, J. E.; Swales, C.; Tanner, R.; Thomas, P.; Tumber, A.; Drewes, G.; Oppermann, U.; Patel, D. J.; Lee, K.; Wilson, D. M. 2012, 'A selective jumonji H3K27 demethylase inhibitor modulates the proinflammatory macrophage response', *Nature*, vol. 488, no. 7411, Aug 16, pp. 404-408.

70. Lakin, GE, Sinkin, JC, Chen, R, Koltz, PF & Girotto, JA 2012, 'Genetic and epigenetic influences of twins on the pathogenesis of craniosynostosis: a meta-analysis', *Plast Reconstr Surg*, vol. 129, no. 4, Apr, pp. 945-954.

71. Lan, F, Bayliss, PE, Rinn, JL, Whetstine, JR, Wang, JK, Chen, S, Iwase, S, Alpatov, R, Issaeva, I, Canaani, E, Roberts, TM, Chang, HY & Shi, Y 2007, 'A histone H3 lysine 27 demethylase regulates animal posterior development', *Nature*, vol. 449, no. 7163, Oct 11, pp. 689-694.

72. Lang, D, Lu, MM, Huang, L, Engleka, KA, Zhang, M, Chu, EY, Lipner, S, Skoultchi, A, Millar, SE & Epstein, JA 2005, 'Pax3 functions at a nodal point in melanocyte stem cell differentiation', *Nature*, vol. 433, no. 7028, Feb 24, pp. 884-887.

73. Lederer, D, Grisart, B, Digilio, MC, Benoit, V, Crespin, M, Ghariani, SC, Maystadt, I, Dallapiccola, B & Verellen-Dumoulin, C 2012, 'Deletion of KDM6A, a histone demethylase interacting with MLL2, in three patients with Kabuki syndrome', *Am J Hum Genet*, vol. 90, no. 1, Jan 13, pp. 119-124.

74. Lee, HQH, J. M.; Wray, A. C.; Lo, P. A.; Chong, D. K.; Holmes, A. D.; Greensmith, A. L. 2012, 'Analysis of morbidity and mortality in surgical management of craniosynostosis', *J Craniofac Surg*, vol. 23, no. 5, Sep, pp. 1256-1261.

75. Lenton, KA, Nacamuli, RP, Wan, DC, Helms, JA & Longaker, MT 2005, 'Cranial suture biology', *Curr Top Dev Biol*, vol. 66, pp. 287-328.

76. Lhuissier, E, Aury-Landas, J, Allas, L, Boittin, M, Boumediene, K & Baugé, C 2019, 'Antiproliferative effect of the histone demethylase inhibitor GSK-J4 in chondrosarcomas', *IUBMB Life*, vol. 71, no. 11, Nov, pp. 1711-1719.

77. Li, Y, Zhang, M, Sheng, M, Zhang, P, Chen, Z, Xing, W, Bai, J, Cheng, T, Yang, FC & Zhou, Y 2018, 'Therapeutic potential of GSK-J4, a histone demethylase KDM6B/JMJD3 inhibitor, for acute myeloid leukemia', *J Cancer Res Clin Oncol*, Mar 28.

78. Logan, M, Martin, JF, Nagy, A, Lobe, C, Olson, EN & Tabin, CJ 2002, 'Expression of Cre Recombinase in the developing mouse limb bud driven by a Prxl enhancer', *Genesis*, vol. 33, no. 2, Jun, pp. 77-80.

79. Lu, X, Sawh-Martinez, R, Jorge Forte, A, Wu, R, Cabrejo, R, Wilson, A, Steinbacher, DM, Alperovich, M, Alonso, N & Persing, JA 2019, 'Classification of Subtypes of Apert Syndrome, Based on the Type of Vault Suture Synostosis', *Plast Reconstr Surg Glob Open*, vol. 7, no. 3, Mar, p. e2158.

80. Luger, K, Rechsteiner, TJ & Richmond, TJ 1999, 'Expression and purification of recombinant histones and nucleosome reconstitution', *Methods Mol Biol*, vol. 119, pp. 1-16.

81. Magge, SNS, K.; Sajja, A.; DeFreitas, T. A.; Hofherr, S. E.; Broth, R. E.; Keating, R. F.; Rogers, G. F. 2017, 'Identical Twins Discordant for Metopic Craniosynostosis: Evidence of Epigenetic Influences', *J Craniofac Surg*, vol. 28, no. 1, Jan, pp. 14-16.

82. Mani, P, Jarrell, A, Myers, J & Atit, R 2010, 'Visualizing canonical Wnt signaling during mouse craniofacial development', *Dev Dyn*, vol. 239, no. 1, Jan, pp. 354-363.

83. Marchac, D & Renier, D 1990, 'New aspects of craniofacial surgery', *World J Surg*, vol. 14, no. 6, Nov-Dec, pp. 725-732.

84. Marino, S, Staines, KA, Brown, G, Howard-Jones, RA & Adamczyk, M 2016, 'Models of ex vivo explant cultures: applications in bone research', *Bonekey Rep*, vol. 5, p. 818.

85. Markunas, CA, Wilcox, AJ, Xu, Z, Joubert, BR, Harlid, S, Panduri, V, Håberg, SE, Nystad, W, London, SJ, Sandler, DP, Lie, RT, Wade, PA & Taylor, JA 2016, 'Maternal

Age at Delivery Is Associated with an Epigenetic Signature in Both Newborns and Adults', *PLoS One*, vol. 11, no. 7, p. e0156361.

86. Milekic, MH, Xin, Y, O'Donnell, A, Kumar, KK, Bradley-Moore, M, Malaspina, D, Moore, H, Brunner, D, Ge, Y, Edwards, J, Paul, S, Haghighi, FG & Gingrich, JA 2015, 'Age-related sperm DNA methylation changes are transmitted to offspring and associated with abnormal behavior and dysregulated gene expression', *Mol Psychiatry*, vol. 20, no. 8, Aug, pp. 995-1001.

87. Miller, SA, Mohn, SE & Weinmann, AS 2010, 'Jmjd3 and UTX play a demethylase-independent role in chromatin remodeling to regulate T-box family member-dependent gene expression', *Mol Cell*, vol. 40, no. 4, Nov 24, pp. 594-605.

88. Miraoui, H, Severe, N, Vaudin, P, Pages, JC & Marie, PJ 2010, 'Molecular silencing of Twist1 enhances osteogenic differentiation of murine mesenchymal stem cells: implication of FGFR2 signaling', *J Cell Biochem*, vol. 110, no. 5, Aug 1, pp. 1147-1154.

89. Miyake, N, Mizuno, S, Okamoto, N, Ohashi, H, Shiina, M, Ogata, K, Tsurusaki, Y, Nakashima, M, Saitsu, H, Niikawa, N & Matsumoto, N 2013, 'KDM6A point mutations cause Kabuki syndrome', *Hum Mutat*, vol. 34, no. 1, Jan, pp. 108-110.

90. Mohammad, KS, Chirgwin, JM & Guise, TA 2008, 'Assessing new bone formation in neonatal calvarial organ cultures', *Methods Mol Biol*, vol. 455, pp. 37-50.

91. Moioli, EK, Clark, PA, Xin, X, Lal, S & Mao, JJ 2007, 'Matrices and scaffolds for drug delivery in dental, oral and craniofacial tissue engineering', *Adv Drug Deliv Rev*, vol. 59, no. 4-5, May 30, pp. 308-324.

92. Moore, LD, Le, T & Fan, G 2013, 'DNA Methylation and Its Basic Function', *Neuropsychopharmacology*, vol. 38, no. 1, 2013/01/01, pp. 23-38.

93. Morales Torres, C, Laugesen, A & Helin, K 2013, 'Utx is required for proper induction of ectoderm and mesoderm during differentiation of embryonic stem cells', *PLoS One*, vol. 8, no. 4, p. e60020.

94. Morinobu, M, Ishijima, M, Rittling, SR, Tsuji, K, Yamamoto, H, Nifuji, A, Denhardt, DT & Noda, M 2003, 'Osteopontin expression in osteoblasts and osteocytes during bone formation under mechanical stress in the calvarial suture in vivo', *J Bone Miner Res*, vol. 18, no. 9, Sep, pp. 1706-1715.

95. Morozov, VM, Li, Y, Clowers, MM & Ishov, AM 2017, 'Inhibitor of H3K27 demethylase JMJD3/UTX GSK-J4 is a potential therapeutic option for castration resistant prostate cancer', *Oncotarget*, vol. 8, no. 37, Sep 22, pp. 62131-62142.

96. Moss, ML 1958, 'Fusion of the frontal suture in the rat', *Am J Anat*, vol. 102, no. 1, Jan, pp. 141-165.

97. Nacamuli, RP, Fong, KD, Warren, SM, Fang, TD, Song, HM, Helms, JA & Longaker, MT 2003, 'Markers of osteoblast differentiation in fusing and nonfusing cranial sutures', *Plast Reconstr Surg*, vol. 112.

98. Nam, HK, Vesela, I, Siismets, E & Hatch, NE 2019, 'Tissue nonspecific alkaline phosphatase promotes calvarial progenitor cell cycle progression and cytokinesis via Erk1,2', *Bone*, vol. 120, Mar, pp. 125-136.

99. Nguyen, TM, Arthur, A, Paton, S, Hemming, S, Panagopoulos, R, Codrington, J, Walkley, CR, Zannettino, AC & Gronthos, S 2016, 'Loss of ephrinB1 in osteogenic progenitor cells impedes endochondral ossification and compromises bone strength integrity during skeletal development', *Bone*, vol. 93, Dec, pp. 12-21.

100. Opperman, LA 2000, 'Cranial sutures as intramembranous bone growth sites', *Dev Dyn*, vol. 219.

101. Ota, K, Tong, KI, Goto, K, Tomida, S, Komuro, A, Wang, Z, Nishio, K & Okada, H 2017, 'The H3K27 demethylase, Utx, regulates adipogenesis in a differentiation stage-dependent manner', *PLoS One*, vol. 12, no. 3, p. e0173713.

102. Ouyang, Z, Chen, Z, Ishikawa, M, Yue, X, Kawanami, A, Leahy, P, Greenfield, EM & Murakami, S 2014, 'Prx1 and 3.2kb Col1a1 promoters target distinct bone cell populations in transgenic mice', *Bone*, vol. 58, Jan, pp. 136-145.

103. Ozkul, Y & Galderisi, U 2016, 'The Impact of Epigenetics on Mesenchymal Stem Cell Biology', *J Cell Physiol*, vol. 231, no. 11, Nov, pp. 2393-2401.

104. Perlyn, CA, DeLeon, VB, Babbs, C, Govier, D, Burell, L, Darvann, T, Kreiborg, S & Morriss-Kay, G 2006, 'The craniofacial phenotype of the Crouzon mouse: analysis of a model for syndromic craniosynostosis using three-dimensional MicroCT', *Cleft Palate Craniofac J*, vol. 43, no. 6, Nov, pp. 740-748.

105. Proctor, MR 2012, 'Endoscopic cranial suture release for the treatment of craniosynostosis--is it the future?', *J Craniofac Surg*, vol. 23, no. 1, Jan, pp. 225-228.

106. Rao, RA, Dhele, N, Cheemadan, S, Ketkar, A, Jayandharan, GR, Palakodeti, D & Rampalli, S 2015, 'Ezh2 mediated H3K27me3 activity facilitates somatic transition during human pluripotent reprogramming', *Scientific Reports*, vol. 5, no. 1, 2015/02/04, p. 8229.

107. Reinhold, MI, Kapadia, RM, Liao, Z & Naski, MC 2006, 'The Wnt-inducible transcription factor Twist1 inhibits chondrogenesis', *J Biol Chem*, vol. 281, no. 3, Jan 20, pp. 1381-1388.

108. Rice, DP, Aberg, T, Chan, Y, Tang, Z, Kettunen, PJ, Pakarinen, L, Maxson, RE & Thesleff, I 2000, 'Integration of FGF and TWIST in calvarial bone and suture development', *Development*, vol. 127.

109. Rice, DP, Rice, R & Thesleff, I 2003, 'Molecular mechanisms in calvarial bone and suture development, and their relation to craniosynostosis', *Eur J Orthod*, vol. 25, no. 2, Apr, pp. 139-148.

110. Richtsmeier, JT, Baxter, LL & Reeves, RH 2000, 'Parallels of craniofacial maldevelopment in Down syndrome and Ts65Dn mice', *Dev Dyn*, vol. 217, no. 2, Feb, pp. 137-145.

111. Rojas, A, Aguilar, R, Henriquez, B, Lian, JB, Stein, JL, Stein, GS, van Wijnen, AJ, van Zundert, B, Allende, ML & Montecino, M 2015, 'Epigenetic Control of the Bone-master Runx2 Gene during Osteoblast-lineage Commitment by the Histone Demethylase JARID1B/KDM5B', *J Biol Chem*, vol. 290, no. 47, Nov 20, pp. 28329-28342.

112. Rojas, A, Sepulveda, H, Henriquez, B, Aguilar, R, Opazo, T, Nardocci, G, Bustos, F, Lian, JB, Stein, JL, Stein, GS, van Zundert, B, van Wijnen, AJ, Allende, ML & Montecino, M 2019, 'Mll-COMPASS complexes mediate H3K4me3 enrichment and transcription of the osteoblast master gene Runx2/p57 in osteoblasts', *J Cell Physiol*, vol. 234, no. 5, May, pp. 6244-6253.

113. Rutland, P, Pulleyn, LJ, Reardon, W, Baraitser, M, Hayward, R, Jones, B, Malcolm, S, Winter, RM, Oldridge, M, Slaney, SF & et al. 1995, 'Identical mutations in the FGFR2 gene cause both Pfeiffer and Crouzon syndrome phenotypes', *Nat Genet*, vol. 9, no. 2, Feb, pp. 173-176.

114. Sahar, DE, Longaker, MT & Quarto, N 2005, 'Sox9 neural crest determinant gene controls patterning and closure of the posterior frontal cranial suture', *Dev Biol*, vol. 280, no. 2, Apr 15, pp. 344-361.

115. Sakaki, H, Okada, M, Kuramoto, K, Takeda, H, Watarai, H, Suzuki, S, Seino, S, Seino, M, Ohta, T, Nagase, S, Kurachi, H & Kitanaka, C 2015, 'GSKJ4, A Selective Jumonji H3K27 Demethylase Inhibitor, Effectively Targets Ovarian Cancer Stem Cells', *Anticancer Res*, vol. 35, no. 12, Dec, pp. 6607-6614.

116. Salimi, A & Pourahmad, J 2018, 'Animal Tests for Evaluation of Cognitive Impairment in Neonatal Mouse', *Methods Mol Biol*, vol. 1797, pp. 545-554.

117. Seenundun, S, Rampalli, S, Liu, QC, Aziz, A, Palii, C, Hong, S, Blais, A, Brand, M, Ge, K & Dilworth, FJ 2010, 'UTX mediates demethylation of H3K27me3 at muscle-specific genes during myogenesis', *Embo J*, vol. 29, no. 8, Apr 21, pp. 1401-1411.

118. Senarath-Yapa, KC, M. T.; McArdle, A.; Wong, V. W.; Quarto, N.; Longaker, M. T.; Wan, D. C. 2012, 'Craniosynostosis: molecular pathways and future pharmacologic therapy', *Organogenesis*, vol. 8, no. 4, Oct-Dec, pp. 103-113.

119. Seruya, M, Oh, AK, Boyajian, MJ, Posnick, JC, Myseros, JS, Yaun, AL & Keating, RF 2011, 'Long-term outcomes of primary craniofacial reconstruction for craniosynostosis: a 12-year experience', *Plast Reconstr Surg*, vol. 127, no. 6, Jun, pp. 2397-2406.

120. Shi, Y, He, G, Lee, WC, McKenzie, JA, Silva, MJ & Long, F 2017, 'Gli1 identifies osteogenic progenitors for bone formation and fracture repair', *Nat Commun*, vol. 8, no. 1, Dec 11, p. 2043.

121. Shin, HR, Bae, HS, Kim, BS, Yoon, HI, Cho, YD, Kim, WJ, Choi, KY, Lee, YS, Woo, KM, Baek, JH & Ryoo, HM 2018, 'PIN1 is a new therapeutic target of craniosynostosis', *Hum Mol Genet*, vol. 27, no. 22, Nov 15, pp. 3827-3839.

122. Shpargel, KB, Sengoku, T, Yokoyama, S & Magnuson, T 2012, 'UTX and UTY demonstrate histone demethylase-independent function in mouse embryonic development', *PLoS Genet*, vol. 8, no. 9, Sep, p. e1002964.

123. Shpargel, KB, Starmer, J, Wang, C, Ge, K & Magnuson, T 2017, 'UTX-guided neural crest function underlies craniofacial features of Kabuki syndrome', *Proc Natl Acad Sci U S A*, vol. 114, no. 43, Oct 24, pp. E9046-e9055.

124. Shpargel, KB, Starmer, J, Yee, D, Pohlers, M & Magnuson, T 2014, 'KDM6 demethylase independent loss of histone H3 lysine 27 trimethylation during early embryonic development', *PLoS Genet*, vol. 10, no. 8, Aug, p. e1004507.

125. Sims, RJ, 3rd, Nishioka, K & Reinberg, D 2003, 'Histone lysine methylation: a signature for chromatin function', *Trends Genet*, vol. 19, no. 11, Nov, pp. 629-639.

126. Springer, IN, Warnke, PH, Terheyden, H, Açil, Y, Bülhoff, A, Kuchenbecker, S, Bolte, H, Russo, PA, Vairaktaris, EG & Wiltfang, J 2007, 'Craniectomy and noggin application in an infant model', *J Craniomaxillofac Surg*, vol. 35, no. 3, Apr, pp. 177-184.

127. Sui, A, Xu, Y, Li, Y, Hu, Q, Wang, Z, Zhang, H, Yang, J, Guo, X & Zhao, W 2017, 'The pharmacological role of histone demethylase JMJD3 inhibitor GSK-J4 on glioma cells', *Oncotarget*, vol. 8, no. 40, Sep 15, pp. 68591-68598.

128. Sun, J, Ermann, J, Niu, N, Yan, G, Yang, Y, Shi, Y & Zou, W 2018, 'Histone demethylase LSD1 regulates bone mass by controlling WNT7B and BMP2 signaling in osteoblasts', *Bone Res*, vol. 6, p. 14.

129. Tang, QY, Zhang, SF, Dai, SK, Liu, C, Wang, YY, Du, HZ, Teng, ZQ & Liu, CM 2020, 'UTX Regulates Human Neural Differentiation and Dendritic Morphology by Resolving Bivalent Promoters', *Stem Cell Reports*, vol. 15, no. 2, Aug 11, pp. 439-453.

130. Van der Meulen, JS, F.; Van Vlierberghe, P. 2014, 'The H3K27me3 demethylase UTX in normal development and disease', *Epigenetics*, vol. 9, no. 5, May, pp. 658-668.

131. Van Meer, P & Raber, J 2005, 'Mouse behavioural analysis in systems biology', *Biochem J*, vol. 389, no. Pt 3, Aug 1, pp. 593-610.

132. Villavicencio, EH, Yoon, JW, Frank, DJ, Fuchtbauer, EM, Walterhouse, DO & Iannaccone, PM 2002, 'Cooperative E-box regulation of human GLI1 by TWIST and USF', *Genesis*, vol. 32, no. 4, Apr, pp. 247-258.

133. Vu, HL, Panchal, J, Parker, EE, Levine, NS & Francel, P 2001, 'The timing of physiologic closure of the metopic suture: a review of 159 patients using reconstructed 3D CT scans of the craniofacial region', *J Craniofac Surg*, vol. 12, no. 6, Nov, pp. 527-532.

134. Walport, LJ, Hopkinson, RJ, Vollmar, M, Madden, SK, Gileadi, C, Oppermann, U, Schofield, CJ & Johansson, C 2014, 'Human UTY(KDM6C) is a male-specific N-methyl lysyl demethylase', *J Biol Chem*, vol. 289, no. 26, Jun 27, pp. 18302-18313.

135. Wang, C, Lee, JE, Cho, YW, Xiao, Y, Jin, Q, Liu, C & Ge, K 2012, 'UTX regulates mesoderm differentiation of embryonic stem cells independent of H3K27 demethylase activity', *Proc Natl Acad Sci U S A*, vol. 109, no. 38, Sep 18, pp. 15324-15329.

136. Wang, FS, Lian, WS, Lee, MS, Weng, WT, Huang, YH, Chen, YS, Sun, YC, Wu, SL, Chuang, PC & Ko, JY 2017, 'Histone demethylase UTX counteracts glucocorticoid deregulation of osteogenesis by modulating histone-dependent and -independent pathways', *J Mol Med (Berl)*, vol. 95, no. 5, May, pp. 499-512.

137. Wang, JC, Nagy, L & Demke, JC 2016, 'Syndromic Craniosynostosis', *Facial Plast Surg Clin North Am*, vol. 24, no. 4, Nov, pp. 531-543.

138. Wang, Y, Sun, M, Uhlhorn, VL, Zhou, X, Peter, I, Martinez-Abadias, N, Hill, CA, Percival, CJ, Richtsmeier, JT, Huso, DL & Jabs, EW 2010, 'Activation of p38 MAPK pathway in the skull abnormalities of Apert syndrome Fgfr2(+P253R) mice', *BMC Dev Biol*, vol. 10, Feb 22, p. 22.

139. Welstead, GG, Creyghton, MP, Bilodeau, S, Cheng, AW, Markoulaki, S, Young, RA & Jaenisch, R 2012, 'X-linked H3K27me3 demethylase Utx is required for embryonic development in a sex-specific manner', *Proc Natl Acad Sci U S A*, vol. 109, no. 32, Aug 7, pp. 13004-13009.

140. Wes, AM, Paliga, JT, Goldstein, JA, Whitaker, LA, Bartlett, SP & Taylor, JA 2014, 'An evaluation of complications, revisions, and long-term aesthetic outcomes in nonsyndromic metopic craniosynostosis', *Plast Reconstr Surg*, vol. 133, no. 6, Jun, pp. 1453-1464.

141. Wilk, K, Yeh, SA, Mortensen, LJ, Ghaffarigarakani, S, Lombardo, CM, Bassir, SH, Aldawood, ZA, Lin, CP & Intini, G 2017, 'Postnatal Calvarial Skeletal Stem Cells Expressing PRX1 Reside Exclusively in the Calvarial Sutures and Are Required for Bone Regeneration', *Stem Cell Reports*, vol. 8, no. 4, Apr 11, pp. 933-946.

142. Wilkie, AO 2000, 'Epidemiology and genetics of craniosynostosis', *Am J Med Genet*, vol. 90.

143. Wilkie, AO & Morriss-Kay, GM 2001, 'Genetics of craniofacial development and malformation', *Nat Rev Genet*, vol. 2, no. 6, Jun, pp. 458-468.

144. Wilkie, AO, Slaney, SF, Oldridge, M, Poole, MD, Ashworth, GJ, Hockley, AD, Hayward, RD, David, DJ, Pulleyn, LJ, Rutland, P & et al. 1995, 'Apert syndrome results from localized mutations of FGFR2 and is allelic with Crouzon syndrome', *Nat Genet*, vol. 9, no. 2, Feb, pp. 165-172.

145. Wilkinson, CC, Stence, NV, Serrano, CA, Graber, SJ, Batista-Silverman, L, Schmidt-Beuchat, E & French, BM 2020, 'Fusion patterns of major calvarial sutures on volume-rendered CT reconstructions', *J Neurosurg Pediatr*, Feb 7, pp. 1-10.

146. Xu, J, Deng, X, Watkins, R & Disteche, CM 2008, 'Sex-specific differences in expression of histone demethylases Utx and Uty in mouse brain and neurons', *J Neurosci*, vol. 28, no. 17, Apr 23, pp. 4521-4527.

147. Yan, N, Xu, L, Wu, X, Zhang, L, Fei, X, Cao, Y & Zhang, F 2017, 'GSKJ4, an H3K27me3 demethylase inhibitor, effectively suppresses the breast cancer stem cells', *Exp Cell Res*, vol. 359, no. 2, Oct 15, pp. 405-414.

148. Yang, D, Okamura, H, Nakashima, Y & Haneji, T 2013, 'Histone demethylase Jmjd3 regulates osteoblast differentiation via transcription factors Runx2 and osterix', *J Biol Chem*, vol. 288, no. 47, Nov 22, pp. 33530-33541.

149. Yang, D, Yu, B, Sun, H & Qiu, L 2017, 'The Roles of Histone Demethylase Jmjd3 in Osteoblast Differentiation and Apoptosis', *J Clin Med*, vol. 6, no. 3, Feb 23.

150. Yang, DC, Yang, MH, Tsai, CC, Huang, TF, Chen, YH & Hung, SC 2011, 'Hypoxia inhibits osteogenesis in human mesenchymal stem cells through direct regulation of RUNX2 by TWIST', *PLoS One*, vol. 6, no. 9, p. e23965.

151. Yapp, CC, A. J.; Price, A.; Oppermann, U.; Snelling, S. J. 2016, 'H3K27me3 demethylases regulate in vitro chondrogenesis and chondrocyte activity in osteoarthritis', *Arthritis Res Ther*, vol. 18, no. 1, Jul 7, p. 158.

152. Ye, L, Fan, Z, Yu, B, Chang, J, Al Hezaimi, K, Zhou, X, Park, NH & Wang, CY 2012, 'Histone demethylases KDM4B and KDM6B promotes osteogenic differentiation of human MSCs', *Cell Stem Cell*, vol. 11, no. 1, Jul 6, pp. 50-61.

153. Yokota, M, Kobayashi, Y, Morita, J, Suzuki, H, Hashimoto, Y, Sasaki, Y, Akiyoshi, K & Moriyama, K 2014, 'Therapeutic effect of nanogel-based delivery of soluble FGFR2 with S252W mutation on craniosynostosis', *PLoS One*, vol. 9, no. 7, p. e101693.

154. Yoshida, T, Phylactou, LA, Uney, JB, Ishikawa, I, Eto, K & Iseki, S 2005, 'Twist is required for establishment of the mouse coronal suture', *J Anat*, vol. 206, no. 5, May, pp. 437-444.

155. Yousfi, M, Lasmoles, F, Lomri, A, Delannoy, P & Marie, PJ 2001, 'Increased bone formation and decreased osteocalcin expression induced by reduced Twist dosage in Saethre-Chotzen syndrome', *J Clin Invest*, vol. 107, no. 9, May, pp. 1153-1161.

156. Yousfi, M, Lasmoles, F & Marie, PJ 2002, 'TWIST inactivation reduces CBFA1/RUNX2 expression and DNA binding to the osteocalcin promoter in osteoblasts', *Biochem Biophys Res Commun*, vol. 297, no. 3, Sep 27, pp. 641-644.

157. Zhang, F, Xu, L, Xu, L, Xu, Q, Li, D, Yang, Y, Karsenty, G & Chen, CD 2015, 'JMJD3 promotes chondrocyte proliferation and hypertrophy during endochondral bone formation in mice', *J Mol Cell Biol*, vol. 7, no. 1, Feb, pp. 23-34.

158. Zhang, FX, L.; Xu, L.; Xu, Q.; Karsenty, G.; Chen, C. D. 2015, 'Histone demethylase JMJD3 is required for osteoblast differentiation in mice', *Sci Rep*, vol. 5, Aug 25, p. 13418.

159. Zhao, HF, J.; Ho, T. V.; Grimes, W.; Urata, M.; Chai, Y. 2015, 'The suture provides a niche for mesenchymal stem cells of craniofacial bones', *Nat Cell Biol*, vol. 17, no. 4, Apr, pp. 386-396.